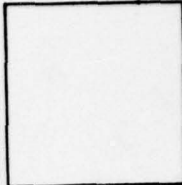
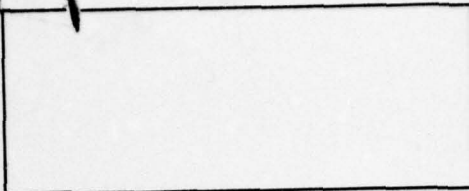
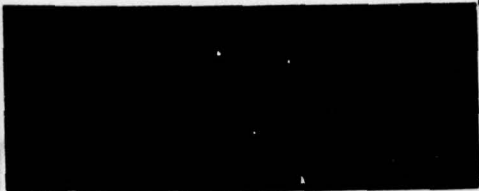


NELC / TR 1988



NELC / TR 1988



①
NW

ADA 034755

EXTENDED LINE-OF-SIGHT OPTICAL COMMUNICATIONS STUDY

GC Moordian, NJ Adrian, PH Levine, and WR Stone

30 June 1976, changed 4 November 1976

Research and Development, 1 July 1975 to 30 June 1976

Prepared for
NAVAL ELECTRONIC SYSTEMS COMMAND
WASHINGTON, D.C. 20360

DDC
RECEIVED
JAN 25 1977
RECEIVED
A

APPROVED FOR PUBLIC RELEASE; DISTRIBUTION IS UNLIMITED



NAVAL ELECTRONICS LABORATORY CENTER
SAN DIEGO, CALIFORNIA 92152

UNCLASSIFIED

SECURITY CLASSIFICATION OF THIS PAGE (When Data Entered)

REPORT DOCUMENTATION PAGE		READ INSTRUCTIONS BEFORE COMPLETING FORM
1. REPORT NUMBER NELC Technical Report 1988 (TR 1988)	2. GOVT ACCESSION NO.	3. RECIPIENT'S CATALOG NUMBER (9)
4. TITLE (and Subtitle) EXTENDED LINE-OF-SIGHT OPTICAL COMMUNICATIONS STUDY	5. PERFORMING ORG. REPORT NUMBER 30	
7. AUTHOR(s) GC Mooradian, VJ Adrian, PH Levine, and WR Stone	8. CONTRACT OR GRANT NUMBER(s)	
9. PERFORMING ORGANIZATION NAME AND ADDRESS Naval Electronics Laboratory Center San Diego, CA 92152	10. PROGRAM ELEMENT, PROJECT, TASK AREA & WORK UNIT NUMBERS 11	
11. CONTROLLING OFFICE NAME AND ADDRESS Naval Electronic Systems Command Washington, DC 20360	12. REPORT DATE / 30 June 1976 changed 4 November 1976	
14. MONITORING AGENCY NAME & ADDRESS (if different from Controlling Office) G. C. / Mooradian, V. J. / Adrian, P. H. / Levine W. R. / Stone	13. NUMBER OF PAGES 120	
16. DISTRIBUTION STATEMENT (for this Report) Approved for public release; distribution is unlimited	15. SECURITY CLASS. (of this report) UNCLASSIFIED	
17. DISTRIBUTION STATEMENT (of the abstract entered in Block 20, if different from Report) (14) NELC / TR-1988	15a. DECLASSIFICATION / DOWNGRADING SCHEDULE	
18. SUPPLEMENTARY NOTES		
19. KEY WORDS (Continue on reverse side if necessary and identify by block number) Laser communications Optical communications Remotely piloted vehicles		
20. ABSTRACT (Continue on reverse side if necessary and identify by block number) The objective of this study was to carry out a tradeoff analysis among systems parameters for two types of extended line-of-sight optical communication links: optical forward scatter from the atmosphere and remotely piloted vehicle relay links. The general application of such links is the control of dispersed Naval task force units. An analytical model was developed for the optical scatter link and was found to be in reasonable agreement with limited field data.		

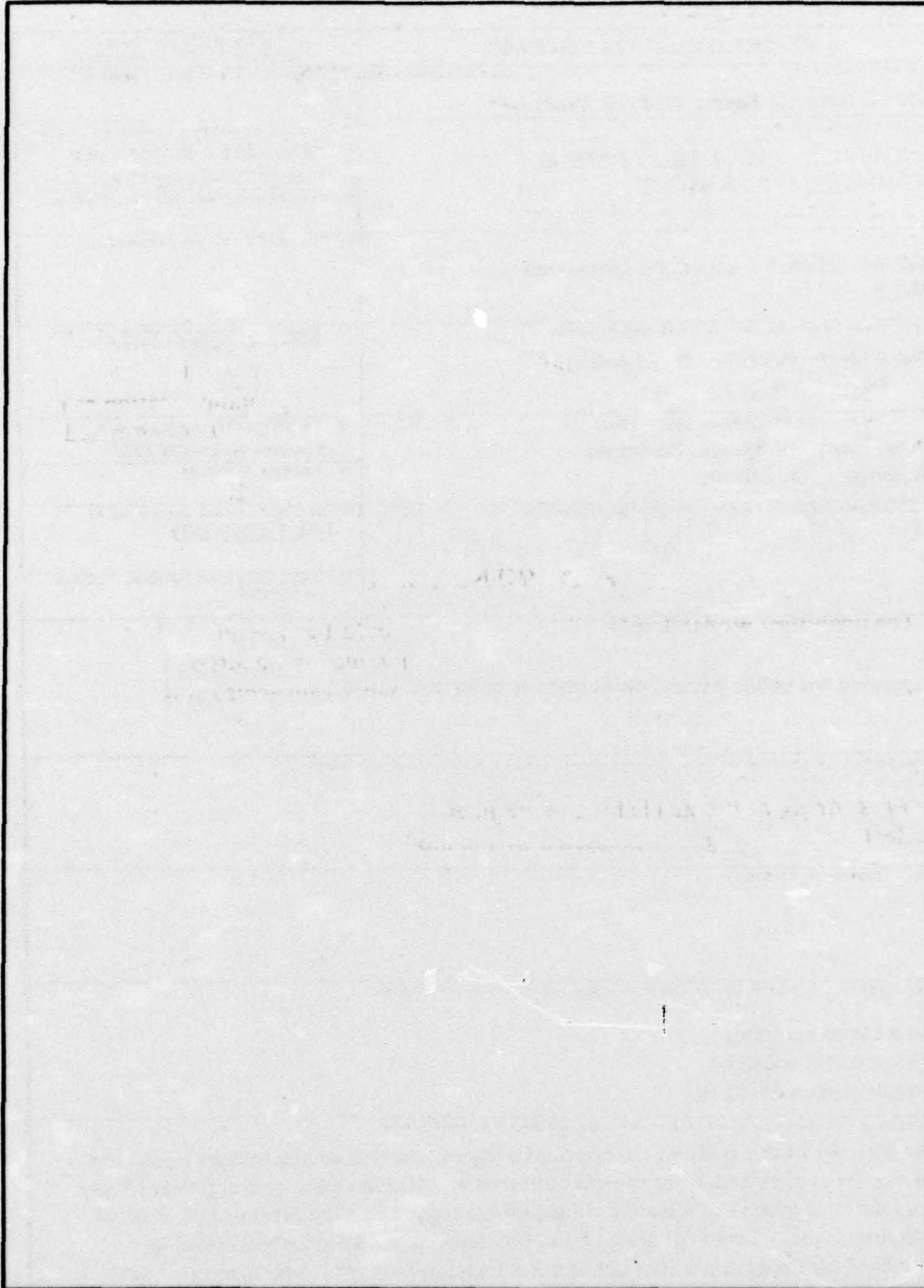
DD FORM 1473 1 JAN 73 EDITION OF 1 NOV 65 IS OBSOLETE

UNCLASSIFIED
SECURITY CLASSIFICATION OF THIS PAGE (When Data Entered)

403940
LB

UNCLASSIFIED

SECURITY CLASSIFICATION OF THIS PAGE(When Data Entered)



UNCLASSIFIED

SECURITY CLASSIFICATION OF THIS PAGE(When Data Entered)

OBJECTIVE

Investigate the potential and suitability of optical communication links with anti-jam and anti-intercept capabilities for task force/group operations at greater than line-of-sight ranges. Specifically, perform a tradeoff analysis among systems parameters for two types of extended line-of-sight optical communications links; optical forward scatter from the atmosphere and remotely piloted vehicle relay links.

CONCLUSIONS

Based upon the analytical model developed for over-the-horizon optical propagation and a systems tradeoff analysis, the following conclusions were drawn: the operating data links can use the same shipboard system; significant performance advantages can be achieved by exploiting decreasing aerosol concentrations with elevation; the primary factor which determines communication-link availability at a given range and data rate is meteorological visibility and, based upon statistical studies of visibility, communication ranges for bit rates of 2400 bits per second and for rates of 75 bits per second were determined for availabilities of both 85 and 70 percent. The communication ranges are considerably greater at night or when low clouds occur to provide a scattering layer.

RECOMMENDATIONS

The analytical model developed in this study should be experimentally tested to assess its validity. Simultaneous pulsed laser propagation measurements at two wavelengths (1.06 and 0.53 μm) should be conducted. The performance gain achieved by the use of elevated beams and exploitation of clouds should be evaluated. Fading rate and other data should be obtained to allow evaluation of time, spatial, and receive angle diversity receiver techniques.

It is strongly recommended that experiments be conducted to verify the meteorological effects upon propagation predicted by the models. An integrated and systematic capability for measuring and predicting the meteorological conditions predominating over the path should be developed.

ASSIGNMENT NO.	
NTIS	White Section <input checked="" type="checkbox"/>
DOC	Blue Section <input type="checkbox"/>
IDENTIFICATION	
DISTRIBUTION AVAILABILITY CODES	
Dist.	AVAIL. CONTROL
A	

ACKNOWLEDGMENT

The mathematical model and system tradeoff analysis used in this report were formulated and reported by VJ Adrian, PH Levine, and WR Stone of Megatek, Inc, under contract N00123-75-C-0328, task MEG-TA-039. This document was approved 4 November 1976 for publication with the present distribution statement.

CONTENTS

	PAGE
SECTION 1. INTRODUCTION	7
Objectives	7
Scope	8
Plan of Report	8
SECTION 2. GENERAL REQUIREMENTS	9
SECTION 3. SYSTEM CONCEPTS AND PERFORMANCE SUMMARY	9
System Types	9
Acquisition	11
Communication Rates	13
State-of-the-Art System Performance	13
SECTION 4. SIGNAL MODEM CONSIDERATIONS	18
Noise Statistics and Signal-to-Noise Ratio	18
Modulation	20
IFF	21
Communication Rate	23
SECTION 5. LINK ANALYSIS	24
Transmission Loss	24
Background Noise	32
Link S/N Ratios	37
Link Availability	46
SECTION 6. COMPONENTS AND SUBSYSTEMS	53
Lasers	53
Optical Filters	56
Photodetectors	60
Pointing and Tracking Systems	64
Remotely Piloted Vehicles	65
SECTION 7. TRADEOFF CONSIDERATIONS	70
SECTION 8. COVERT CONSIDERATIONS	71
SECTION 9. CONCLUSIONS AND RECOMMENDATIONS	72
Conclusions	72
Recommendations	73
APPENDIX A : INCORPORATION OF THE PROPAGATION MODELS IN THE COMPUTER PROGRAMS	75
APPENDIX B : OTH PROGRAM DESCRIPTION	78
APPENDIX C : LOS PROGRAM DESCRIPTION	89
APPENDIX D : REFERENCES	99
APPENDIX E : PROPAGATION MODEL FOR A LASER-TYPE BEYOND- THE-HORIZON COMMUNICATIONS LINK	101

ILLUSTRATIONS

		PAGE
1.	Error probability versus normalized noise energy, K, for fixed values of $S/N = N^2/N+K$, M-2 (ref 6)	19
2.	Probability of detection versus S/N ratio	21
3.	Probability of random events with Poisson distribution (courtesy RCA) (ref 8)	22
4.	Water-vapor concentration as a function of temperature and relative humidity (ref 13)	26
5.	Infrared absorption loss	26
6.	Beyond-the-horizon propagation mechanisms (cloud-free case)	27
7.	Path loss, pencil beam	29
8.	Path loss, 4-degree fan beam	29
9.	Path loss at 1.06 μm , scatter link	30
10.	Path loss, line-of-sight link	31
11.	Path loss as a function of range at 1.06 μm	32
12.	Spectral distribution curves related to the sun; shaded areas indicate absorption, at sea level, due to the atmospheric constituents shown (ref 13)	35
13.	Solar spectral irradiance curves at sea level for various optical air masses; the value of the solar constant used in this calculation was 1322 W m^{-2} (ref 13)	35
14.	Day sky background data (ref 15)	36
15.	Night sky background data (ref 15)	36
16.	S/N for pencil beam, V = 10 kilometres	40
17.	S/N for pencil beam, V = 20 kilometres	40
18.	S/N for pencil beam, V = 50 kilometres	41
19.	S/N for fan beam, V = 50 kilometres	41
20.	Forward-scattering function, water haze, M	43
21.	Forward-scattering function, water cloud, C	43
22.	S/N for 1.06 μm	44
23.	Effect of launch angle on S/N	45
24.	S/N for active link, RPV altitude = 2.5 km	47
25.	S/N for active link, RPV altitude = 2.5 km, visibility = 20 km	47
26.	Percent time visibility 5 nautical miles, North Atlantic, July (courtesy McDonnell Douglas) (ref 16)	49
27.	Percent time visibility 5 nautical miles, North Atlantic, January (courtesy McDonnell Douglas) (ref 16)	49

ILLUSTRATIONS (Continued)

	PAGE
28. Percent time visibility 5 nautical miles, North Pacific, January (courtesy McDonnell Douglas) (ref 16)	50
29. Percent time visibility 5 nautical miles, North Pacific, June (courtesy McDonnell Douglas) (ref 16)	50
30. Percent frequency low cloud amount 6/10 or more, North Atlantic, January (courtesy McDonnell Douglas) (ref 16)	51
31. Percent frequency low cloud amount 6/10 or more, North Atlantic, July (courtesy McDonnell Douglas) (ref 16)	51
32. Percent frequency low cloud amount 6/10 or more, North Pacific, January (courtesy McDonnell Douglas) (ref 16)	52
33. Percent frequency low cloud amount 6/10 or more, North Pacific, July (courtesy McDonnell Douglas) (ref 16)	52
34. Interference filter	56
35. Shift of center wavelength of typical interference filters with angle of incidence	57
36. Filter optical passband as a function of the optical wavelength (ref 25)	59
37. UV-visible photoemitter characteristics (courtesy RCA) (ref 8)	59
38. Visible photoemitter characteristics (courtesy RCA) (ref 8)	61
39. Near infrared-visible photoemitter characteristics (courtesy RCA) (ref 8)	61
40. Wavelength dependence of quantum efficiency and responsivity for several high-speed photodiodes (ref 28)	64
41. Minimum platform altitude required to achieve line-of-sight.	65

TABLES

	PAGE
1. 1.06- μm shipboard system parameters	14
2. RPV terminal	15
3. Performance prediction, daytime	16
4. Performance prediction, night	16
5. Information rate	23
6. Time dispersion	38
7. Nominal system parameters	42
8. Pulse laser	54
9. Continuous-wave lasers	55
10. Characteristics of avalanche photodiodes	63
11. Current small RPV programs	67
12. Effect of component parameters on S/N of a specific system	71

SECTION 1. INTRODUCTION

The wide dispersal of elements of a modern task force requires coordinated intra-element, real-time communications. At present, the Fleet cannot operate with positive Command Control, and Communications (C³) without making itself vulnerable to enemy detection and countermeasures. The Naval Telecommunications Architect has stipulated that the post-1985 Naval Telecommunications System must have survivability equal to the forces served in the face of both physical and electromagnetic attack. It is planned that this goal will be achieved through media diversification and anti-jam, low-probability-of-intercept (AJ/LPI) capabilities. For intra task force (group) netting, hf systems with AJ/LPI capabilities have been specified as the prime service, but hf will require considerable augmentation to accomplish the full capability needed for the Naval Tactical System (NTS).

Optical systems are strong candidates for this augmentation role for a number of reasons. These include reduced susceptibility to jamming, intercept, spoofing, and direction finding; a reduction in spectrum crowding; and potentially high data rates. Optical links also have potential limitations including meteorological effects, multiplatform transmissions, and range limitations imposed by the horizon.

The true potential of electro-optic communications systems needs to be better defined in order to determine its proper future (1985 era) use in the NTS intra-task group application. This use is to be scoped in relation to other candidate future systems such as hf and JTIDS (Joint Tactical Information Data System). Systems concept engineering is needed, as is more extensive data on performance capabilities and limitations. The candidate concepts are being explored in a variety of projects within the electro-optical communications program at NELC. The particular aspect addressed by "Extended Line-of-Sight Optical Communications System Exploratory Development" is to examine and demonstrate the feasibility for maintaining optical links to distances well beyond the horizon. This report represents a theoretical analysis of the concept of optical communications to beyond line-of-sight ranges.

OBJECTIVES

The primary objective of this study was to carry out a tradeoff analysis among system parameters for two types of beyond line-of-sight optical communication links: Forward Scatter Channel and Remotely Piloted Vehicle (RPV) Relay. The general application of such communications links is for the control of dispersed task force units.

The tradeoff study for the forward-scatter channel originally intended to use available scatter models. However, discrepancies were noted between the models and data. This type of discrepancy was particularly apparent in the observed small spot size on the horizon compared to the large diffuse illumination predicted by many models.¹ Thus, an added objective was to generate a forward-scatter model which would allow for realistic engineering estimates of scattered power at ranges beyond the horizon.

¹ Naval Research Laboratory Report 6152, *Experimental Observations of Forward Scattering of Light in the Lower Atmosphere*, by JA Curcio and LF Drummer, Jr, 30 September 1964

SCOPE

The tradeoff study was broadly divided into two parts: analysis of the optical channel, or link analysis, and equipment-dependent factors. The link analysis, embodying consideration of background noise and transmission loss, is more complex analytically and is presented in a form such that it usually need not be repeated for a change in system parameters. The results of the link analysis are presented as signal-to-noise ratios (S/N) for a group of nominal system parameters. The resulting S/N for a change in a parameter, eg radiated power, can usually be rapidly determined.

A forward scatter propagation model which appears consistent with previous field data was generated.² The model also revealed novel strategies for reducing path loss, eg, the use of vertical fan beams and the use of an optimum elevation angle for pencil beams. This model was used for the scatter channel path loss computations. The scatter link analysis predicted that the near infrared (IR) wavelength would provide the best performance. Consideration of state of the art sources and detectors indicates that 1.06 microns is the preferred wavelength. Therefore, the most complete data for both communication links are presented for that wavelength. Complete link and equipment analysis at all wavelengths would be prohibitive. However, since the final definition of an over-the-horizon system or systems is likely to be an iterative analytical and experimental process, computer programs were generated to provide additional data beyond those presented in this report. The programs were designed for ease of altering channel parameters.

Characteristics of various optical system components and possible tradeoffs are discussed. Emphasis is on the near IR but some discussion is included for ultraviolet through IR wavelengths. A discussion of modern techniques and required S/N is included.

An attempt has been made to include information which might be of use as design concepts change, since this is apt to happen in any new technology. Thus, besides discussing the system concepts presented, additional information of the design handbook type has been included.

PLAN OF REPORT

The general system performance requirements are given in section 2. Section 3 discusses the concepts for the two over-the-horizon links and summarizes the system parameters and expected performance. Section 4 discusses signal modems and S/N requirements for system acquisition. Communication data rates are also considered.

Transmission loss data for both link types are given in section 5. This is combined with background radiation to provide predicted S/N for nominal system parameters. The data presented in section 5 are based on models and computer programs described in detail in the appendixes.

The characteristics of various system components such as lasers, optical filters, and detectors are given in section 6. Tradeoffs between the component parameters are discussed briefly in section 7. Covert and antijamming factors are briefly considered in section 8. Section 9 presents conclusions and recommendations; the more detailed summary is presented in section 3.

²Megatek Report R2005-039-IF-1, *Propagation Model for a Laser-Type Beyond-the-Horizon Communications Link*, by PH Levine, 15 December 1975

SECTION 2. GENERAL REQUIREMENTS

The main use of an over-the-horizon optical link would be to communicate between naval task groups. Communication within a group would generally be on a line-of-sight basis, although slightly extended line-of-sight might be considered within a group for increased dispersal. The range of interest for the links is 25 to 150 nautical miles.

The present Navy Tactical Data System (NTDS) typically uses a rate of 2400 bits per second. This, then, becomes the desired information rate for the system. There are other tactical requirements which can be satisfied with a rate of 75 bits per second. A high degree of jamming and intercept protection is expected, and a general requirement is for the system to be much less susceptible to interference and intercept than high-frequency radio systems. In summary, the requirements are:

Range:	25 to 150 nautical miles
Data Rate:	75 bits per second (minimum) 2400 bits per second (desired)
Covertness:	High anti-jamming margin Low probability of intercept

SECTION 3. SYSTEM CONCEPTS AND PERFORMANCE SUMMARY

This section discusses the concepts for two over-the-horizon (OTH) optical communications links. Modulation and detection considerations are summarized. Link acquisition and communication data rates are discussed. Finally, systems composed of state-of-the-art components and subsystems are defined, and performance predictions are given for each type of link.

SYSTEM TYPES

LINKS

Two different types of OTH optical communications systems are considered. They are: Forward-Scatter Channel and Active RPV Relay. The forward-scatter system makes use of scattering from atmospheric "haze" and aerosols and does not depend upon the presence of clouds. If clouds were present, scatter from them could often be used, depending upon their altitude.

An active relay would receive an optical line-of-sight signal from one ship, would demodulate the signal, and would use it to modulate a laser on the RPV. Thus, an optical receiver and transmitter and a pointing system would be located on the RPV. A power source would be required for the transmitter, receiver, and pointing system.

Both links would use high-power shipboard transmitters with pointing and tracking systems. The receiver would be boresighted to the transmitter for use with the relay link but might be capable of pointing and tracking independently for the scatter channel.

A particular Fleet application might use any one or a combination of links. For example, for a certain ship spacing, a scatter channel might be used at night and during high-visibility daytime conditions. If the visibility began to decrease, as indicated by a decrease in signal level, an RPV could be launched.

HETERODYNE VERSUS DIRECT DETECTION

Heterodyne, or coherent, optical detection systems have been developed at $10.6\ \mu\text{m}$ which approach theoretical sensitivity limits very closely. At $10.6\ \mu\text{m}$, a heterodyne system is about 40 dB more sensitive than a direct-detection receiver limited by 300°K background sources which peak out at $10\ \mu\text{m}$. However, at wavelengths shorter than about $1.1\ \mu\text{m}$, detectors are available with low noise internal gain which give dramatic improvement in direct detection, as compared to available direct detectors at $10\ \mu\text{m}$. In addition, both practical problems and inherent limitations in coherent detection, especially relative to a scatter channel, are compounded at shorter wavelengths. For the reasons discussed here, a direct detection system is assumed (wavelength less than $1.1\ \mu\text{m}$).

The receiving aperture and the field of view in a heterodyne receiver are not independent, but are related by the approximate relation.³

$$A \Omega_r = \lambda^2,$$

or
$$A \frac{\pi}{4} \theta_r^2 = \lambda^2$$

where

A = receiving aperture,

Ω_r = solid angle field of view,

θ_r = plane angle field of view, and

λ = wavelength.

Note that for a fixed field of view, the aperture area varies as the square of the wavelength. For a field of view (FOV) of 1 degree, such as might be used in a scatter channel, the maximum aperture at $1\ \mu\text{m}$ is about 4×10^9 square metres. Even for a FOV of 0.1 degree, which might be used in a line-of-sight (LOS) link, the aperture area is about 4×10^{-7} square metres. A direct-detection receiver does not have to satisfy the coherence requirement and may have a large aperture.

Spatial coherence is degraded due to atmospheric turbulence; ⁴ the coherence diameter varies as $\lambda^{6/5}$. Thus, turbulence is more of a problem at short wavelengths. The coherence properties of the scatter-channel field have not been analyzed but it is expected that coherence would be lower at shorter wavelengths.

Heterodyne systems are more complex, in that a very stable local oscillator is required (this may be the unmodulated transmitter source for a homodyne system). There are also stringent alignment tolerances required to keep the signal and local oscillator in phase over the detector surface.

³Siegman, AE, The Antenna Properties of Optical Heterodyne Receivers, *Proceedings of the IEEE*, v 54, p 1350 to 1356, 1966

⁴Pratt, WK, *Laser Communications Systems*, John Wiley & Sons, 1969

Based upon the above factors and the fact that the path loss is excessive at $10.6 \mu\text{m}$, a direct-detection system is assumed throughout this report. If the atmospheric window at $3.8 \mu\text{m}$ becomes available through the development of new lasers in the future, heterodyne receivers should be considered.

MODULATION

For a direct-detection system, short, high-power pulses enhance the ability of a receiver to discriminate against a fixed background by allowing time gating. The signal-to-noise ratio (S/N) expression given in section 4 shows the advantage quantitatively. As will be discussed in section 5, shortening the pulse much below the time dispersion in a scatter channel does not continue to improve the S/N. However, on a LOS link, it appears that the pulse duration (constant energy) should be as short as practical.

The use of pulse modulation has a number of potentially practical features. The space between pulses can be monitored for interference on any of the link types. The pulses can be used in a light-detection-and-ranging (LIDAR) system for possible detection of approaching missiles, or for monitoring the location of an RPV.

Some types of pulse modulation and expected data rates are discussed in section 4. Pulse-modulation systems have generally been assumed throughout the report, although many results (eg, path loss) apply independent of equipment types. Pulse rates of about 200 pulses per second (pps) are required for a data rate of 2400 bits per second.

Polarization and intensity modulation appear possible for the relay link. Phase modulation should also be possible but could not be detected with a non-heterodyne system. Pulse-rate requirements for a pulsed interrogation beam are discussed in section 4. A minimum rate of 480 pps would be required for a data rate of 2400 bits per second assuming a 15-dB S/N (5 bits per pulse).

ACQUISITION

FORWARD-SCATTER LINK

An acquisition subsystem similar to that used in the OCCULT system is assumed for the forward-scatter link. The pointing system on all ships would rotate continuously and synchronously through 360 degrees of azimuth. A ship initiating acquisition would flip the transmitting beam 180 degrees in azimuth and begin transmitting with a 4 degree vertical fan beam. Because of the synchronous rotation, the receiver FOV of another ship would be pointing at the transmitting ship at the time the beam swept the ship.

The single scattering out of the beam will appear to the receiver as an approximately vertical line source (see appendix E). The forward scatter is peaked in the forward direction but has some angular width, so that the line (starting at the horizon) can be "seen" over several degrees of azimuth. Assume a horizontal FOV, θ_h , for the receiver. The FOV of a single receiver will be limited to about 4 degrees by the interference filter constraints (assume

1A width; see section 6). The receiver would see the line source a fraction, $0.5\theta_h/360^\circ$, of a rotation of the acquisition system. The number of pulses, N_p , entering the receiver would be:

$$N_p = \frac{\theta_h R}{720A},$$

where

θ_h = horizontal field of view in degrees,

A = Azimuthal scan rate – revolutions per second, and

R = Pulse repetition rate – pulses per second.

As an example to indicate approximate scan rates, consider a 4 degree horizontal FOV ($\theta_h = 4^\circ$) and require 4 pulses to occur within the receiver FOV. A range of acquisition-response criteria could then be used. For normal operations, a single detected pulse might initiate a response, while a "quiet" ship might require four pulses, or even more than one group of four pulses, at the proper time interval, before triggering a response. Reference curves useful for determining detection probability and false alarm probability tradeoffs are given in section 4. When more than one pulse is detected, the "center of gravity" direction would be used for the transmitted response. If the laser was operated at the 200 pps nominal rate required for communication at 2400 bits per second, the azimuthal scan period would be 3.6 seconds per revolution. Normally, up to 2 revolutions (7.2 seconds) would be required for azimuthal acquisition.

After azimuthal acquisition, the first ship could switch from a fan beam to a pencil beam and scan the transmit beam in elevation. The received signal level at the second ship would be fed back to the first ship to enable it to select the optimum beam elevation. The second ship would then go through the same procedure to complete acquisition.

The S/N required for acquisition depends on the identification friend or foe (IFF) code and probability requirements. As discussed in section 4, 15-dB S/N should cover most IFF requirements. Many of the S/N curves in this report are for a FOV of 1 degree, while the example assumes a FOV of 4 degrees. Increasing the vertical FOV increases both the received energy and the received background noise. As is discussed in section 5, the S/N increases with increased vertical FOV until the time dispersion is about equal to the pulse duration and there remains constant if the receiver electrical bandwidth is adjusted correctly. For typical pulse lengths (0.02 μ sec) at 1.06 micrometres, the S/N does not generally improve for an elevation FOV greater than 1 degree. Increasing the horizontal FOV from 1 to 4 degrees increases the background noise by 6 dB. The energy for a single pulse is not increased as it was for a vertical FOV. Four pulses are received and filter techniques, such as summing the pulses by use of a tapped delay line, can produce essentially the same S/N as for a FOV of 1 degree. However, it would probably be easier to use a FOV of 1 degree when a single-pulse detection criterion is used. When a 4-pulse IFF code with a 15-dB S/N requirement is used, the 21-dB S/N level on a FOV curve of 1 degree would be used for coverage prediction.

The S/N and resulting IFF detection can be enhanced at the expense of acquisition time. Rather than the example given above, assume a FOV of 1 degree with a resulting 6-dB lower noise level. If the azimuthal scan rate is reduced by a factor of 4, 4 pulses will occur within the receiver FOV. Increasing the pulse-repetition rate does not improve the detection since the laser has an average power limitation so that the peak power is reduced.

If approximate ship locations are known from a previous acquisition or by other means, the acquisition transmission could be applied to a restricted azimuthal region. This would reduce the probability of intercept. If the pointing systems on both ships were restricted in azimuth, the acquisition time could be reduced.

RPV RELAY LINK

The acquisition technique for an RPV relay link would be very similar to that described for the scatter link. The launch ship would activate an azimuthal scan with a vertical fan beam on the RPV when it was at a sufficiently high altitude. Figure 25 in section 5 shows that a beam divergence of 1.8 degrees would provide a range capability of a full (150 nautical miles (RPV at midpoint) for a visibility of 20 kilometres. The fan beam would be approximately 7 degrees by 0.25 degree. Requirements of from 1 to 4 pulses for acquisition result in 4 by 360 to 16 by 360 pulses per azimuthal scan. Use of a rate of 200 pps gives a scan time of between 7.2 and 29 seconds. If the launch ship were to know the approximate location of the other ship, the RPV transmissions could be restricted in azimuth to minimize the probability of intercept and to conserve energy.

COMMUNICATION RATES

The communication rate for a pulse-position modulation system is discussed in section 4. It is shown that a rate of 12 bits per pulse is not far from the theoretical information rate when pulse-time dispersion (for the scatter link) is taken into account.

A data rate of 2400 bits per second requires a 200-pps rate using 12-bit words. For a data rate of 75 bits per second, 12-bit words would still be used and the pulse rate would be reduced. The reduction in pulse rate would be converted into a higher peak-pulse power with a resultant extension in operating range.

STATE-OF-THE-ART SYSTEM PERFORMANCE

SYSTEM PARAMETERS

The link analysis given in section 5 clearly shows the advantage of the near infrared for both a forward-scatter and a LOS optical system. Consideration of the state of the art in laser sources and detectors shows that 1.06 micrometres is the preferred wavelength.

In this section, we consider systems operating at 1.06 micrometres and maximize all system parameters, consistent with available components as discussed in section 6. The parameters for the systems defined in this section differ from the nominal system parameters used in section 5. The nominal system parameters (section 5) were selected to be somewhat typical of a large span of wavelengths and were chosen to be powers of 10 where reasonable.

The system concept synthesized in this study uses the same shipboard equipment for both data links, but with different operating parameters, as indicated in table 1. Most of the parameters are based upon components listed in section 6. Significant advances currently being made in the development of plastic optics, are not discussed in this report.

TABLE 1. 1.06- μm SHIPBOARD SYSTEM PARAMETERS.

Parameter	Constant	Scatter Link			Active RPV	
		Acqui- sition	75 b/s	2400 b/s	Acqui- sition	2400 b/s
Transmitter						
Radiated peak power (MW)		40	1280 ***	40	40	40
Pulse rate (pps)		200	25 ***	200	200	200
Beam divergence (mrad)		1° beam or 4° fan	1.5	1.5	1.5	1.5
Pulse width (μsec)	0.015					
Receiver						
Field of view (deg)		1°	1°	1°	7° X ¼° fan	2°
Aperture area (m^2)	0.2					
Optical bandwidth (μm)	10^{-4}					
Detector responsivity (amp/watt)	0.018					
Gain	*					
Dark current (amp)	10^{-13}					
Electrical bandwidth (Hz)		**	**	**	7×10^7	7×10^7

Notes:

*Photomultiplier gain sufficient to give dark current (or background) limited operation.

**Bandwidth adjusted to be equal to the inverse of the received pulse duration at planned maximum range.

***See text.

However, the use of plastics is expected to reduce large-aperture costs from a few thousand to between ten and a few hundred dollars. A 50.8 cm diameter aperture (0.2 m^2) is assumed for the system.

The Nd: YAG laser is assumed to have 120 watts average power, and a tradeoff between pulse rate and peak power is made for different operating conditions. The tradeoff to 1280 megawatts (6 pps), listed for a data rate of 75 bits per second, may be impractical. However, if it cannot be achieved, it is expected that receiver techniques which average over many pulse intervals may produce similar effects on S/N.

A beam divergence of 1.5 milliradians (mrad) is listed for data transmission on the links. The divergence is not critical on the scatter link as long as it is less than about 17 mrad (1 degree). In the scatter link performance prediction, it is assumed that the beam is pointing at the optimum elevation angle.

The shipboard transmitter parameters for the active RPV link are listed as being the same as for the scatter link. This represents much more power than required for the uplink. The power would normally be reduced to a value just sufficient for satisfactory communications, in order to reduce the probability of intercept. The shipboard receiver also uses a vertical fan-shaped FOV for link acquisition.

The general characteristics of an active RPV terminal used for this performance prediction are listed in table 2. The only vehicle parameter used explicitly in the performance prediction is the altitude. The other parameters, listed for convenience, give the expected capability over the next few years (see section 6 for a discussion of RPVs).

TABLE 2. RPV TERMINAL.

Parameter	Value
Remotely Piloted Vehicle	
Altitude	2.5 km
Loiter time	6 hours
Payload	50 pounds
Transmitter	
Radiated power	1 MW
Pulse rate	200 pps
Beam divergence:	
narrow beam	1 mrad
wide beam	1.8°

The ship-to-RPV link is not explicitly considered here since the range with fairly simple receivers exceeds the down-link range. Two different examples of beam divergence are considered for the active RPV transmitter. The wide-beam case (1.8°) will provide less coverage but will greatly simplify the pointing system.

PERFORMANCE

Table 3 gives the performance predictions for daytime background and 2 visibility values. The contour maps in section 5 show that 10-km visibility is typically available about 85 percent of the time. Data indicate that a 20-km visibility would be available about 70 percent of the time. The link availability neglects the presence of clouds which can either degrade or enhance a channel as discussed in section 5.

A 15-dB S/N is taken as the requirement for data communications. This S/N should provide low error rates but includes little margin for signal fading.

The channel acquisition is based on acceptance of a single pulse with a 15-dB S/N. If IFF codes are used to minimize false alarms, the acquisition times will be increased over those listed in the table. For the forward-scatter link, the use of a pencil beam of 1 degree and a fan beam of 4 degrees are considered. The estimate for the fan beam is conservative relative to that of the pencil beam since it assumed that only the energy at the best 1-degree elevator segment is used. In reality, other portions of the beam will contribute energy, but then pulse time dispersion effects must be included. Other tradeoffs between acquisition time and range are possible, and this area should receive additional attention.

TABLE 3. PERFORMANCE PREDICTION, DAYTIME.

Link Type	Visibility = 20 km (Availability \cong 70%)			Visibility = 10 km (Availability \cong 85%)		
	Acquisition		Communication Range (km)	Acquisition		Communication Range (km)
	Range (km)	Time		Range	Time	
<u>Forward Scatter</u>						
Pencil beam	50	32 sec	100	55	32 sec	85
4° fan	45	8 sec		50	8 sec	
<u>Active RPV</u>						
Narrow beam		165*	440			290
Wide beam (1.80)				300		
Fan beam	300	8 sec		210	8 sec	

*Takes into account loss due to time dispersion (section 5), effects negligible at other ranges.

TABLE 4. PERFORMANCE PREDICTION, NIGHT.

Link Type	Visibility = 20 km (Availability \cong 70%)			Visibility = 10 km (Availability \cong 85%)		
	Acquisition		Communication Range (km)	Acquisition		Communication Range (km)
	Range (km)	Time		Range	Time	
<u>Forward Scatter</u>						
Pencil beam	100	32 sec	200*	48	32 sec	140*
4° fan	88	8 sec		44	8 sec	
<u>Active RPV</u>						
Narrow beam		300*	500			340
Wide beam				400		
Fan beam	400	8 sec		300	8 sec	

*Takes into account loss due to dispersion, effect negligible at other ranges.

It is noted that an active relay channel provides the full 150-nmi communication coverage with an 85-percent availability. The scatter link gives a 100-km communication range with 70-percent availability. This range can be extended to 165 km by reducing the data rate to 75 bits per second.

Table 4 shows that considerably better performance is provided at night. The scatter link can provide a data rate of 75 bits per second over the 150-nmi range.

SECTION 4. SIGNAL MODEM CONSIDERATIONS

The purpose of this section is to describe general considerations for IFF and communication signal design, and to establish signal-to-noise ratio requirements. Some examples are given, but the final design and specification of parameters will depend upon the specific Fleet application. As discussed earlier, the emphasis is on pulse-modulation systems. Information is presented on IFF design to allow for tradeoffs between false-alarm and detection probabilities. The effect on S/N of several system parameters are considered.

NOISE STATISTICS AND SIGNAL-TO-NOISE RATIO

Photodetection is most correctly analyzed as a Laquerre counting process.⁵ However, under most conditions of interest, Poisson statistics apply and the Poisson detection process has been analyzed in some detail.⁶

Following Karp, the average number of electrons produced by a received optical pulse of peak power P_c and duration T is given by

$$K_S = \eta P_c T / h\nu,$$

where η is the photodetector quantum efficiency, ν is the optical frequency, and h is Planck's constant. Similarly, the number of electrons produced by background radiation in a time T is given by

$$K_N = \eta P_b T / h\nu,$$

where P_b is the received background average power. Note that K_N is proportional to T for a constant background, so that the use of short pulses and corresponding short signal intervals decreases the amount of interfering radiation.

The number of electrons "counted" in a time slot that contains the signal, is a Poisson-distributed random variable with mean $K_N + K_S$, and the number of electrons counted in a slot containing only noise is a Poisson random variable with mean K_N . The ratio of the square of the electron count (ie square of detector current), when no noise is present, to the *variance* of the count, when noise is present, has many of the characteristics of a S/N and is usually referred to in this way. For Poisson statistics this becomes:

$$S/N = K_S^2 / (K_S + K_N).$$

The error probability for Poisson statistics depends upon both signal and noise energy, and not upon merely their ratio. An example of an error probability curve is shown in figure 1. It is noted that the error probability approaches the familiar Gaussian case for a large background count. It appears that the familiar Gaussian statistics can be used for daytime

⁵ Gagliardi, RM, "The Effect of Timing Errors in Optical Digital Systems," *IEEE Transactions on Communication Technology*, COM-20, p 87 to 93, 1972

⁶ Gagliardi, RM and S, Karp. "M-ary Poisson Detection and Optical Communications," *IEEE Transactions on Communication Technology*, COM-17, p 208 to 216, 1969

background conditions while the more precise Poisson statistics would apply at night. Since a system would generally be designed for worst-case conditions, the emphasis is on Gaussian statistics.

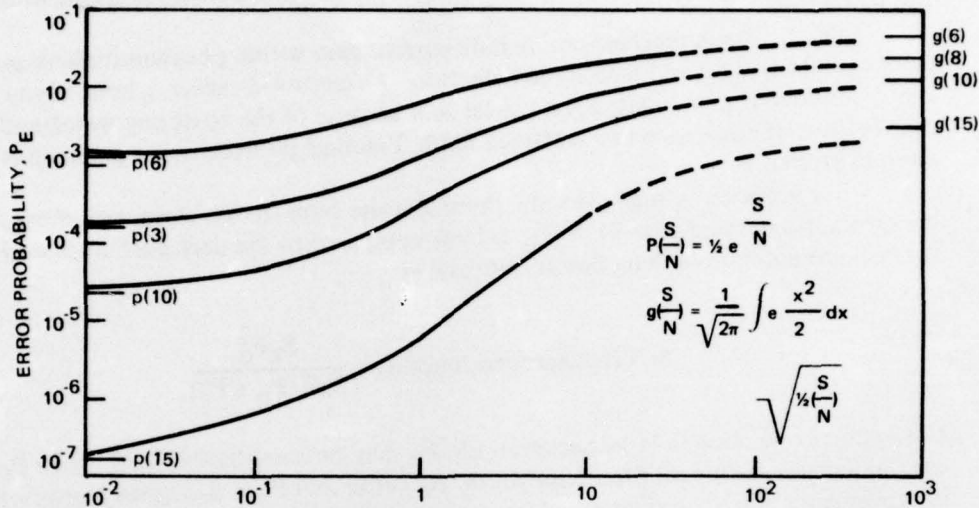


Figure 1. Error probability versus normalized noise-energy, K , for fixed values of $S/N = N^2/N + K$, $M=2$ (courtesy IEEE) (ref 6).

The S/N expression can be cast in more useful engineering terms by noting that the signal photocurrent, I_c , is the product of the electron charge, q , and the number of photons per unit time. The current may also be expressed as the product of the detector responsivity, S_d , (ampere per watt) and the incident power or,

$$I_c = (nq/h\nu)P_c = S_d P_c.$$

A similar expression holds for the background current. Consider a photodetector with internal current gain G , feeding an amplifier presenting a load, R_L . It can be shown⁵ that

$$S/N = \frac{S_d^2 P_c^2 G^2}{2qB (S_d(P_b + P_c) + I_d) G^2 + 4kTB/R_L}$$

where

- S_d is the detector responsivity (ampere/watt),
- q is the electronic charge (coloumbs),
- P_c is the receiver carrier power (watts),
- B is the electrical bandwidth of the system (hertz),
- P_b is the background power incident on the detector (watts),
- I_d is the detector dark current (amperes),
- k is Boltzmann's constant (joules/K),
- T is the thermal noise temperature (K), and
- R_L is the load resistance (ohms).

For practical amplifiers, T will be greater than the ambient temperature. This expression, neglecting the thermal noise term (second term in the denominator), is used in the link analysis given in section 5. For sufficiently high gain G , the S/N is independent of the thermal noise.

Practical gain mechanisms include current gain within photomultipliers and avalanche photodiodes and heterodyne detection. As discussed earlier, a heterodyne system is not considered a candidate for a scatter link because of the operating wavelength and possible loss of coherence in a scattered field. Practical photodetector parameters are given in section 6.

For sufficiently high gain, the thermal noise term can be neglected. When the background-generated current, $S_d P_b$, is large compared to the dark current, the expression for background-limited detection is obtained as

$$S/N \text{ (background limited)} = \frac{S_d P_c^2}{2qB (P_b + P_c)}$$

For systems operating in large backgrounds, P_b may be considerably larger than P_c . In this case, a decrease in optical filter bandwidth, B_o (note that $P_b \propto B_o$), gives a proportional improvement in S/N : reduction of bandwidth by a factor of 2 improves S/N by 3 dB. (A reduction in the electrical bandwidth, B , has the same effect, but B must be wide enough to respond to the pulse envelope.) An increase of 2 in S_d (or quantum efficiency) improves S/N by 3 dB. The S/N is increased 6 dB by a doubling of transmitter power (or P_c), rather than 3 dB as might be expected intuitively. A doubling of the receiving antenna aperture doubles both P_c and P_b and thus increases P_c^2/P_b by 3 dB.

The S/N expression indicates that it is advantageous to concentrate the laser pulse energy in a short pulse in order to obtain high peak power. Cutting the duration in half gives a 3-dB S/N advantage, since P_c^2 is increased 6 dB while the noise is increased 3 dB, due to a doubling of the required electrical bandwidth, B . Pulse lengthening due to propagation time dispersion will limit this improvement.

MODULATION

Pulse modulation has been assumed for both the scatter and active RPV links. Common types of pulse systems are pulse amplitude, pulse position (PPM), and pulse internal (PIM) modulation. Because of possible amplitude fluctuations in the scatter link, and primarily because of the low pulse rate (for high peak power), pulse-amplitude modulation is not considered for the active links. Pulse-position modulation requires accurate synchronization (for example, by the use of precision frequency standards) but has some advantage over PIM in S/N and covertness, in both communications and IFF.

Pulse-time dispersion will limit the width of independent or orthogonal intervals for both PPM and PIM. For a scatter link, the time dispersion can be as large as 2 microseconds (table 5) for a fan beam and a field of view of 4 degrees. However, for likely system parameters the dispersion should be considerably less than 0.5 microsecond, and this value will generally be considered for the independent interval.

IFF

IFF coding tradeoffs between false-alarm rates and probability of detection will vary with Fleet vehicles and tactics. For example, a submarine wants to have a very low probability of being triggered into an unnecessary transmission. False-alarm probability changes very rapidly with S/N so that a reasonable example establishes the approximate S/N requirement.

An example of an IFF code consisting of three pulses has been analyzed⁷. The required S/N, for a false alarm rate of 0.5 per hour with a detection probability of 0.99, was calculated for a range of pulse rates from 10 to 200 pps, and from 1 to 4096 time-code intervals per pulse. A S/N of 12 to 13.5 dB covered the range. A 15-dB S/N appears to be a conservative requirement.

Curves of detection probability as a function of false alarm and S/N are included to aid in the design of specific IFF codes. Figure 2 is based on a Rayleigh noise distribution, or the envelope of Gaussian noise, and would apply for daytime background conditions. P_n in the figure is the probability that the noise exceeds a threshold, while P_d is the probability that the signal (plus noise) exceeds the same threshold. This curve is for single pulse probabilities. (See Anderson⁷ for computations involving more than one pulse.) If an IFF code is to be created specifically for night use, Poisson statistics would probably apply. Probability curves for this case are given in figures 2 and 3.

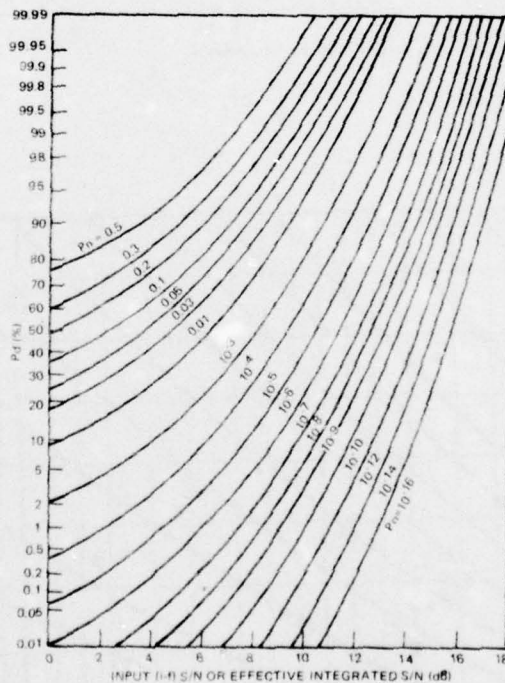
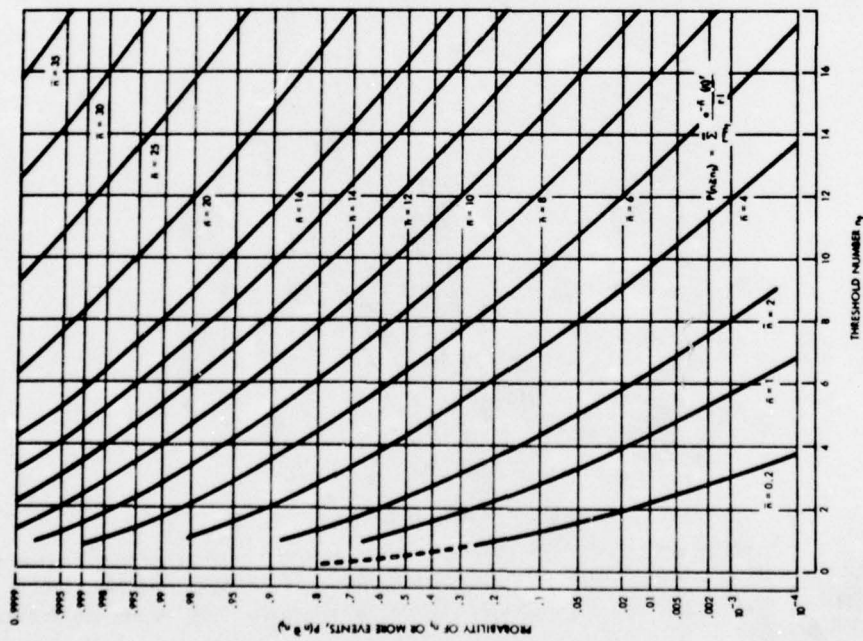
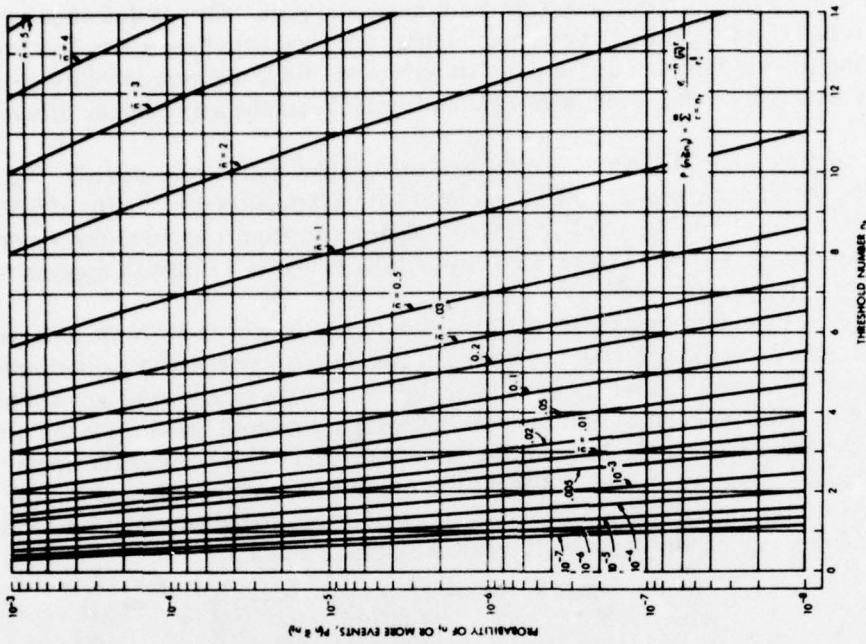


Figure 2. Probability of detection versus S/N ratio.

⁷Naval Electronics Laboratory Center Technical Document 447, *Periscope Aircraft-Submarine Optical Communications System (PERASOCS): Preliminary Definition and Analysis*, by R. Anderson, D. Adrian, and WR Stone, 1 September 1974



Probability of n_1 or more random events with Poisson distribution when the expected mean number of events is n as a function of the threshold number n_t (Part 1 of 2).



Probability of n_1 or more random events with Poisson distribution when the expected or mean number of events is n as a function of the threshold number n_t . Curves for $10^{-7} < n < 10^{-4}$ are approximate (Part 2 of 2).

Figure 3. Probability of random events with Poisson distribution (courtesy RCA) (ref 8).

COMMUNICATION RATE

When the system switches from acquisition to communications, the tradeoff between false alarm and detection probability changes. That is, additional false indications are acceptable if the pulse detection can be enhanced enough to reduce the overall error rate. In a fixed-threshold system, the threshold level would have to be altered. However, another strategy, such as maximum-likelihood detection, should probably be used.

The information rate for a pulse position modulation system has been shown to be approximately:^{9,10}

$$H = (\log_2 M) / M \Delta T - P_E \{ (\log_2 M) M \Delta T \},$$

where

- M = number of slots,
- ΔT = duration of slot, and
- P_E = probability of error.

The P_E term is small for the S/N considered here for communications and is ignored in obtaining approximate information rate. The information rate for PIM should be close to that of PPM with some capacity used for synchronization. To obtain the maximum information rate for a given pulse rate, assume that the period between pulses is divided into slots of 0.5-microsecond duration. This duration is dictated by pulse-time dispersion in a scatter link. For a LOS link, the slot duration could probably be shorter. Table 5 gives the information capacity for several pulse rates. It is noted that the capacity increases with a decrease in M (increase in pulse rate). The information rate is also given assuming one 12-bit word per pulse. Optical communication systems using 12-bit words have been implemented¹¹ and it is noticed that very little is generally gained by going to more than 4096 slots.

TABLE 5. INFORMATION RATE.

Pulse Rate	Period (msec)	M (no)	H (bits/sec)	Data Rate Using 12 bits/pulse (bits/sec)
10	100	200,000	176	120
20	50	100,000	332	240
50	20	40,000	265	600
100	10	20,000	1430	1200
200	5	10,000	2660	2400

⁸ RCA, *Electro-Optics Handbook*, 1974

⁹ Karp, S and RM Gagliardi, "The design of a Pulse-Position Modulated Optical Communication System," *IEEE Transactions on Communication Technology*, COM-17, p 670 to 676, 1969.

¹⁰ Karp, S, EL O'Neill and RM Gagliardi, "Communication Theory for the Free-Space Optical Channel," *Proceedings of the IEEE*, v 10, p 1611 to 1625, 1970

¹¹ Naval Electronics Laboratory Center Technical Note 2672, *Voice Communication with a Flashlamp-Excited Blue-Green Dye Laser*, by JE Celto, EJ Schimitschek and JA Trias, 24 April 1974*

*NELC technical notes are informal documents intended primarily for use within the Center.

SECTION 5. LINK ANALYSIS

The link analysis is separated into four parts. First, the transmission loss as a function of range and wavelength is given for both the scatter and direct (relay) propagation links. The optical background noise is also described. The S/N is determined as a function of range and wavelength for nominal system parameters. The value of this computation is that it indicates the preferred operating wavelengths and allows a rapid assessment of the S/N resulting from a change in system parameters. Heavy rain, dense fog, and clouds can produce losses of from 20 to 30 dB per kilometer and obliterate an optical channel. Estimates of link availability are also given.

TRANSMISSION LOSS

In the visible portion of the spectrum, the major loss mechanism is aerosol scattering. The aerosol scattering also permits OTH communications as discussed quantitatively in appendix E. Near the low wavelength end of the visible region, molecular (Rayleigh) scattering begins to contribute to the loss. In the ultraviolet (UV) region, Rayleigh scattering becomes more important, and absorption by ozone causes very large losses for wavelengths below 0.3 μm . Because of these losses, the UV region has not been considered in detail.

In the IR region, the effects of absorption by water vapor and carbon dioxide need to be considered. These losses are minor for windows in the near IR but become pronounced at larger wavelengths. The absorption losses are superimposed upon the scatter losses. IR absorption loss is first considered, and then OTH propagation in the visible and IR regions is discussed.

IR ABSORPTION LOSS

In the absence of haze or clouds, the major loss mechanism in the IR region is absorption by atmospheric components, particularly water vapor and carbon dioxide. The computation of radiative transfer is very complicated and numerous approximate methods have been applied.^{1,2} For a single frequency, the transmittance over a homogeneous path is of the same general form as for scatter, ie,

$$T(\lambda) = \exp(-k(\lambda)w),$$

where

T is the transmittance,
k is a coefficient,
 λ is wavelength, and
w is the amount of absorber in the path.

^{1,2} LaRocca, AJ, "Methods of Calculating Atmospheric Transmittance and Radiance in the Infrared," *Proceedings of the IEEE*, v 63, p 75 to 94, 1975

However, considering absorption over an entire absorption "line" and the effects of adjacent absorption lines leads to various expressions for transmittance. For weak absorption lines or short distances, the above form is often applicable. For strong absorption lines or long distances the following form is often used:¹⁴

$$T(\lambda) = \exp(-k(\lambda)w)^{1/2}.$$

This expression is often used for water vapor in part of the IR spectrum, and the following expression is used for other IR wavelengths.¹⁴

$$T(\lambda) = \exp[-k(\lambda)w/(1 + 2k_2(\lambda)w)^{1/2}].$$

For large w , this approximates the previous form for transmittance.

Transmittance tables for H₂O and CO₂ are given by Valley (tables 10-13 and 10-14).¹³ The table for CO₂ covers the range of absorption concentration of interest in the present study. The CO₂ concentration is about 0.294 pascal (30 atm-cm) per kilometer of sea level path and decreases with altitude. A value of 0.245 pascal (25 atm-cm), corresponding to an average altitude of 1 km, was used to obtain the absorption for transmission windows between 1 and 4.6 μm . For CO₂ laser transmission at 10.6 μm , the laser transition occurs in reverse in the atmospheric CO₂. This absorption is combined with water vapor absorption. A typical loss value is about 1 dB/1.6 km.

Absorption loss in water depends upon the total water vapor concentration over the path (scatter depends on drop size). The relationship between precipitable water and relative humidity and temperature is shown in figure 4. In determining absorption, we assume a temperature of 20°C and 50-percent relative humidity. The 0.9 cm/km is reduced to 0.84 to account for a drop in water content with altitude. The transmittance table in Valley is only applicable to 50 cm of water (60-km path). The transmittance values for longer ranges were generally extrapolated assuming an exponential $(kw)^{1/2}$ variation. When the variation in the table was still close to exponential (w) at maximum w , this variation was used to $2w$ and then the $w^{1/2}$ variation was assumed. With the extrapolation used, loss values for ranges beyond about 100 km are somewhat suspect.

The absorption loss as a function of range for various transmission windows is plotted in figure 5. The loss is similar for wavelengths close to those indicated but generally becomes extremely large at intermediate wavelengths. The IR absorption loss is combined with the scatter loss in the next section for the different types of propagation channels. Absorption loss for wavelengths below 1 μm is considered negligible and is ignored.

¹³ United States Air Force, *Handbook of Geophysics and Space Environment*, SL Valley, Editor, 1965

¹⁴ Naval Electronics Laboratory Center Technical Note 2714, *Radiated Background Noise in the 10-45 GHz Band*, by DB Sailors, DJ Adrian and PH Levine, 24 June 1974*

*NELC technical notes are informal documents intended primarily for use within the Center.

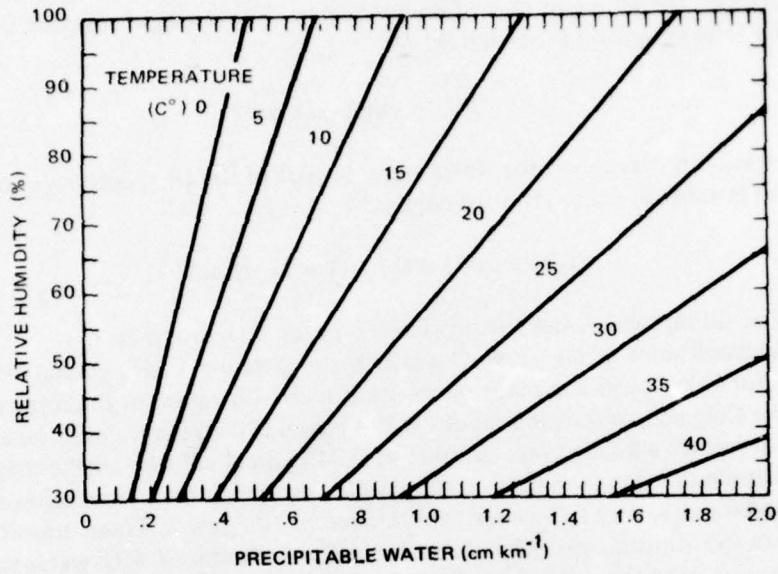


Figure 4. Water-vapor concentration as a function of temperature and relative humidity (ref 13).

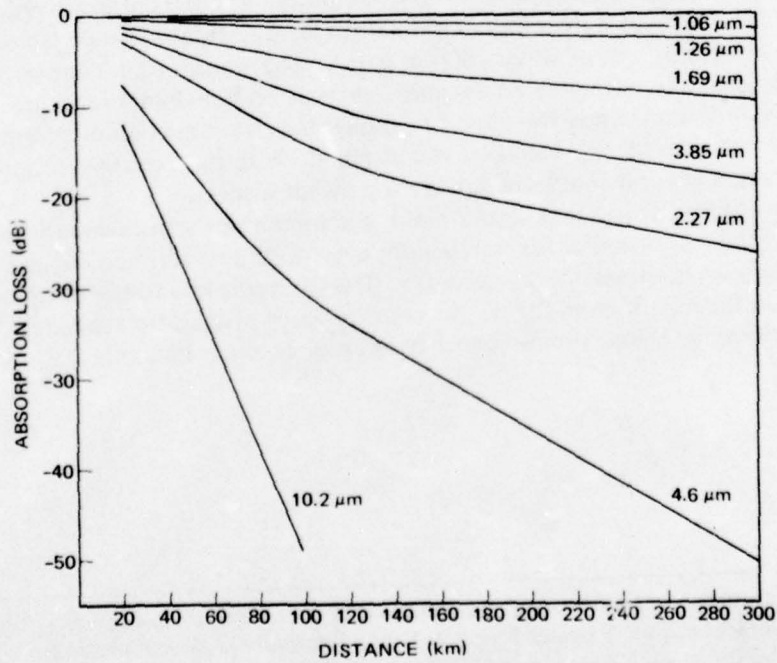


Figure 5. Infrared absorption loss.

FORWARD-SCATTER LINK

A forward-scatter optical communication channel, where the scattering arises from atmospheric "haze" aerosols, has been analyzed.² The referenced report is included as appendix E for convenience. As illustrated in figure 6, the two primary mechanisms for OTH propagation (with absence of clouds) are single and multiple scattering from atmospheric aerosols. Ignoring absorption and noting that scattering tends to be peaked in the forward direction, it is meaningful to think in terms of an "aura" of multiply (forward) scattered photons surrounding the laser beam. This aura will, in general, attenuate less rapidly with distance than the direct beam and, were it not for the effect of the nearby Earth's surface, would be the dominant source of radiance at long ranges. However, the effect of the Earth's surface is to remove energy from the aura by a combination of absorption and diffuse scattering so that, for near-surface transmitter/receiver links, the aura will attenuate more rapidly with range than that of the singly scattered component. For this reason, the computed transmission loss is for the singly scattered component. It should be borne in mind, however, that at ranges less than about 100 kilometers, the aura can, under favorable conditions,² be the dominant component (by about 10 dB).

A BASIC language program (see appendix B) was written to compute the scatter transmission loss as a function of visibility, wavelength, distance, and transmitter vertical beam width. The scatter model was developed in terms of the extinction coefficient. As discussed in the appendix, the commonly used simple relationship between extinction coefficients and visibility or meteorological range, underestimates the extinction coefficients by as much as an order of magnitude for some wavelengths and visibilities. However, it has been possible to combine the semi-empirical model of Elterman with other theoretical and experimental results to obtain a model of sufficient accuracy for the range of visibilities and wavelengths required for the system tradeoff studies. This is discussed further in appendix A.

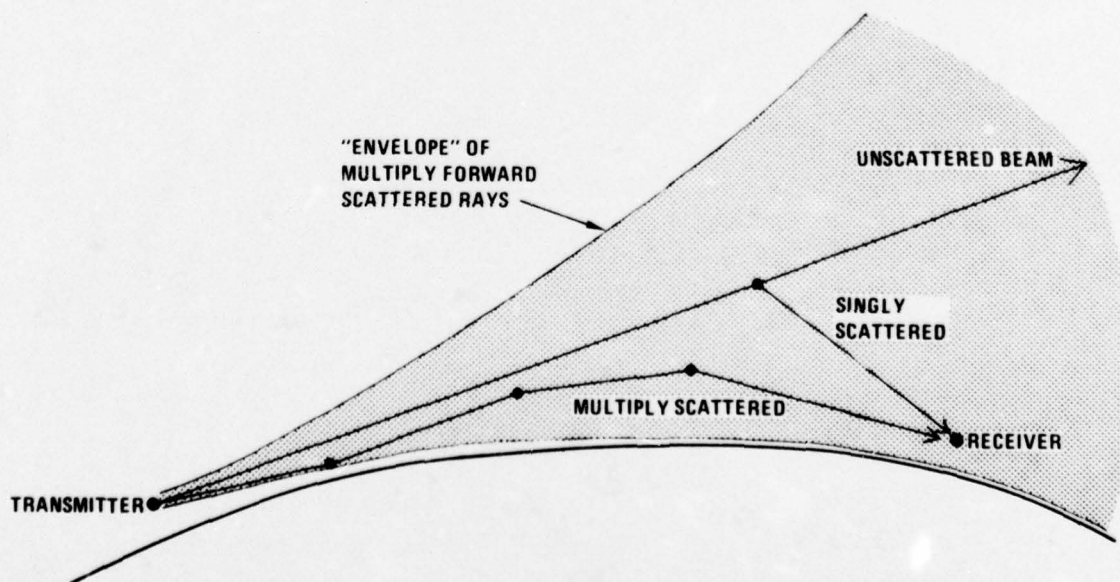


Figure 6. Beyond-the-horizon propagation mechanisms (cloud-free case).

The computed transmission loss does not include the aerosol scattering "gain" in the forward direction but it is included in the S/N computations presented later. The absorption loss in the IR band has been combined with the scatter transmission as a multiplicative factor in the data presented here. Dotted lines connect the IR windows for ease of viewing the data. Absorption between windows is generally such as to preclude communications at any significant distance.

Figure 7 shows the path loss versus wavelength and distance for a pencil beam. The vertical lapse rate of the aerosol concentration is 1.3 km for the figure. This figure indicates the advantage of a system operating in the near IR. The background noise varies with wavelength as shown in the next section and the resulting S/N indicates an even greater advantage for near IR (eg, 1.06 μm) compared to visible (eg, 0.53 μm). Experimental comparison of scatter at 1.06 and 0.53 μm would appear to be an important step in evaluating the forward-scatter model.

Figure 8 shows the loss assuming a 4 degree vertical fan-beam transmitter. The other parameters are the same as for figure 7. Comparison of the two figures shows the signal enhancement produced at long ranges by the fan beam. As discussed, (in LINK S/N RATIOS) this advantage will be effected by time dispersion for short-pulse systems. It is also noted that the fan beams tend to shift the wavelength for minimum path loss towards the lower IR range. Considering available laser sources, 1.06 μm is clearly the most probable operating wavelength. The path loss at 1.06 μm as a function of visibility and range is shown in figure 9.

4° FAN BEAM
V = 20 km
H_T = H_R = 25 km

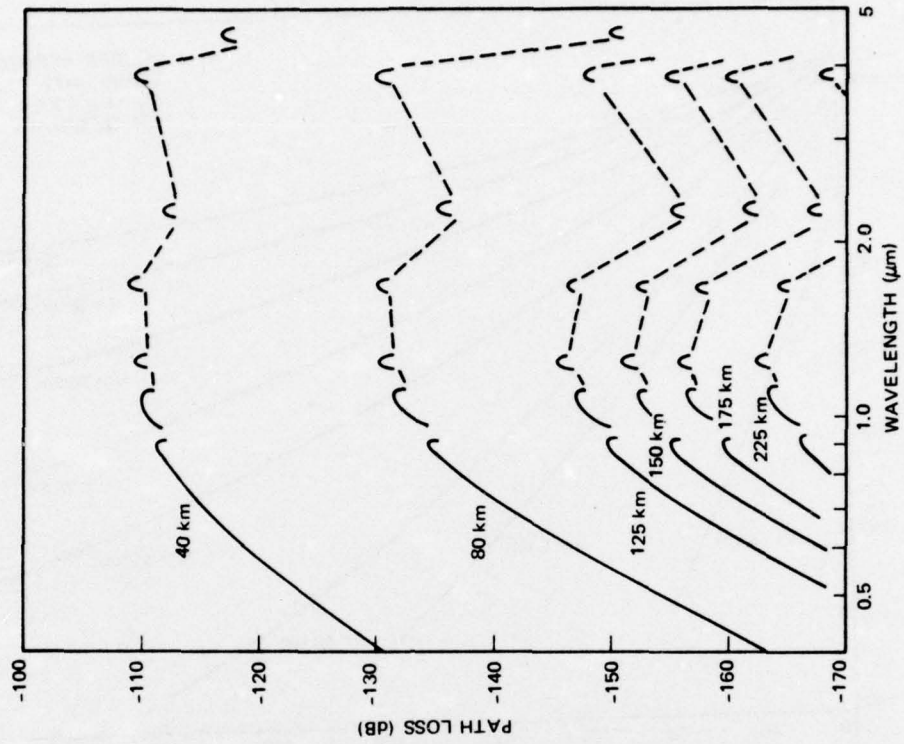


Figure 8. Path loss, 4-degree fan beam.

PENCIL BEAM
V = 20 km
H_T = H_R = 25 km

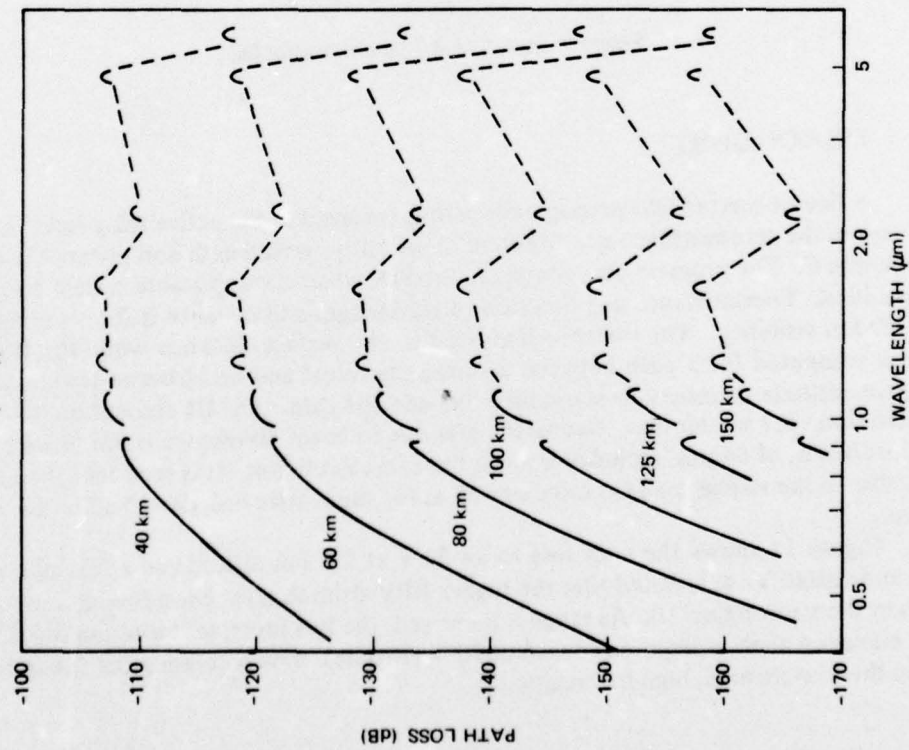


Figure 7. Path loss, pencil beam.

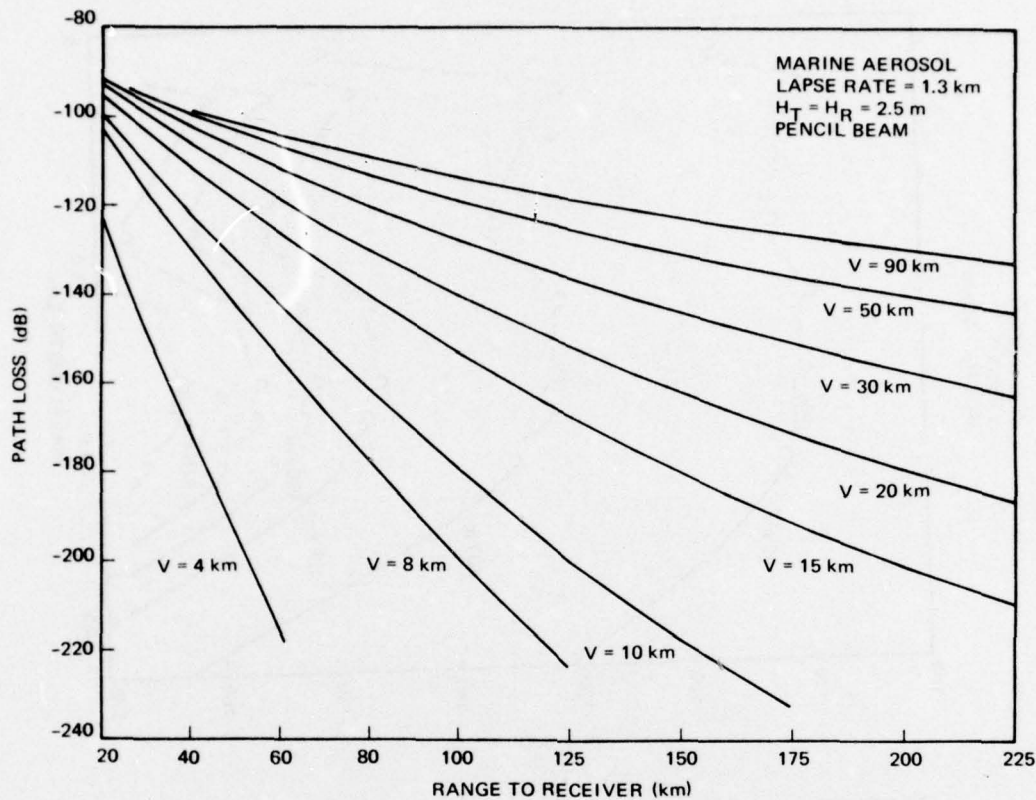


Figure 9. Path loss at $1.06 \mu\text{m}$, scatter link.

LINE-OF-SIGHT

A line-of-sight (LOS) propagation path is involved in the active relay link. A program to compute the transmittance as a function of visibility, wavelength and distance is described in appendix C. The program also computes the S/N when the applicable system parameters are specified. Transmittance as a function of wavelength and distance is shown in figure 10 for a 20-km visibility. The distance indicated is the surface distance while the transmittance is computed for a path between a surface terminal and an airborne terminal at the minimum altitude necessary to maintain a line-of-sight path. The IR absorption loss is superimposed upon the scatter loss. Geometric loss due to beam divergence is not included in the path loss but is, of course, included later in the S/N calculation. It is seen that the near IR is preferable to the visible for LOS links as well as for the scatter link described in the previous section.

Figure 11 shows the path loss to an RPV at 2.5 km altitude as a function of range and visibility. It is noted that the higher RPV altitude gives considerable smaller path loss than shown in figure 10. As range is increased, the loss increases more rapidly since a lower elevation angle is required (constant RPV altitude), thus increasing the fraction of the path in the low-altitude, high-loss region.

VISIBILITY = 20 km
AIRBORNE TERMINAL HEIGHT = MINIMUM FOR LINE OF SIGHT
SURFACE TERMINAL HEIGHT = 7 km

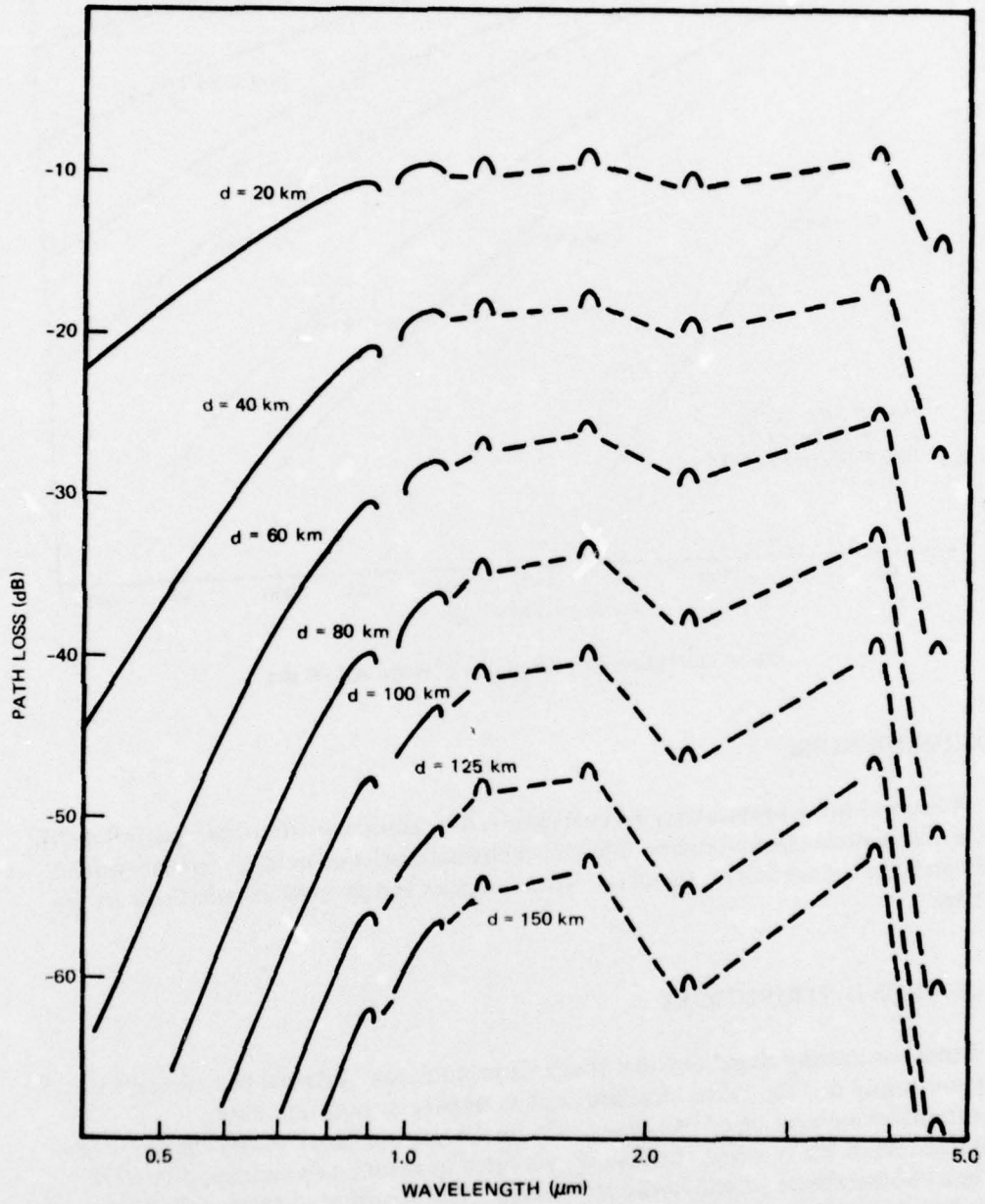


Figure 10. Path loss, line-of-sight link.

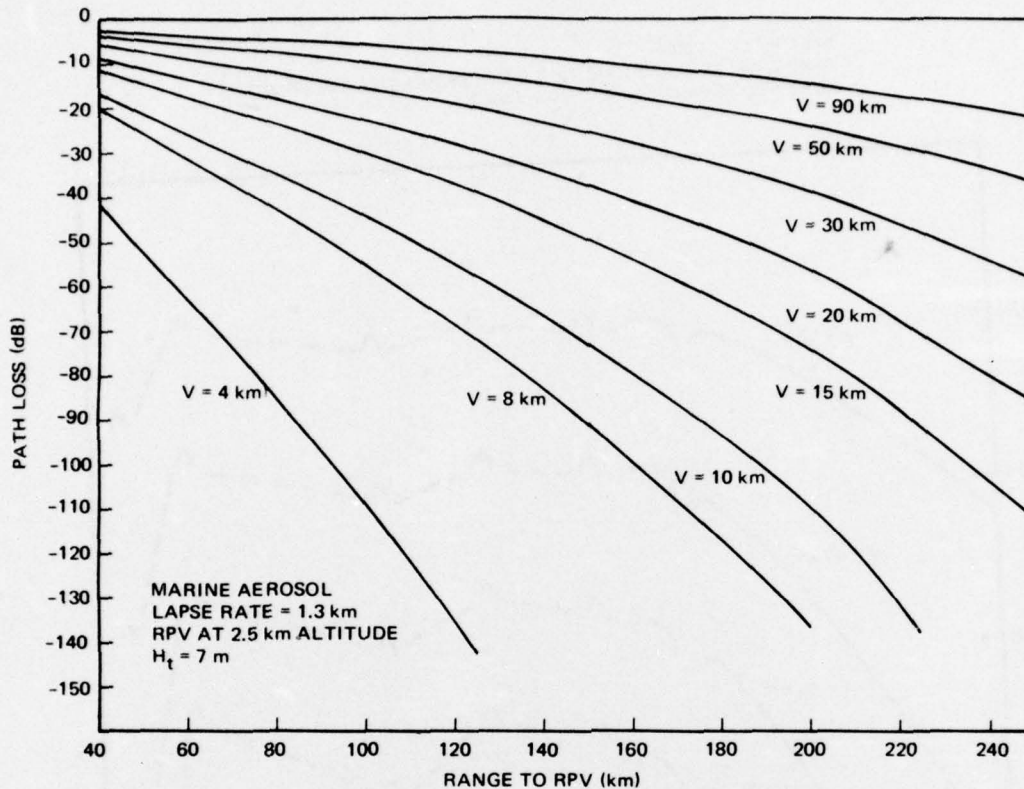


Figure 11. Path loss as a function of range at $1.06 \mu\text{m}$.

BACKGROUND NOISE

Noise and noise sources may be characterized by source distribution, spectral distribution, and statistical characteristics. Statistical characteristics of noise in optical systems were discussed in the section on signal modems. Sources and spectral distributions are discussed here.

SOURCE DISTRIBUTIONS

Some contrasting characteristics of source location are: internal or external (background); uniformly distributed or localized; and stationary or nonstationary.

Internal noise may be of two types. Thermal noise originates within the amplifiers and load resistors of the receiver. Internally generated quantum noise is caused by dark current in a photoemissive or photovoltaic detector. The quantum or photon-fluctuation noise produced by external radiation is proportional to the power incident on the detector. Thus, both the signal and background radiation contribute to the noise. The photon noise associated with the signal (self noise) is included in the program listed in the appendix although, at long operating ranges, it is negligible compared to the background.

The importance of the distributed versus discrete source has to do with the measure of background. If the source fills the receiver field of view, the spectral radiance, $N(\lambda)$, ($\text{watt m}^{-2} \text{steradian}^{-1} \mu\text{m}^{-1}$) is an appropriate measure. However, if the source does not fill the field of view (discrete source) the irradiance, $H(\lambda)$, ($\text{watt m}^{-2} \mu\text{m}^{-1}$) is more appropriate.

When a source is contained within the receiver field of view, the received background power, P_b , in terms of H is given by

$$P_b = H(\lambda)A_r t_o t_a B_o ,$$

where

- A_r = receiving aperture,
- B_o = optical bandwidth,
- t_o = transmittance of the receive optics,
- t_a = transmittance of the atmosphere, and
- λ = wavelength.

When a source completely fills the receiver field of view, the received power may be expressed in terms of the radiance, N , as

$$P_b = N(\lambda)\Omega_r A_r t_o t_a B_o ,$$

where

- Ω_r = solid angle receiver field of view.

For a conical field of view, the solid angle is related to the plane angle of view, θ_r , by

$$\begin{aligned} \Omega_r &= 2\pi(1-\cos \theta_r/2) \\ &= \frac{\pi\theta_r^2}{4} , \text{ for small angles.} \end{aligned}$$

This latter relation holds for systems considered in this study. For a nonconical field of view, eg, cylindrical optics, the effective solid angle needs to be either determined, or roughly approximated by replacing θ_r^2 in the above expression by the product of the linear FOVs in the largest and the smallest direction.

The major background radiation sources are the sun and sky. The sun may be considered a discrete or a distributed source depending upon whether the receiver FOV is larger or smaller than the 0.5-degree angle subtended by the sun. The spectral distribution for the sun is given in the next section, but it is generally assumed in this study that the receiver does not look directly at the sun. The sky background may be considered as a distributed uniform source for any FOV considered in this study. The relative locations of natural sources may be considered approximately stationary when viewed from a ship. This may no longer be true for an aircraft.

Intentional or unintentional man-made interference sources will generally be point sources. However, scattering of this energy, eg by clouds, may generate a distributed interference source. Interference source locations may well be nonstationary.

SPECTRAL CHARACTERISTICS

The spectral distribution for the sun is shown in figure 12.¹⁵ It is noted that a blackbody at 5999 K fits the curve quite well. In fact, the blackbody approximation is reasonably good through the millimetre portion of the radio band.¹⁴ Figure 12 also shows the spectral distribution at sea level. The effect of absorption by water vapor, carbon dioxide, and ozone is apparent. The spectral irradiance within the atmosphere depends upon the density and composition of the air along the path of the beam. Figure 13 illustrates the depletion of the solar beam in passing through clear air to sea level as a function of the optical air mass and zenith angle. Detailed tables of solar irradiance are given in Valley.¹³

The daytime sky background radiance is due to scattering of incident solar radiation and to emission by atmospheric particles heated by incident radiation. The visible radiance is predominately scattered radiation, and the infrared is mainly atmospheric emission. Both the level and the spectral distribution depend upon the characteristics of the scatterer. Radiance from sunlit clouds may be an order of magnitude higher than from a clear sky. Sky background data for several conditions are shown in figure 14. Atmospheric absorption bands, illustrated in figures 12 and 13, are not included. The dashed line is discussed in the next section of this report.

Night sky background radiance data are shown in figure 15. The main source in the visible is scattered moonlight. At night, aurora and airglow can be important for some wavelengths near 1.6 μm . Thermal emission predominates for wavelengths greater than 2.5 μm , in contrast to a value of 4 to 5 μm during the day.

ANALYTICAL APPROXIMATION TO BACKGROUND

An analytical approximation to the background was needed for the link performance computer program. From figures 14 and 15, it is seen that a 283 K blackbody radiation curve serves as a fairly good envelope to the measured values. Examination of curves in the IR band^{15,5} indicate that 288 K may be slightly better. In fact, the 283 K indicated for figures 14 and 15 may well be a misprint. The radiance may be derived from Planck's law for spectral radiant emittance, $W(\lambda)$,

$$W(\lambda) = \frac{2\pi c^2 h^{-4}}{\lambda^5} \frac{1}{\exp\{hc/\lambda kT\} - 1}$$

¹⁵ Kopeika, NS and J Boldogna, "Background Noise in Optical Communication Systems," *Proceedings of the IEEE*, v 10, p 1571 to 1577, 1970

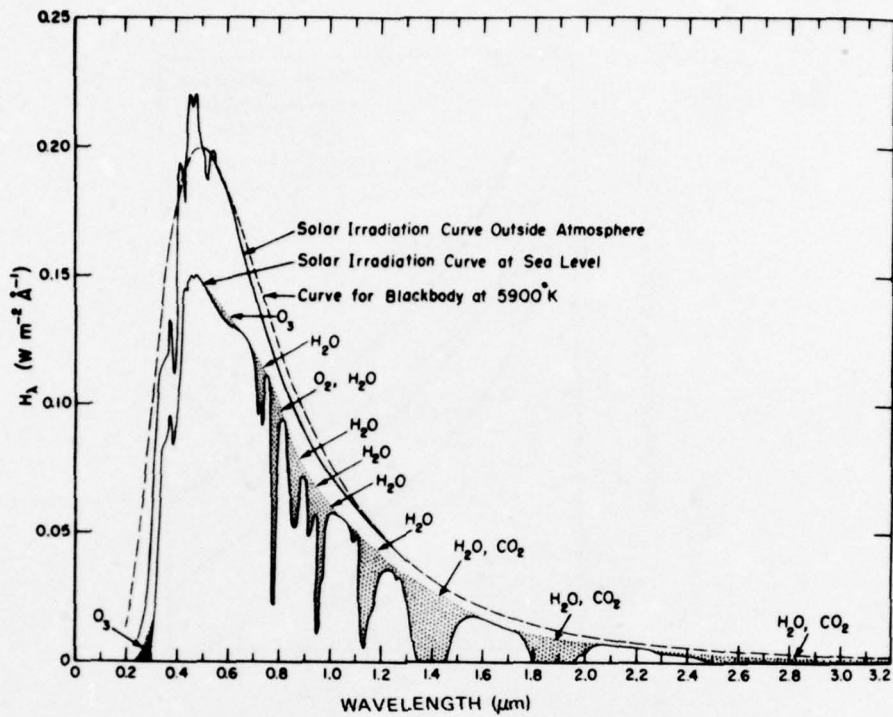


Figure 12. Spectral distribution curves related to the sun; shaded areas indicate absorption, at sea level, due to the atmospheric constituents shown (ref 13).

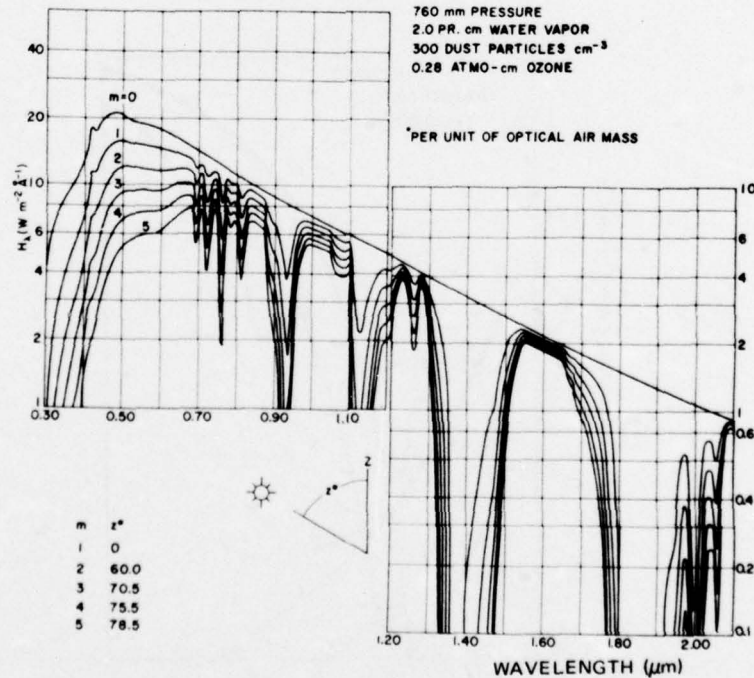


Figure 13. Solar spectral irradiance curves at sea level for various optical air masses; the value of the solar constant used in this calculation was 1322 W m^{-2} (ref 13).

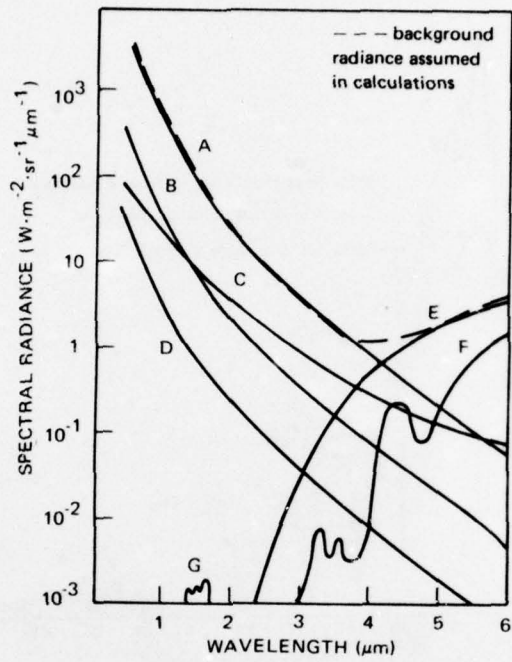


Figure 14. Day sky background data (ref 15).

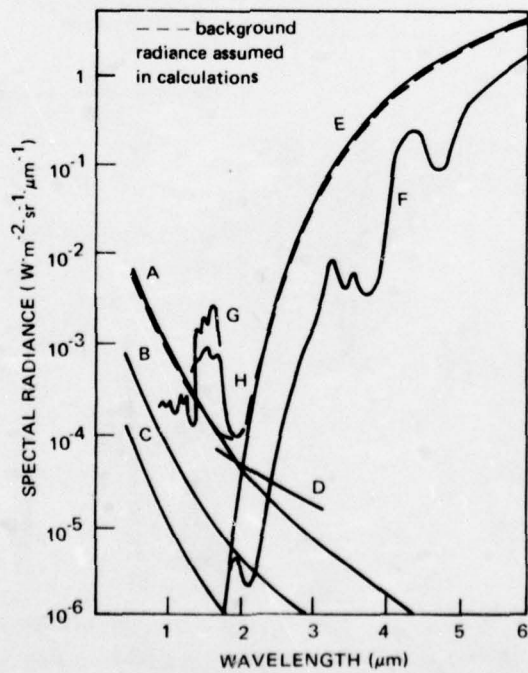


Figure 15. Night sky background data (ref 15).

where

- c = velocity of light,
- λ = wavelength,
- T = temperature of background radiation source,
- h = Planck's constant, and
- k = Boltzmann's constant

If it is assumed that the source is a diffuse radiator (Lambert surface), it can be shown that¹⁵

$$N(\lambda) = W(\lambda)/\pi .$$

The expression for N with T = 288 K is used for the emission portion of the sky noise.

The scattering of sunlight is a function of wavelength, so that a blackbody term alone cannot be used for this component. Comparison of the blackbody radiation for 5900 K and the measured data yielded an empirical multiplying factor of

$$4 \times 10^{-5} / \lambda^{3/2} ,$$

where λ is in μm . The empirical expression for the daytime background is then

$$N(\lambda) = \frac{4.75 \times 10^3}{\lambda^{13/2} (e^{2.44/\lambda} - 1)} + \frac{1.2 \times 10^8}{\lambda^5 (e^{50/\lambda} - 1)} \quad (\text{daytime}),$$

where λ is in μm . The dashed curve in figure 14 shows a plot of this expression. A similar approach for the night sky background gives

$$N(\lambda) = \frac{8.3 \times 10^{-3}}{\lambda^{13/2} (e^{2.44/\lambda} - 1)} + \frac{1.2 \times 10^8}{\lambda^5 (e^{50/\lambda} - 1)} \quad (\text{night}).$$

This expression is plotted as the dashed curve in figure 15.

LINK S/N RATIOS

PULSE DISPERSION EFFECTS

The transmission loss given earlier is actually the value for loss of energy. The curves also give power loss for continuous-wave transmission or pulse transmission where the pulse duration is long compared to the time dispersion introduced by the media. However, time-dispersion effects must be considered when obtaining the S/N for a short-pulse system. The received energy will be spread over a time equal to the sum of the pulse duration and dispersion.

We first consider the time dispersion for a pencil transmitter beam and a finite field of view. Referring to figure E3 of appendix E, let the elevation angles be equal (ie, $\beta_1 = \beta_2 = \beta$)

and denote the dashed line by Z_3 . The difference in propagation time within the receiver field of view, F , ($F = d\beta_2$ in the figure) is:

$$\begin{aligned} \Delta T &= \frac{\Delta Z}{c} [dZ_1 + Z_3 - Z_2], \\ &= \frac{Z_2}{c} \left[\frac{\sin F + \sin 2\beta}{\sin (2\beta + F)} \right] - 1, \end{aligned}$$

where c is the velocity of light. The law of sines was used in the derivation. Next we let:

$$\begin{aligned} D &= 2Z_2 \text{ and} \\ \beta &= D/2R, \end{aligned}$$

where D is the distance between receiver and transmitter and R is the "4/3 earth" radius (see appendix E) of 8493 kilometres. After some trigonometric manipulations and replacing the sines of angles by their arguments, we obtain the time dispersion for a pencil beam:

$$\Delta T = \frac{D^2 F}{4Rc} \quad (\text{pencil beam}).$$

Table 6 lists the time dispersion in microseconds for several distances.

TABLE 6. TIME DISPERSION.

Path D in km	Time in Microseconds			
	Pencil Beam FOV		Fan, Beam Fan Angle = FOV	
	1°	4°	1°	4°
50	0.004	0.017	0.025	0.41
100	0.017	0.069	0.050	0.81
200	0.069	0.28	0.10	1.6
300	0.156	0.62	0.15	2.4

For a fan beam, we assume an equal fan and FOV angle, F . The difference in propagation time between the upper and lower edge of the beam is then found to be approximately (assuming lower edge as a flat earth):

$$\Delta T = \frac{\Delta D}{c} = \frac{D}{c} (1/\cos F - 1) \quad (\text{fan beam}).$$

Time-dispersion values are shown in table 6. Some of the dispersion values are significantly longer than typical pulse lengths (eg about $0.02 \mu\text{sec}$ for a Nd:YAG laser).

If the dispersion equals the pulse duration (eg, at 100 km, for a pencil beam and 1-degree field of view), the peak power is reduced to half that expected from the path-loss computations. Further increase in the FOV would increase the signal energy but not the peak power. The increased energy comes from increased pulse stretching. Consider the S/N expression,

$$\text{SNR (background limited)} = \frac{S_d P_c^2}{2qB (P_b + P_c)}$$

The required bandwidth, B, is inversely proportional to the received pulse duration, T+ΔT, where T is the transmitted pulse duration and ΔT the dispersion. Since P_c is also inversely proportional to the received pulse duration, the S/N is approximately,

$$\text{SNR} = \frac{K}{T + \Delta T}$$

Once T is smaller than ΔT, there is little advantage in reducing it further. It is noted that the bandwidth must be varied as ΔT varies. This could be done stepwise, for example, with 2-to-1 changes in bandwidth (3-dB changes in noise).

Now consider the effect of varying the FOV. Once the FOV is large enough that the time dispersion is comparable to the pulse duration, a further increase will give no increase in peak P_c. The background P_b will increase but B may be reduced, thus keeping the S/N constant. It is advantageous to increase the FOV until the background current term exceeds the dark current. In addition, a wider FOV would relax pointing accuracy requirements.

The time dispersion or extended source effects might conceivably be put to some use, such as angle diversity. For example, 2 detectors could be used, each with a different elevation look angle. The pulse received at the higher angle should lag the other by an amount depending upon the transmitter distance. This would allow discrimination against interference (intentional or unintentional) with a different time relationship. Some advantages of diversity reception could also be achieved in that 2 scattering volumes with possibly different short-term characteristics would be viewed.

FORWARD-SCATTER LINK

The program described in appendix B was used to compute the S/N data given in this section. The IR absorption loss discussed earlier in this section is included in the data. Dashed lines connect the IR windows for ease of following the curves. In general, there will be excessive absorption loss in the wavelength regions indicated by the dashed lines. The computed values are applicable when pulse dispersion can be ignored. For some of the data, corrections are applied for time-dispersion effects as described in the last section.

Figures 16 through 18 show the S/N variation as a function of wavelength and distance for three different visibilities using a pencil transmitter beam pointing at the horizon. The noise level for most of the curves is the maximum noise (analytic expression). The results for the noise curve, D of figure 14 is indicated in figure 16. The system parameters given in table 7 are used independently of wavelength, in order to indicate the generally preferred wavelength region. As can be seen in section 6, there is not generally a strong regular variation of system parameters with wavelength. The figures indicate the advantage of the near IR. Consideration of available laser sources and detectors indicates that 1.06 μm is the best operating frequency at present. The 3.8-μm region should be considered in the future if component advances, especially chemical (deuterium fluoride) lasers, continue.

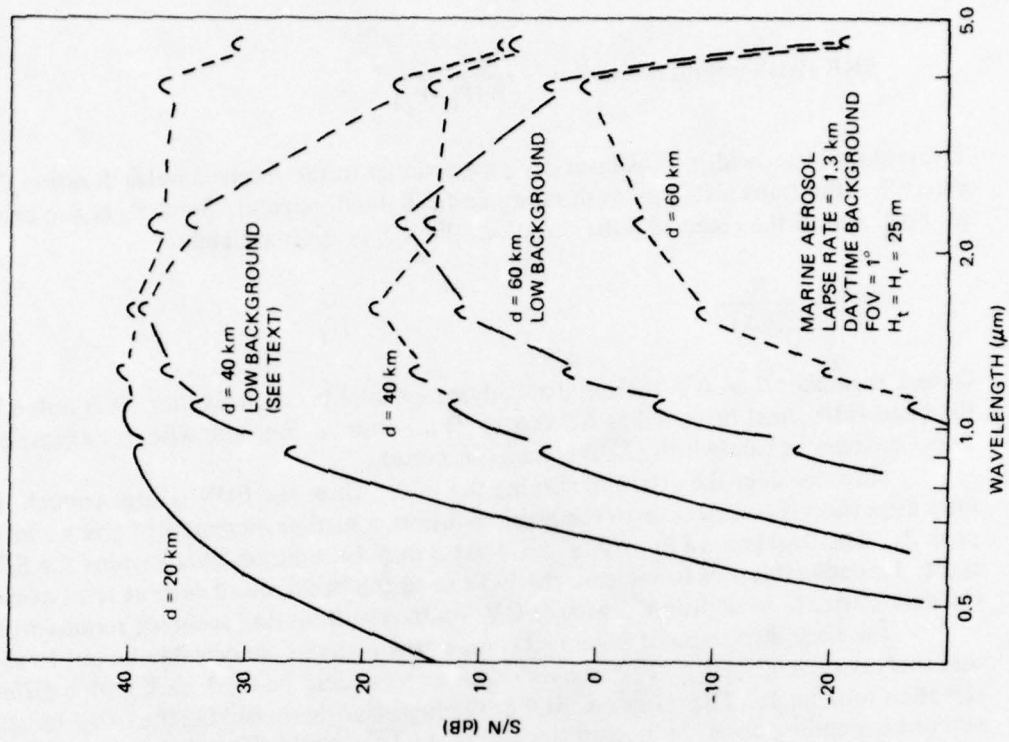


Figure 16. S/N for pencil beam, $V=10$ km (FOV = 1 degree).

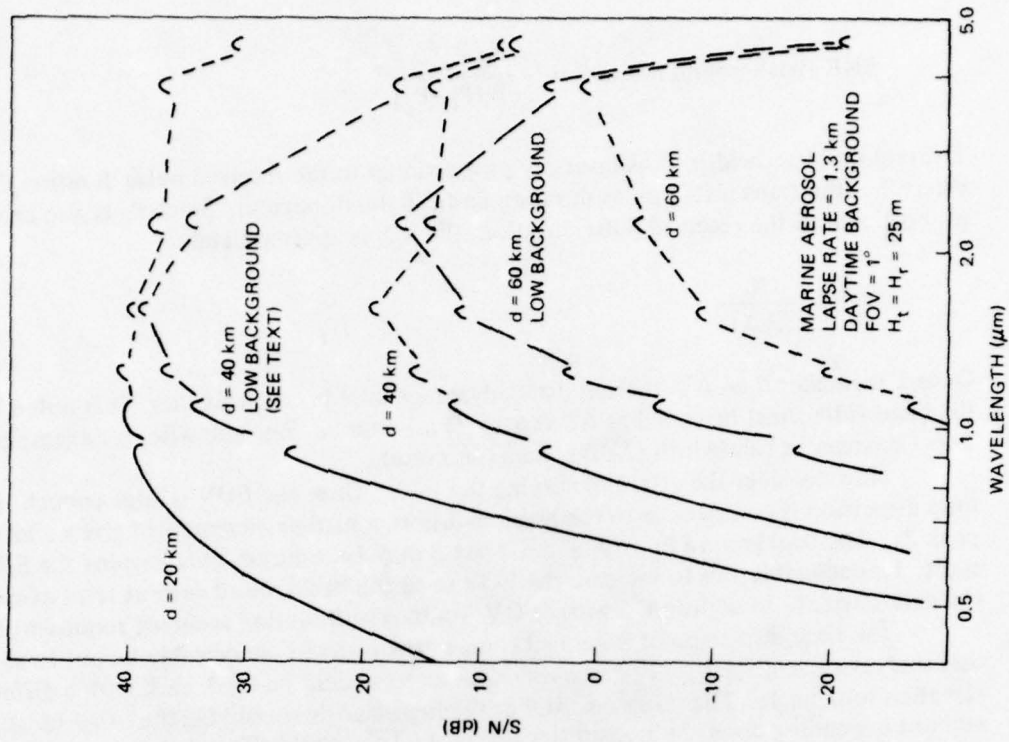


Figure 17. S/N for pencil beam, $V=20$ km.

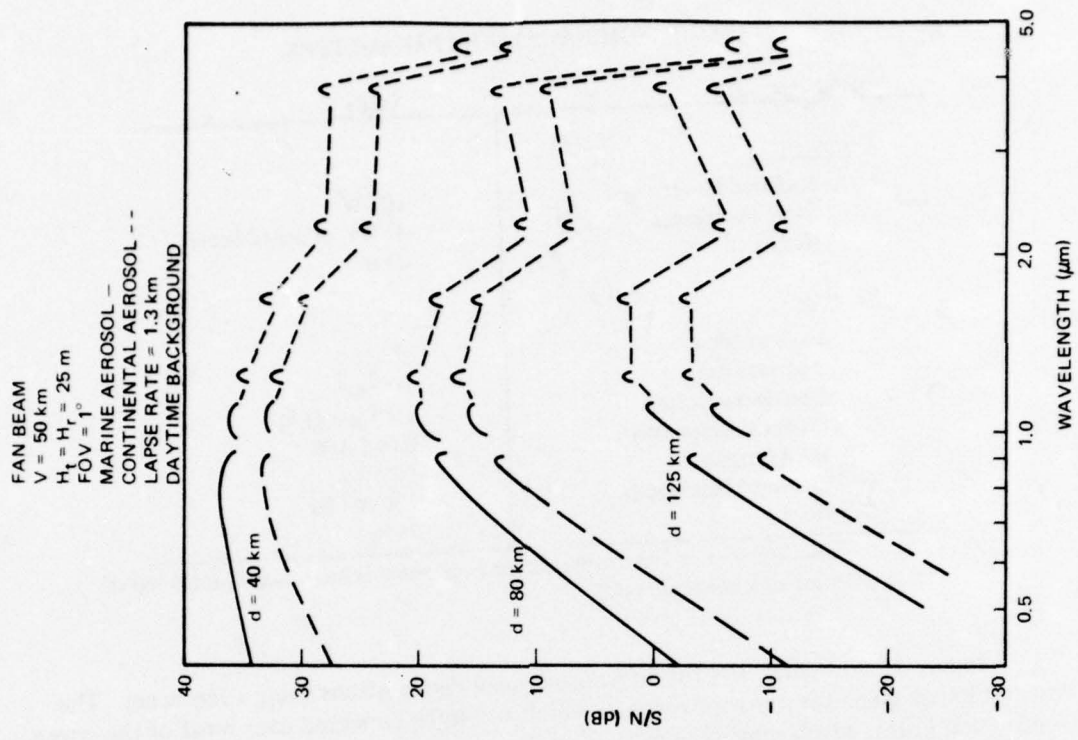


Figure 19. S/N for fan beam, $V=50$ km.

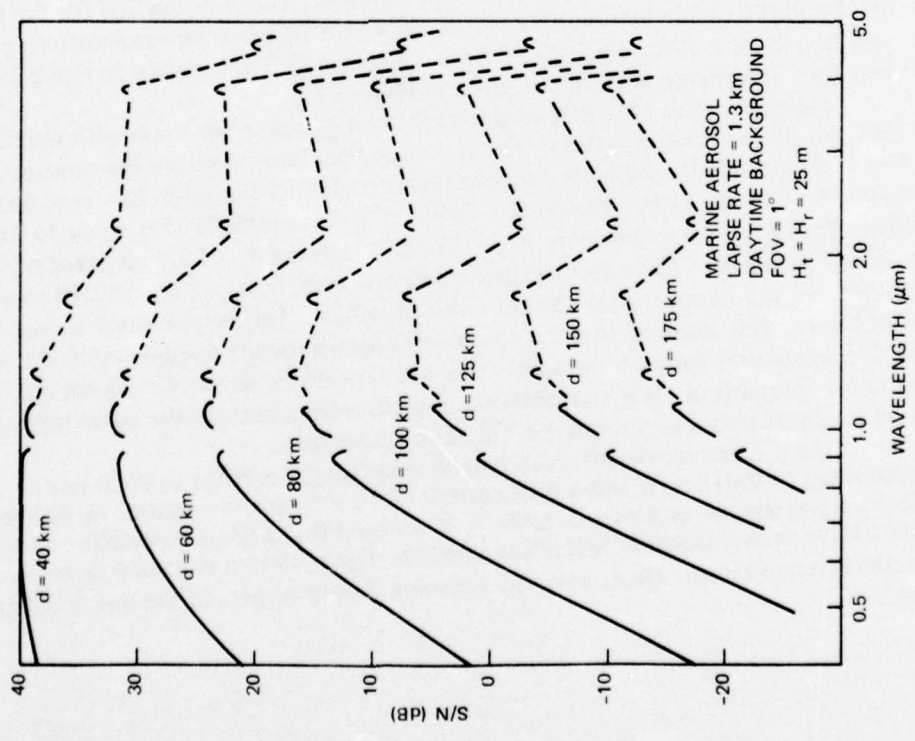


Figure 18. S/N for pencil beam, $V=50$ km.

TABLE 7. NOMINAL SYSTEM PARAMETERS.

Parameter	Value
<u>Transmitter</u>	
Radiated Power	10^6 W
Beam Divergence	4° fan, or pencil beam
Height	25 m
<u>Receiver</u>	
Field of View	1°
Aperture Area	10^{-2} m ²
Optical Bandwidth	10^{-4} μm (1Å)
Detector Responsivity	0.065 A/W
Dark Current	10^{-14} A
Electrical Bandwidth	7×10^7 Hz
Height	25 m

(Background or dark current limited operation is used, based on the use of a detector with adequate gain).

Figure 19 compares S/N for different aerosol distributions using a fan beam. The best results are given for a marine aerosol, which would be expected over most of the ocean. Continental hazes, which may exist near coast lines, are expected to generally produce signals a few dB smaller than marine aerosols. The difference between the S/N for the two aerosols is greater in the visible than in the near IR. The Deirmerdjian forward-scattering function for a maritime M haze at wavelengths of 0.45, 1.19, and 10.0 μm is given in figure 20. Similar curves for a Deirmerdjian cloud are given in figure 21.

Figure 22 shows the S/N versus range for a 4-degree fan beam with visibility as a parameter, for a 1.06-μm system. The system parameters used were the same as given in table 7. The presently available detector responsivity at 1.06 μm is, however, only 0.018 ampere/watt (A/W) rather than 0.065 A/W. The curves would also apply to far ranges (where $P_b > P_c$) for a responsivity of 0.018 and a laser power of 1.9 megawatts (which is presently available). The effect of time dispersion on S/N (assuming a 0.015-μsec pulse) is indicated in the figure for the 20-km visibility curve. The same reduction would apply to all curves. It is assumed that the electrical filter bandwidth is adjusted to the inverse of the dispersion time for each distance. The pencil beam results at $V = 20$ km are shown in the figure for comparison. It is seen that the time dispersion reduces the advantage of the fan beam for short pulses as discussed in the previous section.

Figure 23 shows the effect of launch angle on the S/N for a pencil beam. A detector responsivity of 0.018 A/W and a dark current of 10^{-13} ampere was used in the computation. Other parameters are as shown in table 7. It is noted that a beam elevated at about 4 degrees gives a large enhancement in S/N at long ranges. The optimum elevation depends on aerosol distribution and range. Thus, elevation scanning should be part of the link-acquisition procedure.

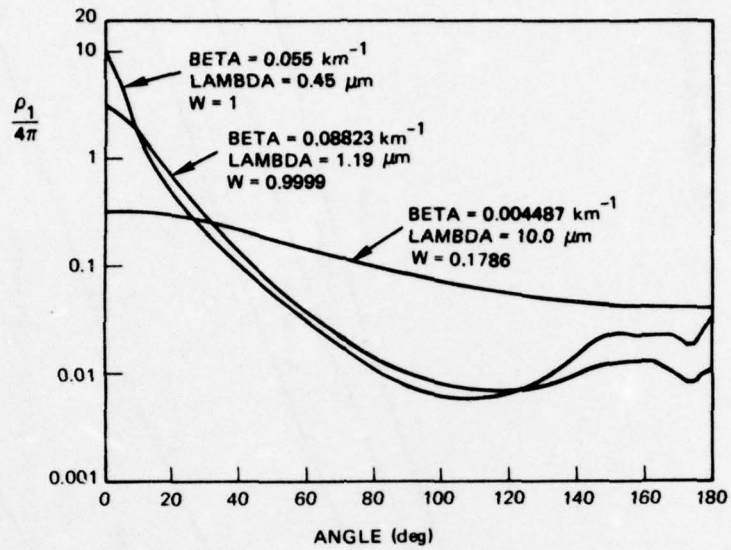


Figure 20. Forward-scattering function, water haze, M.

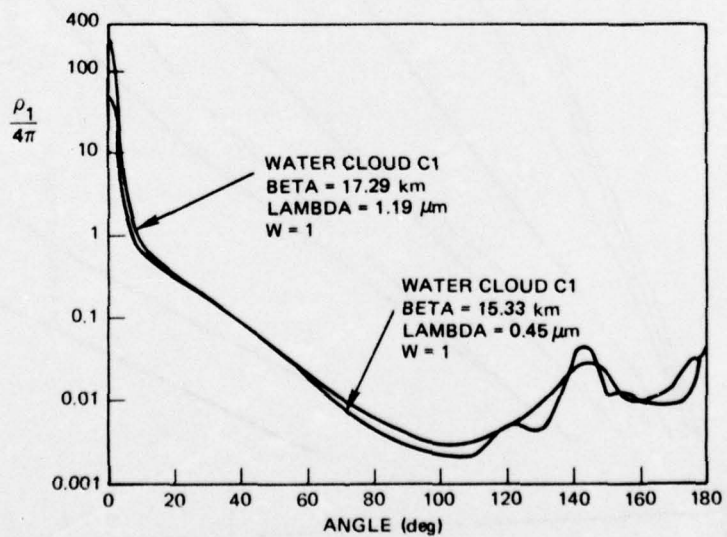


Figure 21. Forward-scattering function, water cloud, C₁.

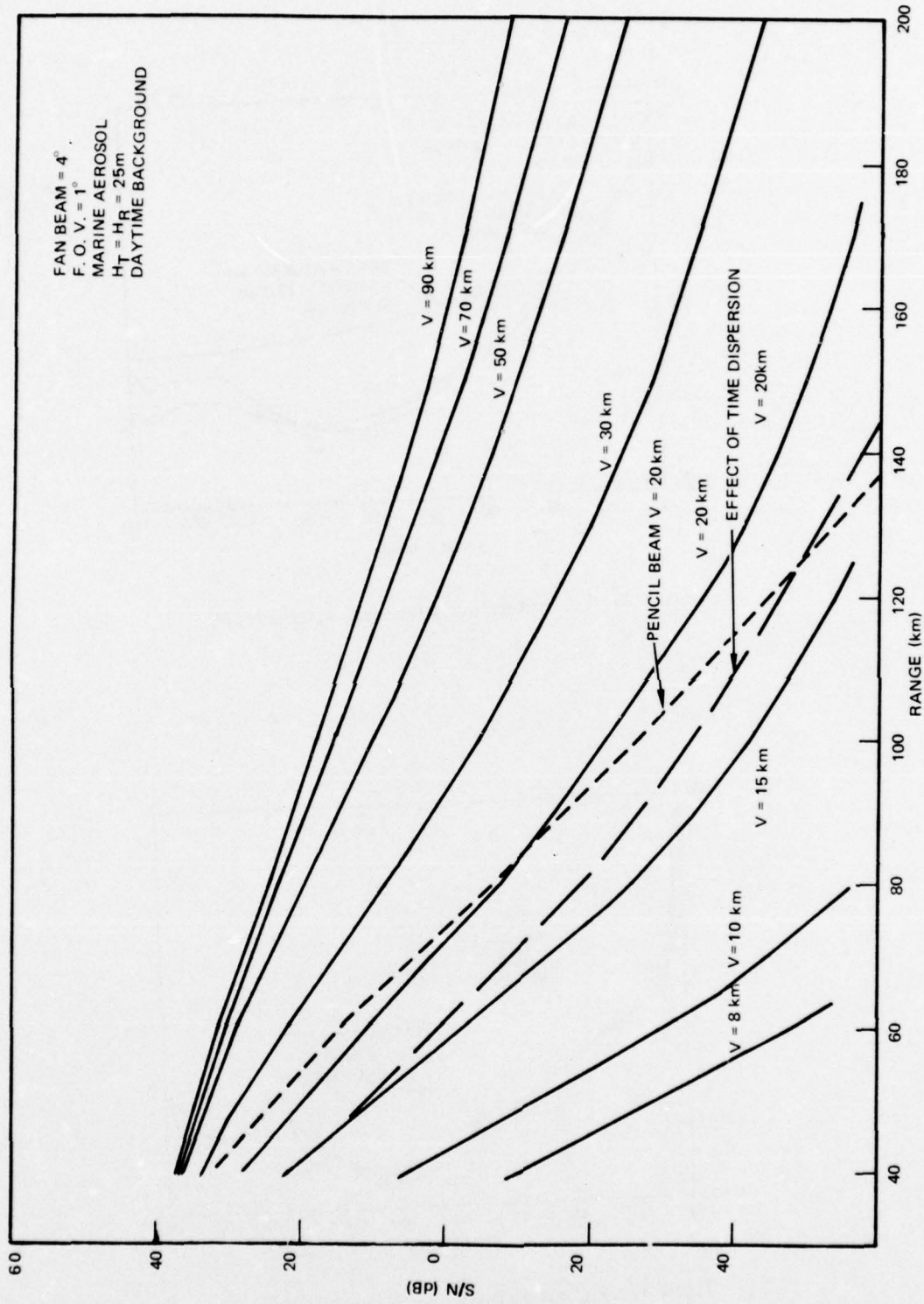


Figure 22. S/N for 1.06 μm .

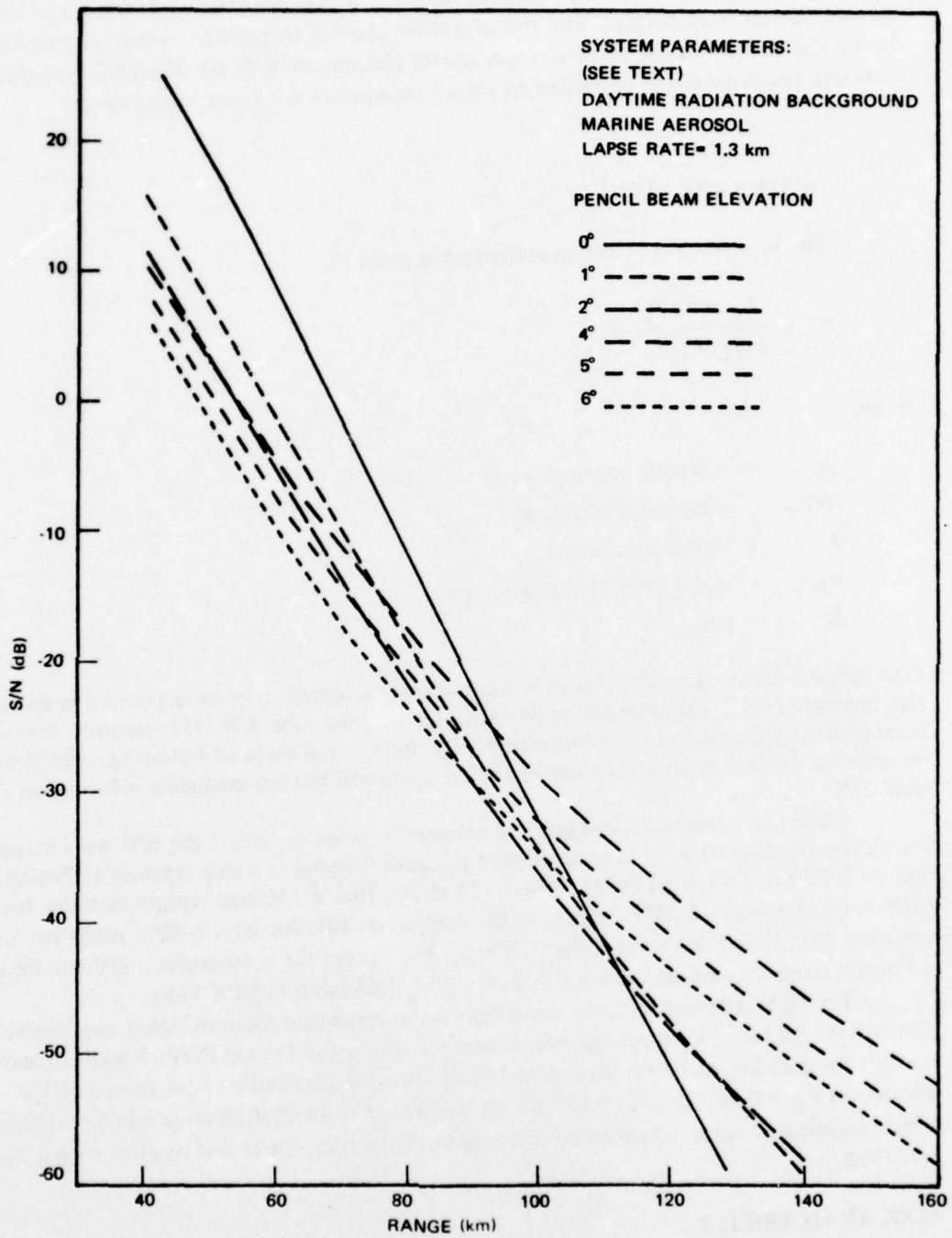


Figure 23. Effect of launch angle on S/N.

Examination of figures 18 and 23 shows that a 15-dB S/N (for $S_d = 0.018$ A/W, $P=1.9$ MW, $\lambda=1.06$ μm) could be expected for ranges less than 60 km and 100 km for visibilities of 20 and 50 km respectively. The use of a 40-megawatt transmitter would extend these ranges to 80 and 160 km. The effects of parameter changes on S/N are discussed in section 4 and coverage predictions for an optimum set of parameters are given in section 3.

ACTIVE RPV LINK

The received power for an active link is given by,

$$P_c = \frac{A_r T(R) P_t}{\pi(\theta_D R/2)^2}$$

where

- A_r = receiving aperture area,
- $T(R)$ = path loss at range, R,
- P_t = transmitter power,
- θ_D = transmitter divergence, and
- R = range.

Loss in the receiver optics is ignored but could be considered to be incorporated in an effective aperture area. The received power was used to determine S/N. It is assumed that sufficient gain is used in the photomultiplier so that the thermal noise of following amplifiers can be ignored. Dark current is included in the computation but has negligible effect upon daytime S/N.

Using the transmitter and receiver parameters given in table 7 the S/N was computed for a range of visibilities. It is assumed that the path is between a ship (system at 7-m altitude) and an RPV (at 2.5-km altitude). Figure 24 shows that a 150-nmi communication range ($S/N = 15$ dB) with an RPV located at the midpoint (140-km ship-to-RPV path) could be achieved with visibilities greater than 10 km. S/N curves for a 10-degree FOV should allow a simpler receiving pointing control system to be used (ship-to-RPV link).

The RPV pointing accuracy for transmission presents a more stringent requirement. The curves in figure 24 assume that the receiver is within the 1-mrad FOV. Figure 25 shows the S/N for a 20-km visibility. Curves are also shown for a transmitter divergence of 1.8 degrees (or $\theta_D = 0.06^\circ$ and $P_R = 10^3$ W). It is noted that the desired range can be achieved with a pointing accuracy of about \pm degree on both the transmitter and receiver with a visibility of 20 km.

LINK AVAILABILITY

Weather affects the link availability in 2 ways. First, the path loss, in any of the link types, is a strong function of visibility or meteorological range. Second, clouds can affect the links in different ways. On an RPV link, a cloud on the path will attenuate the signal. In a

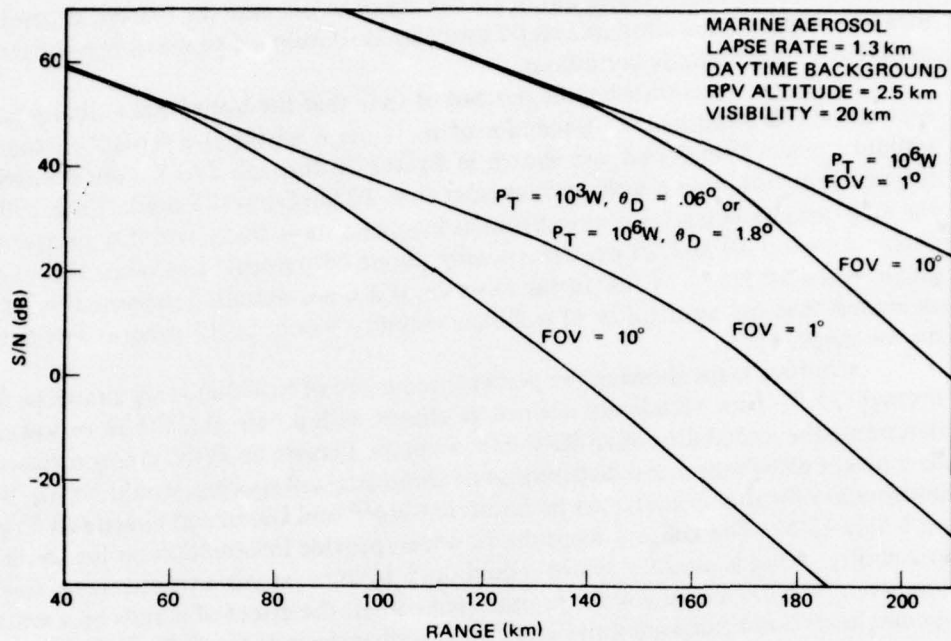


Figure 24. S/N for active link, RPV altitude = 2.5 km.

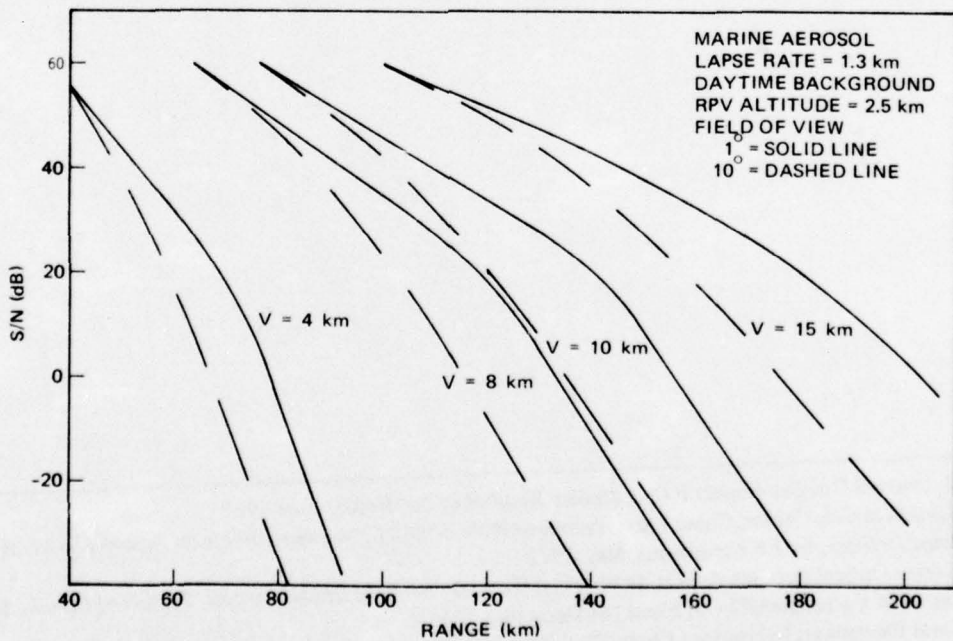


Figure 25. S/N for active link, RPV altitude = 2.5 km, visibility = 20 km.

scatter link, a cloud can either attenuate the signal or increase the scatter, depending upon location. Operational strategies could probably be developed to maximize scatter-link availability under cloudy conditions.

Contour maps showing the percent of time that the horizontal visibility is less than 5 nmi have been published.¹⁶ Examples of these maps, giving the percent of time that the visibility is less than 5 nmi, are shown in figures 26 through 29. We are primarily interested in visibilities significantly greater than 10 km (almost 5 nmi). Examination of the data samples taken from nine different locations show that a visibility greater than 20 km occurs between 10 and 20 percent (usually about 15 percent) less often than a visibility greater than 10 km.¹⁷ Thus, in the absence of a more definitive information, it can be estimated that the availability of a 20-km visibility would be 15 percent less than shown on the maps.

Contour maps showing the percent frequency of low clouds are shown in figures 30 through 33.¹⁶ Low clouds are defined as clouds with a base at 2438 m or lower. To determine the availability of an RPV link, a comprehensive analysis, taking into account the base height distribution and distribution of cloud size and spacing, would be required. Some information for such a study can be found in Cato¹⁸ and Green and Greenwell¹⁹ published on 1 May 1975. The contour maps do, however, provide information on the lower limit of availability. That is, an RPV system could operate some, as yet undetermined, fraction of the time even with low cloud cover. As indicated earlier, the effect of clouds on a scatter system is complicated and can sometimes improve as well as degrade the link. If the cloud base is greater than 915 or 1220 metres, the scatter signal can be greatly enhanced.

¹⁶McDonnell Douglas Report F-063, *Marine Weather of the World*, June 1968

¹⁷Naval Weapons Center, China Lake, Technical Note 4056-16, *Weather Effects on Infrared Systems for Point Defence*, by FE Nicodemus, May 1972

¹⁸Electro-Optical Systems Report 4440, Final III, *Laser Systems Study, Part III, Effects of Clouds*, by GA Cato, LW Carrus and KJ von Essen, 14 December 1975

¹⁹Naval Electronics Laboratory Center Technical Note 2923, *Optical SATCOM: Effects of Clouds on Global Availability of Optical Satellite Communications Links*, by SW Green and RA Greenwell, 1 May 1975*

*NELC technical notes are informal documents intended primarily for use within the Center.

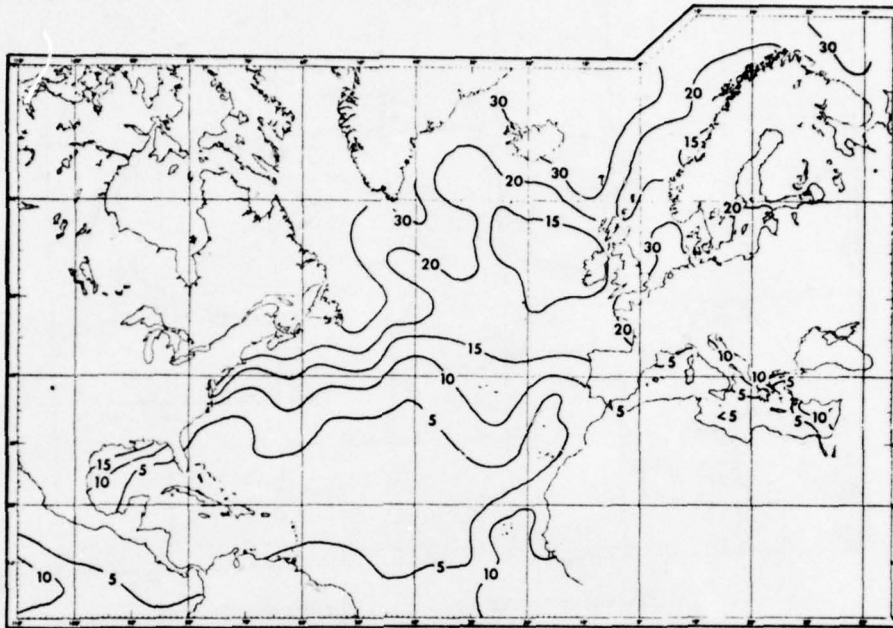


Figure 26. Percent time visibility 5 nautical miles, North Atlantic, July (courtesy McDonnell Douglas) (ref 16).

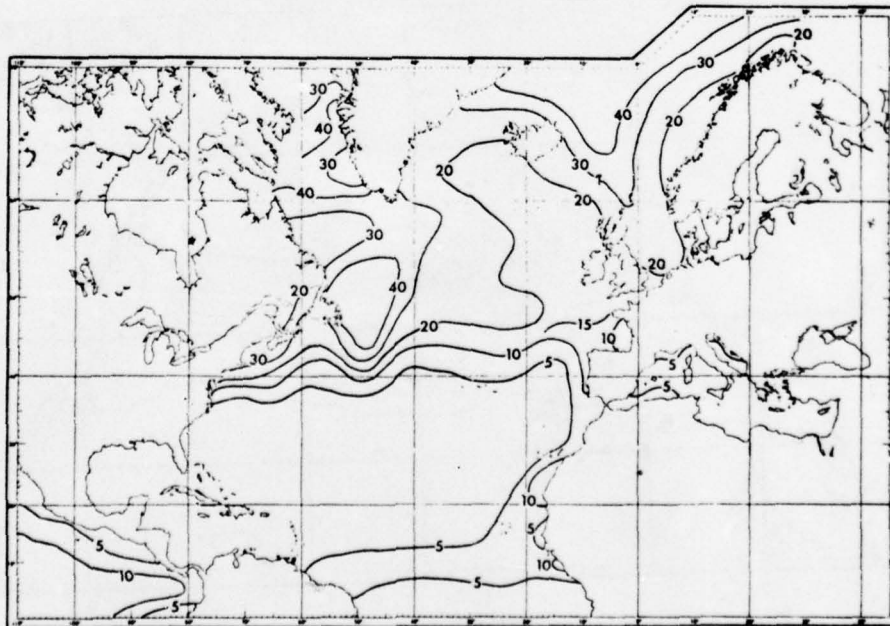


Figure 27. Percent time visibility 5 nautical miles, North Atlantic, January (courtesy McDonnell Douglas) (ref 16).

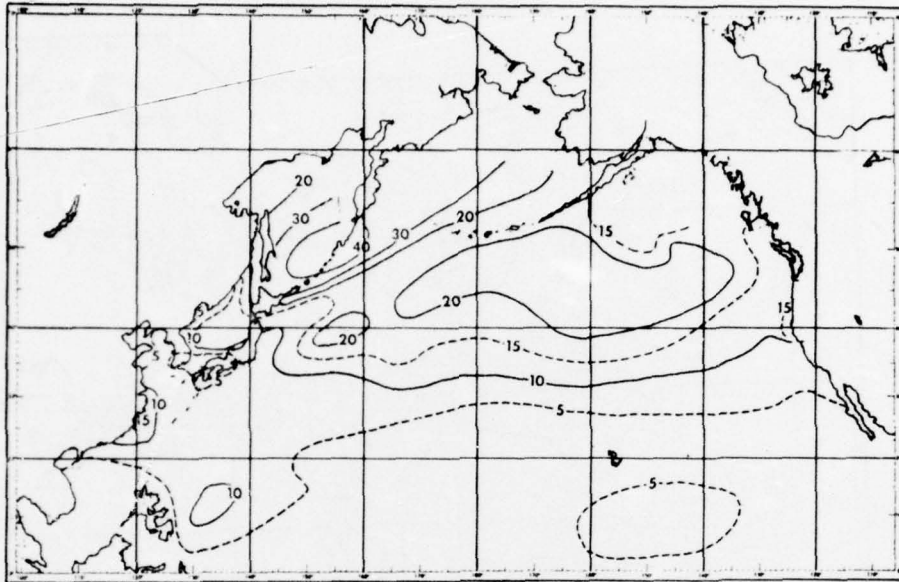


Figure 28. Percent time visibility 5 nautical miles, North Pacific, January (courtesy McDonnell Douglas) (ref 16).

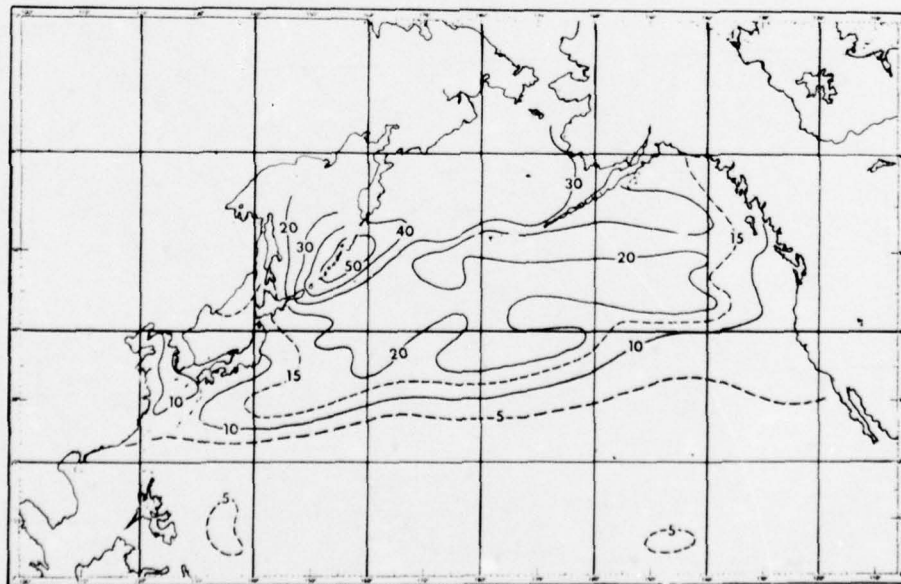


Figure 29. Percent time visibility 5 nautical miles, North Pacific, June (courtesy McDonnell Douglas) (ref 16).

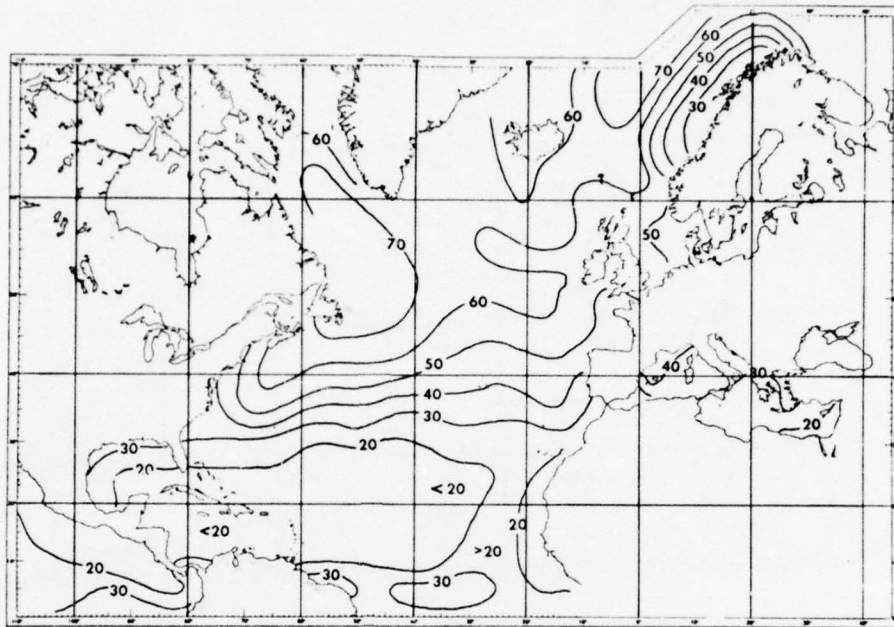


Figure 30. Percent frequency low cloud amount 6/10 or more, North Atlantic, January (courtesy McDonnell Douglas) (ref 16).

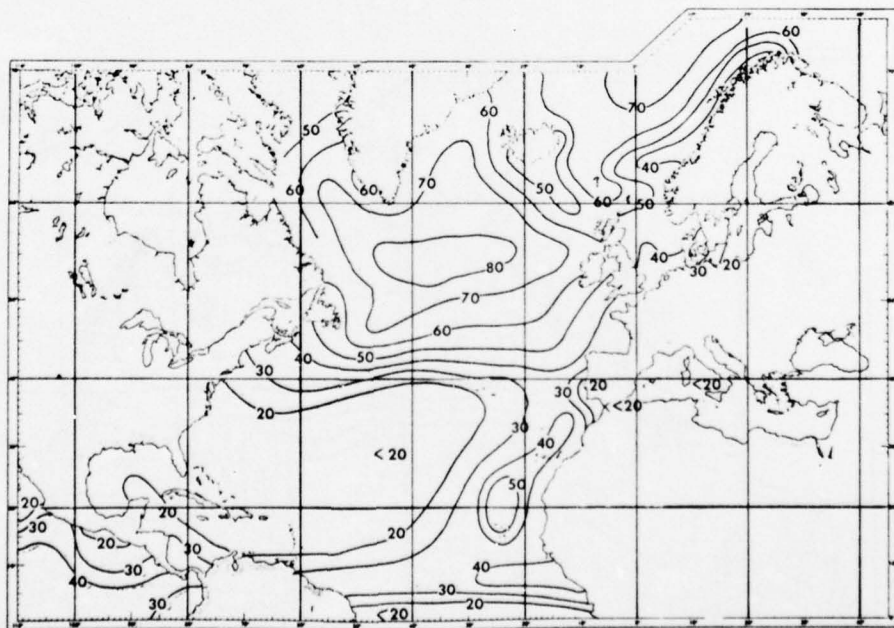


Figure 31. Percent frequency low cloud amount 6/10 or more, North Atlantic, July (courtesy McDonnell Douglas) (ref 16).

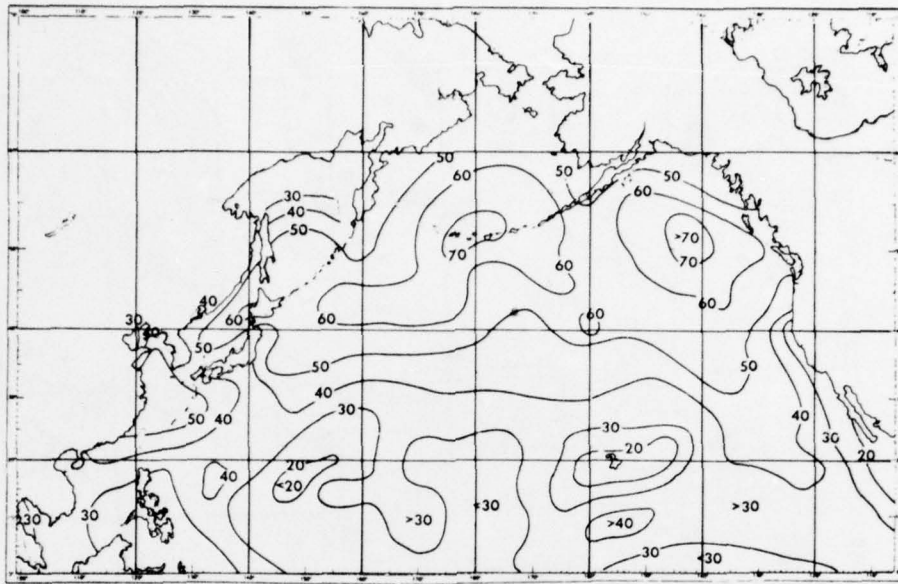


Figure 32. Percent frequency low cloud amount 6/10 or more, North Pacific, January (courtesy McDonnell Douglas) (ref 16).

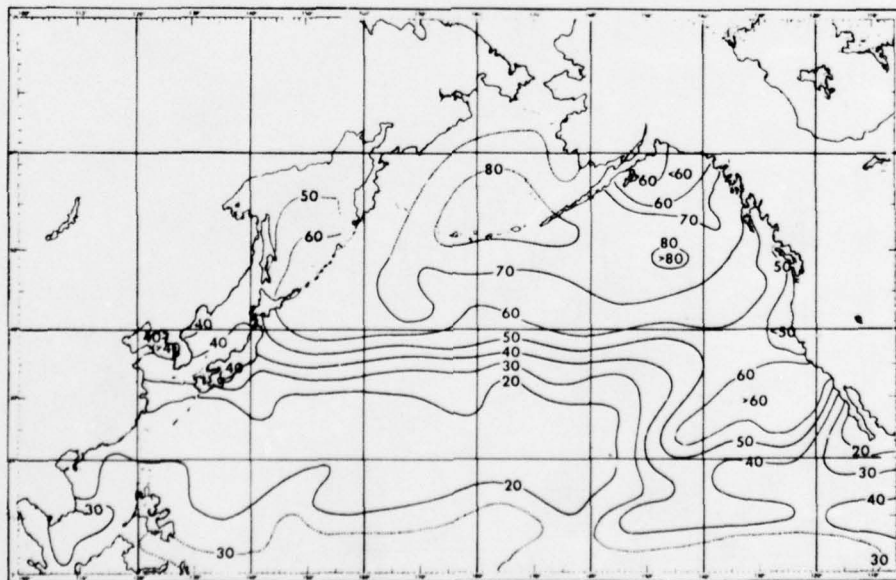


Figure 33. Percent frequency low cloud amount 6/10 or more, North Pacific, July (courtesy McDonnell Douglas) (ref 16).

SECTION 6. COMPONENTS AND SUBSYSTEMS

The major components involved in system tradeoff considerations are briefly described in this section. The range of practical parameters for each component is generally listed as a function of wavelength. Approximate costs are given where available to aid in tradeoff considerations. Components to be discussed include the following: lasers, optical filters, detectors, pointing control systems, and remotely piloted vehicles (RPVs).

LASERS

Laser action has been demonstrated in various media including gases, liquids, crystalline solids, and glasses. A huge number of continuous and pulsed sources have been developed with useful power outputs at wavelengths which span the optical spectrum. However, there are a relatively small number of high peak-power laser types. These are discussed briefly in this section. Summaries of laser types and characteristics are found in Geusic²⁰ and RCA⁸, while the performance of commercially available lasers is given in *Laser Focus*.²¹

The principal high-power pulse lasers for different wavelength regions are listed in table 8. Pulse parameters, beam divergence, and cost are listed for commercial units. It should be noted that peak power and pulse-repetition rate can generally be altered, keeping the average power constant. Dye and chemical lasers are under active development and much higher powers are likely in the future.

Principal high-power continuous wave laser types are listed in table 9. Costs for various output powers are listed for use in tradeoff considerations.

²⁰ Geusic, JE, WB Bridges and JI Panklove, "Coherent Optical Sources for Communications," *Proceedings of the IEEE*, v 10, p 1419 to 1439, June 1970

²¹ *1975 Laser Focus Buyers' Guide*, Advanced Technology Publications, Inc, 1975

TABLE 8. PULSE LASERS.

Wavelength	Type	Energy Joules	Output Peak Power MW	Pulse Width μ s	Pulse Rate (pps)	Beam Divergence mrad	Approximate Price Range (1976)
(μ m) 0.337 0.53	Nitrogen Neodymium Yag- frequency doubled	0.01 0.1 0.15	1 5 10	0.01 0.02 0.014	50 30 10	1 4 3.5	\$k 23 40-60 50
Selected within 0.45 to 0.69 0.49 1.06	Dye Dye Nd: YAG	0.1 0.12 0.05 0.1 0.15 0.45	2 0.25 5 6 10 30 50 80	0.5 0.01 0.015 0.015 0.015 0.02 0.015	30 10 2400 50 30 20 30 30	— 3 to 5 1.2 3 to 5 2 0.8	— 15 to 30 27 30 to 40 35 to 55 75
2.8 to 3 3.5 to 4 10.6	Hydrogen Fluoride Deuterium Fluoride Carbon Dioxide	0.7 1 0.5 3 800	1.4 2 2.5 30 8000	0.5 0.5 0.2 0.1 0.1	1 to 2 1 to 2 200 300 0.1	0.5 0.3 1.2 0.6 0.5	15 15 15 30 90

TABLE 9. CONTINUOUS-WAVE LASERS.

Wavelength μm	Type	Output (watts)		Beam Divergence	Commercial Units
		Principal Mode	Multimode	mrad	Approx Price Range (1976)
0.337 0.351 to 0.52	Nitrogen Argon	0.1			\$k
		4		0.6	
		5		0.5	
		8		0.5	
0.53	Nd: YAG Frequency doubled Ruby/Glass	16	20	0.6	8
		2			10.5
					13
0.69 to 1 1.06	Nd: YAG	15	to 20	5	16
			15	6 to 8	20
			25	5 to 8	6 to 12
			50	5 to 8	8 to 15
			200	6 to 8	10 to 18 (20 to 26 MIL SPEC)
			800-1000	5 to 15	13 to 30
2.6 to 3.5 10.6	Hydrogen Fluoride Carbon Dioxide	4000		16 to 20	20 to 40
		3		4	100
		50		1 to 2	4
		250	300	1	8 to 13
		500		1.4	30
1000		2.1	35		
					47

OPTICAL FILTERS

Background radiation noise may be reduced in the frequency domain (filtering), the time domain (gated receiver in a pulse system), or spatially (limited FOV). Frequency-selective filtering is considered in this section but the maximum FOV is generally related to bandwidth for narrow-band filters. The major emphasis in this section is upon interference filters, which provide narrow passbands and can be designed over a wide range of optical wavelengths. Acoustically tuned optical filters are also discussed. Some other filter types are briefly considered.

INTERFERENCE FILTERS

Interference filters are commercially available with typical standard bandwidths of 10, 30 and 100Å (about \$200, \$150 and \$100 for 61-cm diameter). Multilayer dielectric-stack filters are available with bandwidths down to about 5Å and solid-spacer Fabray-Perot filters have been developed with an optical bandwidth of 0.5Å.²²

Recently developed filters in the infrared provide bandwidths of from 0.3Å to 8Å in the 1 to 5 μm band.²³ The 0.3Å-filter at 1 μm has a 1-degree allowable FOV.

In its simplest form, an interference filter consists of two partially reflecting surfaces separated by a spacer with refractive index n as indicated in figure 34.

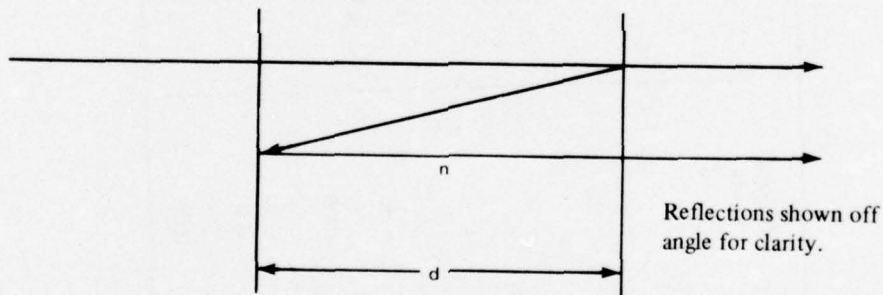


Figure 34. Interference filter.

The signals will be enhanced when the optical path length is,

$$2nd = m\lambda,$$

where m is an integer (order of interference). Peak transmissions occur at wavelengths,

$$\lambda_m = 2nd/m,$$

²² McIntyre, C, et al, "Optical Components and Technology in Laser Space Communications Systems," *Proceedings of the IEEE*, v 10, p 1491 to 1503, 1970

²³ Roche, AI and AM Title, "Tilt Tunable Ultra Narrow Band Filters for High Resolution Infrared Photometry," *Applied Optics*, v 14, p 765 to 769, 1975

so that multiple transmission bands are produced. The separation between transmission bands, or the free spectral range, is,

$$\lambda_s = \lambda_m^2 / 2nd.$$

One way of retaining very narrow bandwidths but increasing the effective λ_s is to operate 2 filters in tandem. The free spectral ranges of the 2 filters are chosen so that undesired coincidences occur in regions where they can be reduced by blocking filters (eg. absorption filters).

When light is incident on the filter at an angle, θ , relative to the normal, the wavelength of peak transmission, λ_0 , in each band is lowered by an amount of $\delta\lambda$ given by,

$$\delta\lambda = \lambda_0 \theta^2 / 2n^2,$$

for small θ . This allows the filter to be fine tuned by tilting but also restricts the FOV for effective filtering. Figure 35 shows a plot of $\delta\lambda/\lambda_0$ versus θ for typical values of refractive index. The figure shows, for example, that a 1 Å bandwidth at 1.06 μm is limited to a ± 2 degree FOV. The values of n vary with the general optical band in a direction to reduce the direct dependence of bandwidth on wavelength.

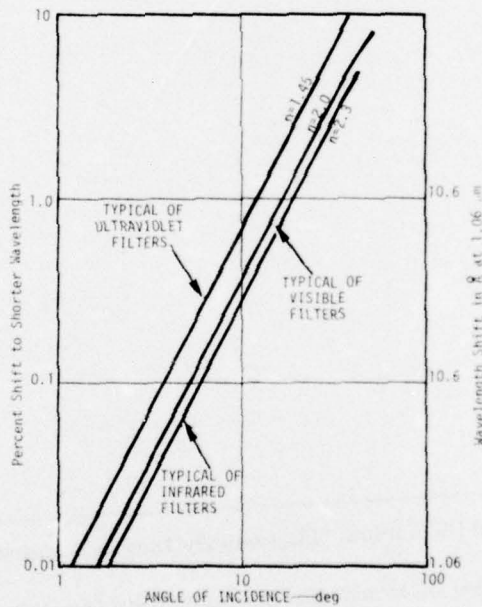


Figure 35. Shift of center wavelength of typical interference filters with angle of incidence.

The temperature stability of solid-spaced interference filters depends both upon the bulk linear coefficient of thermal expansion of the substrate and the temperature dependence of the index of refraction.

The magnitude of the effects depends upon material, operating temperature, and wavelength. While temperature control may be necessary, it is not generally a difficult requirement. For example, in the near-to-mid IR range, a temperature stability on the order of ± 2 degrees C is sufficient for less than a 1Å shift.²³

ACOUSTICALLY TUNED OPTICAL FILTERS

Electronically tunable acousto-optic filters (ATOF) have been developed in the past few years.²⁴⁻²⁷ A tunable filter combined with a tunable laser (eg, dye laser), offers the possibility of spread optical spectrum techniques with resulting countermeasures advantages. Bandwidths roughly comparable to those obtained with interference filters can be achieved. However, the filter is polarization sensitive and requires a microwave power source. Interference filters would be preferable unless the tuning capability is needed.

Figure 36 shows the bandwidth as a function of wavelength. It is noted that a FOV of ± 3 degrees causes little degradation in the bandwidth. Other designs (crystal at different orientation) can produce very large off-angle sensitivity (eg, a 20 times increase in bandwidth for a 1-degree aperture angle).

²⁴ Harris, SE, STK Nieh and DK Winslow, "Electronically Tunable Acousto-Optic Filter," *Applied Physics Letter* 15, p 325, 1969

²⁵ Kusters, JA, DA Wilson and DL Hammond, "Optimum Crystal Orientation for Acoustically Tuned Optical Filters," *Journal of the Optical Society of America*, v 64, p 434 to 440, 1974.

²⁶ Naval Electronics Laboratory Center Technical Report 1990, *Possible Use of Organic Dyes and Inorganic Compounds in Liquid as Wide-Aperture, Narrowband, Optical Filters*, by JA Trias (in preparation)

²⁷ Senitzky, B, "Narrowband Ultraviolet Vapor Filter," *Applied Optics*, v 14, p 238 to 244, 1975

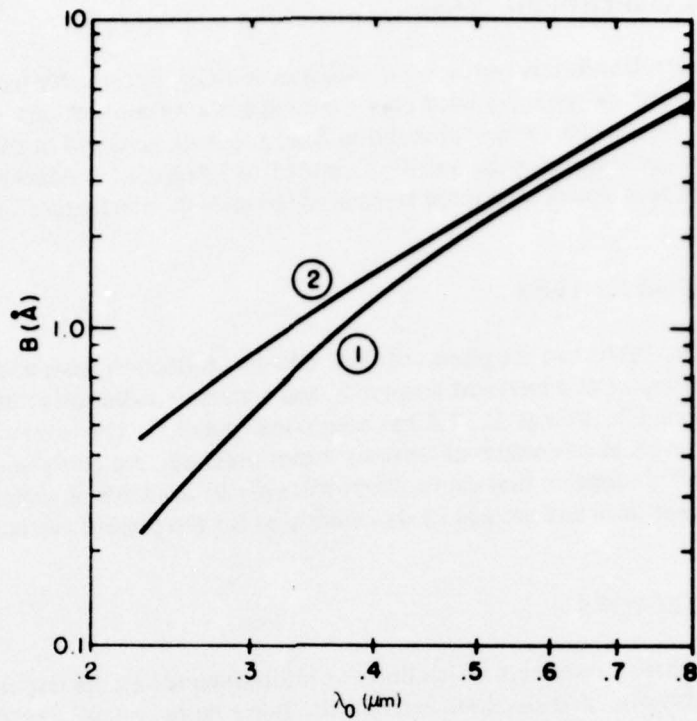


Figure 36. Filter optical passband as a function of the optical wavelength (ref 25).

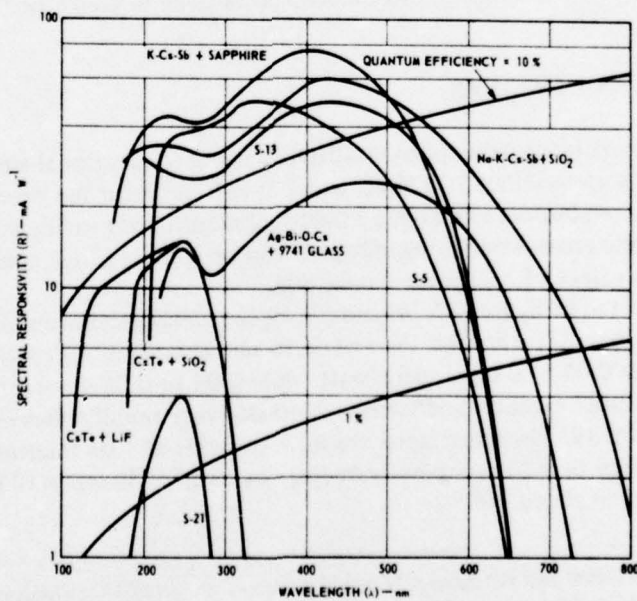


Figure 37. UV-visible photoemitter characteristics (courtesy RCA) (ref 8).

ABSORPTION FILTERS

Absorption filters can be used with a wide FOV, but usually have such a wide bandwidth that they are generally used only for gross filtering applications. Recently, however, a moderate bandwidth (100Å) absorption filter has been achieved in the blue-green with the use of organic dyes having a field of view of ± 45 degrees.²⁶ Absorption filters may also be used to suppress unwanted transmission bands in interference filters.

VAPOR FILTERS

Vapor filters use the phenomena of selective reflection from a vapor. The vapor behaves as a reflector at a resonant frequency and transmits radiation at other frequencies. A mercury vapor UV filter at 2537 Å has been constructed.²⁷ The bandwidth of the filter varies from 0.1Å to 1Å as a function of mercury vapor pressure. An acceptance angle of 7 degrees was achieved. It appears that vapor filters will only be available at certain specific frequencies in the near term and are not likely candidates for the present system.

PHOTODETECTORS

The three parameters which define a photodetector are its responsivity or quantum efficiency, its noise, and envelope bandwidth. For a pulse system, a sufficient bandwidth is required for the detector to respond to a short pulse. Pulse durations as short as about 0.015 microsecond are considered in this study. The advantage of internal detector gain was discussed in section 4. Two types of detectors with internal gain are discussed briefly in this section. A detailed discussion of photodetectors is given in Melchior.²⁸

PHOTOMULTIPLIERS

Commercially available photomultipliers using conventional electrostatic focusing have bandwidths up to about 100 MHz, which is sufficient for the present application. The use of additional electrodes and crossed-field techniques can provide much larger bandwidths. In fact, a dynamic cross-field photomultiplier can be used as a high-speed gated detector to minimize the effect of background radiation.²⁹

As indicated in figures 37, 38 and 39, high-efficiency photomultipliers cover the range from the near UV through the visible to about 0.9 μm . Typical responsivity in the near UV is 0.04 to 0.07 ampere/watt while 0.06 to 0.08 ampere/watt is available in the visible spectrum. Quantum efficiency decreases very rapidly above 0.9 micrometre as indicated in figure 39. However, units are now available at 1.06 micrometre with a 2-percent quantum efficiency or 0.018 ampere/watt responsivity.²³ The gain of photomultipliers typically runs up to about 10^6 .

²⁸ Melchior, H, MB Fisher and FR Arams, "Photodetectors for Optical Communication Systems," *Proceedings of the IEEE*, v 10, p 1466 to 1486, 1970

²⁹ Leverenz, DJ and OL Gaddy, "Subnanosecond Gating Properties of the Dynamic Cross-Field Photomultiplier," *Proceedings of the IEEE*, v 10, p 1487 to 1490, 1970.

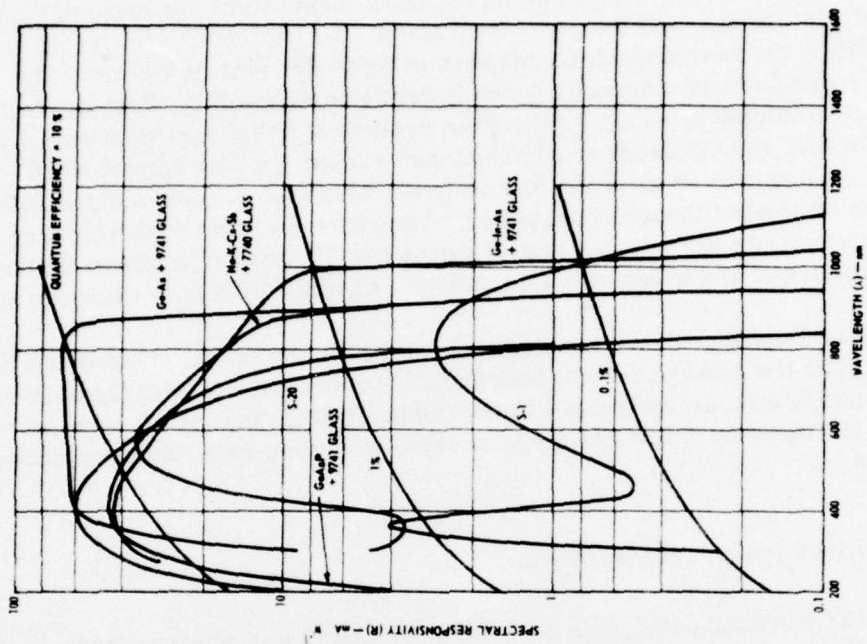


Figure 38. Visible photoemitter characteristics (courtesy RCA) (ref 8).

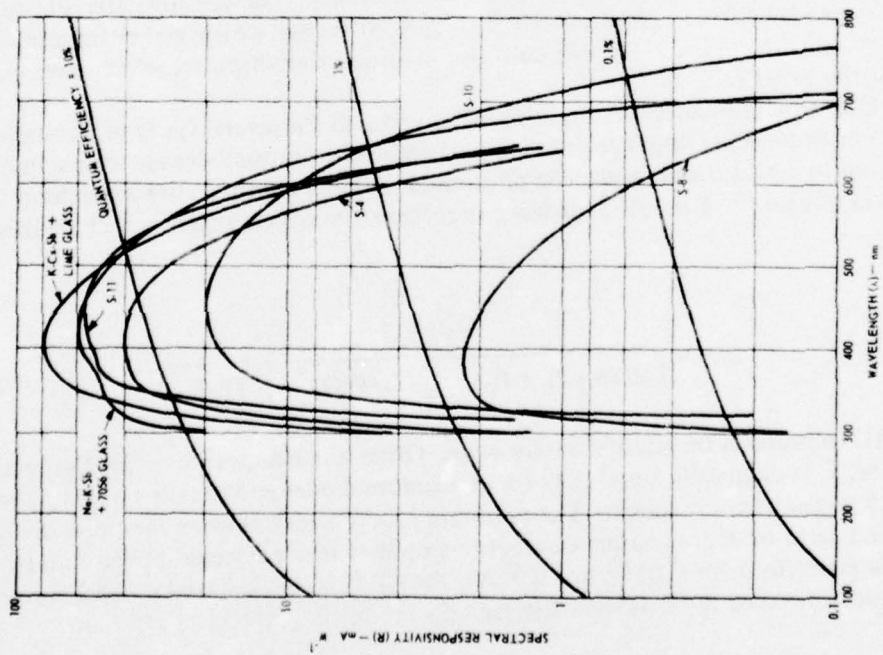


Figure 39. Near infrared-visible photoemitter characteristics (courtesy RCA) (ref 8).

The dark current in a photomultiplier depends upon the type of photoemissive surface, cathode area and temperature. At room temperature, the range of dark current for different surface materials varies from about 10^{-17} to 10^{-13} amperes per square cm. Values for specific materials are given in figure 37. The dark current decreases with temperature and orders of magnitude decreases are possible. Dark-current values for photomultiplier tubes are usually given in amperes rather than amperes per cm^2 and often are given as anode or amplified dark current. A dark current of 10^{-14} ampere was used for most of the link analyses. This value is appropriate at room temperature for most of the spectrum, but 10^{-13} ampere (room temperature) is more typical at $1.06 \mu\text{m}$. For most practical system parameters, the current generated by the daytime background will exceed the dark current. At night the reverse condition usually exists.

Commercial grade photomultiplier tube costs in the visible vary from less than one hundred to a few hundred dollars. Solar-blind UV tubes cost close to a thousand dollars, while near UV costs are comparable to the visible. Prices in the near IR ($1.06 \mu\text{m}$) range up to a few thousand dollars but would be expected to drop once volume production was obtained.

AVALANCHE PHOTODIODES

The avalanche photodiode is a p-n junction detector in which avalanche multiplication is obtained by operation with a high reverse bias voltage. These devices have high internal gain and large bandwidth but have a small light-sensitive area and generate an internal noise which is a function of the gain. The small junction area is required to keep the diode capacitance low (for fast response) and leakage currents small. The sensitive area of avalanche photodiodes varies from about 2×10^{-5} to $2 \times 10^{-3} \text{ cm}^2$ which makes focusing of light onto the area much more difficult than with photomultipliers, which have cathode areas on the order of 1 cm^2 .

Quantum efficiency as a function of wavelength for several types of photodiodes is shown in figure 40. Other characteristics of avalanche photodiodes are shown in table 10. In addition to dark current, avalanche photodiodes have a multiplicative noise term which is a function of gain.²⁸ The S/N expression in section 4 may be written to include this term as:

$$S/N = \frac{S_d^2 P_c^2 G^2}{2qB (S_d(P_b + P_c) + I_d) G^2 F(G) + 4kTB/R_L}$$

where $F(G)$ represents the multiplicative noise. Other quantities were defined in section 4. The factor, F , is essentially equal to G for germanium diodes and usually equal to about the 0.4 to 0.5 power of G for silicon. The optimum gain is achieved when the noise out of the diode (first term in denominator) equals the amplifier thermal noise. Even though the dark current is generally high (10^{-10} to 10^{-9} A), the daytime background current for λ near $1 \mu\text{m}$ is expected to exceed it because of the high S_d (about 0.5 A/W).

TABLE 10. CHARACTERISTICS OF AVALANCHE PHOTODIODES (REF 28).

Diode	Wavelength Range (μm)	Sensitive Area (cm^2)	Dark Current	Avalanche Breakdown Voltage (volts)	Maximum Gain	Multiplication Noise $i^2 \sim M^2 + x$	Current Gain-Bandwidth Product (GHz)	Capacitance (pF)	Series Resistance (Ω)
Silicon n^+p	0.4-1	2×10^{-5}	50 pA at -10V	23	10^4	$x \sim 0.5$	100	0.8 at -23V	6
Silicon $n^+p\pi-p^+$	0.5-1.1	2×10^{-3}		~ 88	200	$x \sim 0.4$	high		
Silicon n^+i-p^+	0.5-1.1			200 to 2000		low	not very high		
PtSi-nSi	0.35-0.6	4×10^{-5}	~ 1 nA at -10V	50	400	$x \sim 1$ for visible illumination	40 for UV excitation	< 1	
Pt-GaAs	0.4-0.88			~ 60	> 100	very low	> 50		
Germanium n^+p	0.4-1.55	2×10^{-5}	2×10^{-8} A at -16V and 300°K	16.8	250 at 300°K $> 10^4$ at 80°K	$x \sim 1$	60	0.8 at -16V	< 10
Germanium n^+p	for 1.54			150					
InAs	0.5-3.5								
InSb at 77°K	0.5-5.5			a few	10	very low			

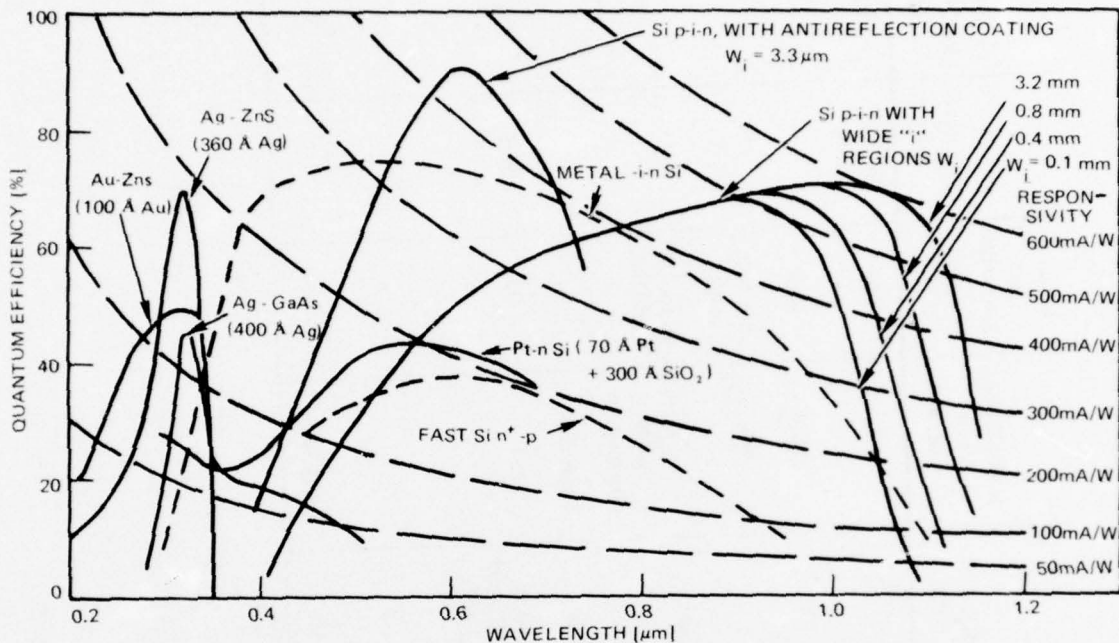


Figure 40. Wavelength dependence of quantum efficiency and responsivity for several high-speed photodiodes (courtesy IEEE) (ref 28).

The S/N for an avalanche diode depends upon the amplifier noise and the form of $F(G)$. Assuming a daytime background, $F = G^{1/2}$ and a low-noise amplifier, an optimum gain on the order of 100 can be obtained. Under these assumptions, the resulting S/N would be just slightly better than the 2-percent quantum efficiency multiplier at $1.06 \mu\text{m}$. The choice between photomultipliers and avalanche diodes requires a detailed consideration of practical design problems. Silicon avalanche photodiodes are in the price range between \$200 and \$2000.³⁰

POINTING AND TRACKING SYSTEMS.

Ship-to-ship and ship-to-RPV-to-ship optical communication links require pointing and tracking systems. Furthermore, as has been demonstrated in the Naval Electronics Laboratory Center OCCULT experiments, high-rate reciprocal pointing and tracking (in which both terminals in a link track each other) can produce orders of magnitude improvement in S/N and acquisition speed over less sophisticated systems. The purpose of this subsection is to briefly summarize what is currently available in such systems.

For shipboard use, the OCCULT system represents the current state of the art. Its specifications call for pointing stability to a given point with peak errors less than ± 0.2 degree ($\pm 3.5 \text{ mrad}$) on a platform experiencing 20-degree rolls with 10-second periods.

³⁰ Medved, D, "Photodiodes for Fast Receivers," *Laser Focus*, v 10, p 45 to 47, 1974

It will be capable of 2-axis (train and elevation) tracking, at rates of 20 degrees per second, either axis. Upon receipt of an acquisition pulse, it will stop searching and return to the correct position ± 0.2 degree in <0.2 seconds, using a 90 degree per second search rate. The system is currently in its prototype test and development stage, with some shipboard tests having been carried out. It appears possible that the pointing accuracy specifications may be exceeded by a factor of two. In its prototype form, it requires 2 metres of standard rack space for the control electronics, plus <0.1 cubic metre for the gimbal and mount. System hardware cost is about \$35 000.

Currently available systems for RPV use are typified by an Army system which is part of a video tracker/laser designator payload weighing a total of 14 kg. It provides a gyro-stabilized platform with tracking in 2 axes, azimuth and elevation. It tracks at a rate of 10-degrees per second, with 360-degree azimuth and 15-degree elevation movement. Pointing accuracy is not known; however, for target-designation purposes (the Army mission) accuracy of <17 mrad (1°) would probably be required. This system has undergone operational tests.

REMOTELY PILOTED VEHICLES

The purpose of this section is to characterize the current and near-term future capabilities of remotely piloted vehicles (RPV) for use as central platforms in OTH optical communication links. Current RPVs range from 11 kg and 2.4 m in wingspan to a remotely piloted F-102A aircraft. Operational requirements for the Navy Fleet and probable system physical specifications for active repeater platforms for use with OTH optical links imply that the smaller RPVs (often termed "mini-RPVs") are adequate. Figure 41 shows the minimum platform altitude (km), H_2 , required to achieve LOS to the platform over a distance, D , km, given a transmitter at altitude H_1 (km). Note that the maximum total communication distance is twice D .

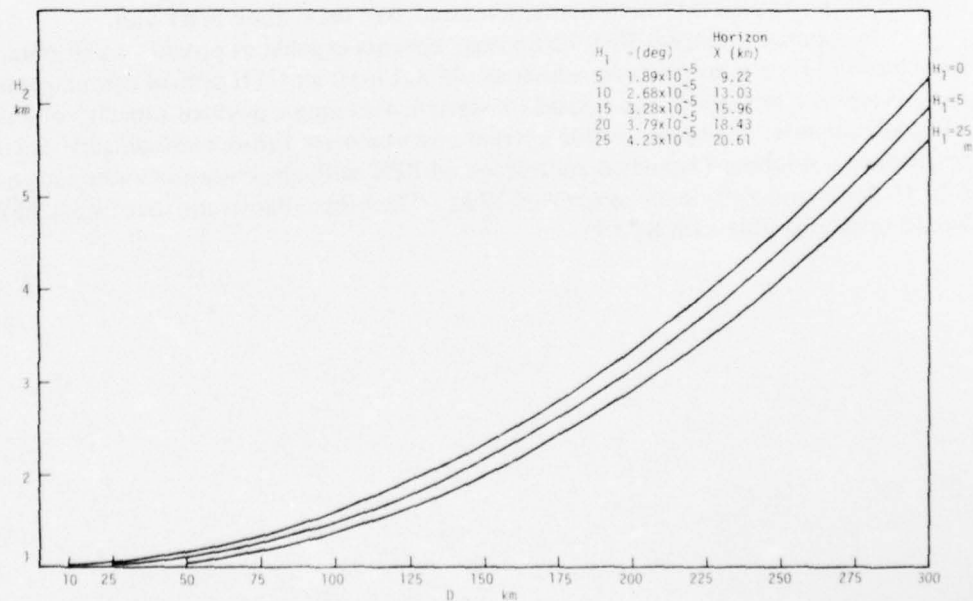


Figure 41. Minimum platform altitude required to achieve line-of-sight.

The ideal RPV would have a radar and optical cross section of zero, a payload of about 90 kg, a range of 150 km, be launched and recovered on-board ship, have an altitude range from 0 to 5 km, and be able to loiter on station as long as desired. Although extreme, most of these specifications are at least approachable within the next 5 years, based on existing RPVs and associated technology. Table 11 summarizes existing small RPVs and those under development. Of special interest for OTH optical communication applications is the Teledyne Ryan mini-RPV, called "STAR" (Ship Tactical Airborne RPV). This RPV was scheduled for flight tests in February 1976. It is to be launched from a ship via pneumatic rail and recovered on-board by landing it in a horizontal net. It can operate either in a preprogrammed mode, thus eliminating the necessity of a command link to the RPV (and increasing the covertness of the RPV), or in a fully controllable command mode. The payload weight can vary from 12 to about 22 kg. With a 12-kg payload, the RPV can fly at a speed of 255 km per hour to a range of 225 km, loiter for 3 hours at a speed of 113 km per hour, and return. Shorter ranges would provide longer loiter times. As presently configured, STAR has a flight ceiling of about 2.5 km (which, from figure 41, is consistent with its flight range of 200 to 225 km for a reasonable loiter time).

The current STAR payload contains a video tracker and laser designator in a 25-cm diameter, hemispherical, optical dome. The package is gyrostabilized. The estimated lifetime is 10 flights, with the limiting factors being recovery and pilot error (although the RPV has flotation). The engine requires maintenance every 100 flight hours. The cost of such an RPV is heavily dependent upon the payload. With the video tracking/laser designator payload, a cost of \$150 000 per vehicle in quantities of 50 is estimated. This could easily drop to \$200 000 in quantities of 1000, without payload.

The optical and radar cross sections of mini-RPVs are small. Physically, the human eye cannot resolve an object the size of an RPV beyond a range of about 25 km (and it is probable that the actual detection range is less than one fifth of this). Non-human optical detectors can be made to have even greater range limitations by the proper choice of RPV surface finish. The radar cross section can be of the order of two seagulls for an RPV using plastic structural materials and skin (as is done in STAR).

In summary, current RPV technology appears capable of providing a shipboard-launched-and-recovered platform which would not limit an OTH optical communications link, except for the time it can remain on station, assuming a payload capacity of about 11-kg is adequate. It appears within current and near-term future technological capability to produce a shipboard launched and recovered RPV with an on-station endurance of 6 to 10 hours and a payload capacity of 23 kg. The other characteristics of such an RPV would be comparable with STAR.

TABLE 11. CURRENT SMALL RPV PROGRAMS (REF 31).

Prime Contractor	Designation	Mission	Agency	Overall Length, Ft Less Booster, Ft	Overall Span, Ft Wings or Fins, Ft	Body Diameter, Ft	Launch Weight, Lb Less Booster, Lb	Powerplant No of Eng Manufacturer Eng Designation	Guidance	Performance		Remarks
										Speed, MPH	Endurance, Min Or Range, nmi	
Developmental Sciences Inc, Industry, CA	Sky Eye	Surveillance	-	6	11.5	1	50-120	1 101 M McCulloch 12.5 hp	Radio command	120	0-360	Pusher, swept wing, carries payloads to 70 lb.
	Remotely piloted blimp (RPMB)	Surveillance monitoring, measurement	-	55	16	13.5	340	1 Kohler 35 hp	Radio command	65	24-hr	High endurance airborne platform with many applications.
Eglen Hovercraft, Inc, Terre Haute, IN	Falcon	Research testbed, surveillance	-	6	8	.75	28	Pusher type Homelite 4.5 hp	Radio command	80-100	2-hr	Off-the-shelf flying testbed for dev of RPV systems.
	Janus	Reconnaissance	-					Homelite 4.5 hp	Radio command	80-100	3-hr	
Fairchild Space and Electronics Co	Look out	-	Navy	12.7	14.7	2.0	195	1 McCulloch MC 101	Radio command	83	60	Ship launch and recovery.
Lockheed Missiles & Space Sunnyvale, CA	Aequare	Strike Support	USAF/ARPA	2.7	2.4	0.348	68	1 9.3 W McCulloch	Radio command	541	222 km	Feasibility RPV for long-range reconnaissance and laser target designation.

TABLE 11. Continued.

Prime Contractor	Designation	Mission	Agency	Overall Length, ft Less Booster, ft	Overall Span, ft Wings or Fins, ft	Body Diameter, ft	Launch Weight, lb	Powerplant No of Eng Manufacturer Eng Designation	Guidance	Performance		Remarks
										Speed, mi/hr	Endurance, Min or Range, mi	
Northrop Corp	VSTT	Target	Army	3.8	1.74	0.4	174	1 Williams Research WR24-17	Radio command	2893	2 hr+	Recoverable gunnery/missile target drone.
Philco-Ford Aeronutronic Division, Newport Bch, CA	Prairel	Reconnaissance & targeting	ARPA/USAF	2.3	4.0	0.24	34	1 K&B, ST-245	Manual	353 max 235 cruise	Man-portable mini-RPV for real time reconnaissance and laser target designation.
	Praire 2	Reconnaissance & targeting	ARPA/USAF	2.9	3.7	0.305	34	1 Kolby Corp distributed by Sakert Riggs, D-238	Manual with auto plotting	400	Configuration optimized for minimum observables
	Calere	Night recon & targeting	ARPA/USAF	2.29	4.0	0.24	38.4	1 K&B, SR-245	Manual	353 max	Thermal imager utilized for full night capability
Teledyne Ryan Aeronautical San Diego, CA	Auto-lander	Demo	USN/NSWC	3.11	3.7	0.305	39.4	1-Kolbo Corp	Manual	400 max	
	Mini RPV (STAR)	Acquisition, recon, strike	USN/USAF	1.5	2.3	Delta	63		Program & command	565	5 hr	Rail launch & net recovery/or conventional landing gear.

TABLE 11. Continued.

Prime Contractor	Designation	Mission	Agency	Overall Length, Less Booster, ft	Overall Span, Wings or Fins, ft	Body Diameter, ft	Launch Weight, Less Booster, lb	Powerplant No of Eng Manufacturer Eng Designation	Guidance	Performance		Remarks
										Speed, mi/hr	Endurance, Min or Range, mmi	
Lockheed Missiles & Space Sunnyvale, CA	PRV STD	Battle field support	Army	1.8	3.6	0.348	54	1 9.3 W McCulloch	Radio command	564	3 hr	Total system demonstrator. Target acquisition and laser designation.
	RTV-2	Research test	...	4	4.5	0.04	163	1-Marine Corp rotary engine RC-B-33.5 W	Radio command	611	2 hr	Twin boom pusher with tricycle gear.
McDonnell Douglas Astronautics Co, Huntington Beach, CA	Mark 2	Reece / Targeting	USAF/ARPA	2.1	3		57	Ross	Radio command	100 kt.	3 hr	Configuration optimized for minimum observables. Long range.
	Acquiline	Reece	...	1.5	2.7	0.348	36	1-Lycoming	Omega	305	555.6 km	
Northrop Corp, Los Angeles, CA	KJ2R-5	Target	Foreign	3.8	3.5	0.037	154	1 Northrop 0-100-3	Radio control	1278	380 km	Over 65,000 produced.
	MQM-74A Chukar	Target	Navy	3.6	1.7	0.037	146	1 WR 24-6	Radio control	2378	713 km	Recoverable gunnery/missile target drone.
	MQM-74C Chukar 2	Target	Navy	3.8	1.7	0.037	165	1 WR 24-7	Radio control	2703	1185 km	Recoverable gunnery/missile target drone.

³¹ Aviation Week and Space Technology, March 17, 1975

SECTION 7. TRADEOFF CONSIDERATIONS

The level of effort in this study has precluded a rigorous system optimization procedure of the type described by Pratt.³² Such an analysis might be premature anyway, especially for the scatter link, since the system performance depends so strongly upon the link characteristics. Taking advantage of propagation characteristics can be expected to give improvements in performance which can be much more significant than the difference between optimum and reasonable component combinations. For example, flying an active RPV at a 2.5 km altitude rather than at the minimum LOS altitude gives a predicted 30-dB S/N improvement at a range of 90 km for a visibility of 20 km.

Since the link analysis indicated that the desired 150 nmi range could not usually be achieved under typical daytime conditions, the "optimization" procedure (section 3) was to select approximately the best state-of-the-art component parameters and determine system performance for both links. An example of the effect of system parameters on the S/N (see section 4) is given in table 12. It is assumed that the detector has sufficient internal gain that the noise contribution of the following amplifier has negligible effect on S/N. Note that peak power and pulse rate can usually be traded off under a fixed average power constraint. The relations given in table 12 can be used for rapid evaluation of tradeoffs and then the appropriate program in the appendix used for an accurate S/N determination.

Costs for the shipboard system are dominated by the laser and pointing and tracking subsystem. This assumes that expected economies are achieved in plastic optics. For the RPV relay, the laser and pointing-control costs are expected to be significant.

A tradeoff or selection of one of the link types over the others does not seem appropriate at this time. As one progresses from a scatter link to an RPV system, both the cost and the communication range increase. Both could use the same shipboard system and be interchangeable as environmental conditions change.

³²Pratt, WK, LS Stokes and R Hinckley, "Optimization of Optical Communication Systems," *Proceedings of the IEEE*, v 10, p 1737 to 1740, 1970

TABLE 12. EFFECT OF COMPONENT PARAMETERS ON S/N OF A SPECIFIC SYSTEM.

Fixed Parameters		Value
Wavelength		1.06 μm
Detector dark current		10^{-3} A/W
Internal detector gain		(see text)
Variable Parameter	Condition	S/N effect proportional to
Peak power, P	Signal power \gg background	10 log P
	Signal power \ll background	20 log P
Responsivity, S_d	Daytime	10 log S_d , 10 log A
Aperture, A	Night, large received signal	10 log S_d , 10 log A
	Night, small received signal	20 log S_d , 20 log A
Optical Bandwidth, B_o	Daytime	-10 log B_o
	Night	no effect, reasonable B_o
Transmitter divergence, θ_D	Scatter link	Complicated (see section 5), small effect for small θ_D
	Line-of-sight link	-20 log θ_D
Receiver FOV	Scatter link, background limited	no effect in vertical plane -10 log FOV horizontal plane
	Line-of-sight link, background limited	-20 log FOV

SECTION 8. COVERT CONSIDERATIONS

Covert considerations have been alluded to throughout this report. This section briefly summarizes general factors which affect covertness. A more quantitative analysis is recommended before system implementation.

Because of their extremely narrow divergence or beamwidth, laser transmissions are difficult to detect. Jamming is also difficult because of the narrow FOV usually used in receivers. However, the aerosol scatter characteristics present a limit on both covertness and antijamming: signal energy is scattered out of the beam and jamming energy is scattered into the receiver. For this reason, if no other, the scattering characteristics of marine hazes should be well defined. In the long term, spread-spectrum techniques, using tuneable lasers and filters, should be incorporated to enhance the covertness of optical systems.

From an intercept standpoint, the transmitted power should be adjusted to be just sufficient to support the required data rate. However, a reserve of transmitter power is desirable to combat jamming. With this power limitation, an intercept receiver could not be at a much greater range than the communication link. For a LOS link, the intercept receiver would have to be at a much shorter range unless it was on-axis (or nearly so) with the beam. Even for a scatter channel, being off-axis restricts the range because of the scattering function. Scattered power is typically down by 10 dB at 30 degrees off axis, decreasing to -20 dB at 65 degrees and -30 dB at 110 degrees, for marine aerosols. In addition, the angular source size of the beam becomes much larger off-axis which requires a very large receiver FOV, significantly increasing background and pulse dispersion. Clearly, this must be further characterized both experimentally and theoretically.

SECTION 9. CONCLUSIONS AND RECOMMENDATIONS

CONCLUSIONS

An analytical model for OTH laser propagation was developed, based upon the single scattering approximation. The model appears to be in reasonable agreement with limited field data on OTH optical propagation at relatively close) ranges up to 40 km. A more conclusive field test of the model, particularly at longer ranges, would be necessary to accurately assess its utility for OTH optical-scatter communications system design. Based upon the use of systems composed of state-of-the-art (1976) components, the following conclusions were drawn from this analysis:

1. The operating wavelength should be in the 1-to-3 μm range for all links;
2. Both relay and scatter OTH data links can use the same shipboard system;
3. Significant performance advantages can be achieved by exploiting propagation characteristics. These include:
 - (a) Use of a vertical fan beam or optimally elevated beams in a scatter link, and
 - (b) Positioning the relay platform at a high altitude to take advantage of the decrease in path loss caused by the vertical decrease in aerosol concentration;

4. The primary factor which determines the percentage of time communication over a given distance at a given bit rate can be achieved is the meteorological visibility. Statistical studies of the occurrence of visibilities greater than a given value are available. The accumulated statistics were analyzed to determine the general availability of an optical scatter-link communications capability having bit rates of 2400 and 75 bits per second at a bit-error rate of less than 10^{-5} . When the statistics are summed for all ocean areas the following results are obtained for daytime:

<u>Availability</u>	<u>2400 bits/sec</u>	<u>75 bits/sec</u>
85%	55 km	85 km
70%	100 km	165 km

The 85-percent availability is equatable to a meteorological visibility condition of 10 km and the 70-percent availability to 20-km visibility. Higher availabilities and longer ranges can be achieved with improved meteorological visibilities. For example, in the Mediterranean, the communication ranges listed for a visibility of 20 km can be achieved with an availability of 95 percent; and

5. The communications ranges are considerably greater (by factors of 2 to 3) at night, or if low clouds occur to provide a scattering layer. It is important to note that areas of operation with lower average visibility (eg, the North Atlantic) also have a high occurrence of low cloud cover. The interpretation of the visibility data on range, data rate, and availability requires further characterization.

Performance predictions for state-of-the-art systems for a number of conditions are given in tables 3 and 4 of section 3. Section 3 discusses the system concepts and gives a more detailed summary than that presented here.

RECOMMENDATIONS

The forward-scatter link analysis presented in this report is based upon a single scattering model. While the model gives reasonable agreement with the limited field data, it is strongly recommended that experiments be designed and carried out to assess the validity of the model. The experiments might well include simultaneous pulsed measurements at two wavelengths (ie, 1.06 and 0.53 μm) since the analysis predicts large differences as a function of wavelength. The performance gain achieved by the use of elevated beams and exploitation of clouds should be evaluated. It is recommended that fading rate and other data be obtained to allow evaluation of time, spatial, and receive-angle diversity receiver techniques.

It is recommended that the development of economical pointing and tracking subsystems be continued, since this is one of the major cost items in a shipboard system. On a long-term basis, the development of tunable lasers in the 1- μm region should be encouraged so that spread-spectrum techniques could be used. Tunable filters are currently available. It is also recommended that careful consideration be given to the potential economies and resulting increase in practical system performance levels which may be realized with the development of low-cost plastic optical systems for communications use.

Because a primary factor determining link availability is that of the meteorological conditions prevailing over the link, it is strongly recommended that experiments be carried out to verify the meteorological effects upon propagation predicted by the models. It is also strongly recommended that an integrated and systematic capability for measuring and predicting the meteorological conditions predominating over a path be developed. This might well take advantage of a combination of optical measurements and existing microwave meteorological measurement capabilities.

APPENDIX A: INCORPORATION OF THE PROPAGATION MODELS IN THE COMPUTER PROGRAMS.

When work on the task covered by this report began it was thought that existing Monte Carlo computer codes would be employed to produce the numerical results required for the system tradeoff studies. This was not done for several reasons. First, an analytical model for the over-the-horizon (OTH) case was developed (see appendix A) which has resulted in several important insights, and considerable simplification in characterizing practical communications links. It was felt that it was important to incorporate this model into a computer program in order to exploit these advantages. Second, the Monte Carlo codes could not model the OTH case without modifications which would not be completed in the time frame necessary to meet task milestones. Third, the line-of-sight (LOS) propagation mode (eg, using an RPV) could be adequately modeled without resorting to the cost and complexity of using the Monte Carlo codes.

Both the OTH and LOS propagation models were incorporated into interactive computer programs written in the BASIC language, for use on a minicomputer. The result is a tool which permits the scientist and system engineer to explore both the propagation models and potential system designs interactively, with high efficiency. The benefits which have resulted from this effort have far outweighed the unanticipated additional effort. This appendix describes how the OTH and LOS models were incorporated into these programs, including the approximations used. The programs themselves are described in appendix C (OTH) and appendix D (LOS), along with user instructions and listings. Because this programming effort was not originally planned, an effort has been made to keep the documentation as brief as possible, consistent with providing enough information for other researchers to make use of the programs.

The OTH model is described in detail in appendix E. However, in order to use it, certain parameters are required. The extinction coefficient, β , must be calculated as a function of wavelength, λ , and meteorological range (also termed visibility), V . As discussed by Woodman³³, the most widely used expressions for calculating $\beta(\lambda, V)$ underestimate β by a factor of from 2 (at $\lambda = 1\mu$, $V = 23.5$ km) to greater than 10 (at $\lambda = 10\mu$, $V = 23.5$ km), with much higher errors for smaller values of V . Note that this underestimates the attenuation by factors of from 5 to $>5 \times 10^3$. Elterman³⁴ has done an extensive study of available models and experimental results, and derived an expression for $\beta(V, \lambda)$ which is consistent and in good agreement with experimental results for the range $.27\mu \leq \lambda \leq 2.17\mu$, for $V \geq 2$ km. Surface aerosol distributions characteristic of hazes with $2 \text{ km} \leq V \leq 13 \text{ km}$ are assumed. Elterman³⁴ considers the effects of such parameters as aerosol distribution, mixing layers, scale height, and the approximations used in deriving his results in great detail, none of which will be repeated here. However, it is clear that, for the system engineering purposes of the work described in this report, the Elterman model is quite adequate for the above range of wavelengths and for $V \leq 13$ km, which Elterman takes as the boundary between haze and clear conditions. The numerical results presented in this report include values for V as high as 390 km. The Elterman formula was used, without modification, for these values of V .

³³Woodman, Douglas P, "Limitations in Using Atmospheric Models for Laser Transmission Estimates," *Applied Optics*, v 13, p 2193 to 2195, 1974

³⁴Elterman, L, "Relationships Between Vertical Attenuation and Surface Meteorological Range," *Applied Optics* v 9, p 1804 to 1810, 1970

This was felt to be justified for two reasons; first, due to the methods used by Elterman,^{3,4} it should produce conservative values for β for $V > 13$ km; second, the values for the extinction coefficient for $13 \text{ km} \leq V \leq 336 \text{ km}$ (the Rayleigh limit) at $\lambda = 0.55\mu$ agree well with the values given by the Elterman formula for these values of V . The Elterman formula is

$$\beta(V, \lambda) = \frac{\beta(4, \lambda) [(3.91/V) - \beta_r]}{[(3.91/4) - \beta_r]} \quad (1)$$

V is in kilometers and β and β_r are km^{-1} . The formula is normalized to $V = 4$ km, hence the numerical factors of 4. β_r is the Rayleigh attenuation coefficient at $\lambda = 0.55\mu$, $\beta_r = 1.162 \times 10^{-2} \text{ km}^{-1}$. The computer programs store a table of values (given by Elterman) for $\beta(4, \lambda)$. Linear interpolation on the logarithms of the tabular values as a function of the logarithm of the wavelength is used to find $\beta(4, \lambda)$ for the particular value of λ desired, and equation (1) then gives $\beta(V, \lambda)$. The use of log-log interpolation was arrived at empirically after trying various polynomial interpolation methods. This method of interpolation produces values of β for intermediate values of λ which are at least as accurate as the model.

Elterman gives values of $\beta(4, \lambda)$ only for $0.27\mu \leq \lambda \leq 2.17\mu$. To extend these values to 10.2μ , some theoretical values of $\beta(23.5, \lambda)$, computed by Barnhardt and Street and given by Woodman (B1), were used. These values were adjusted to a meteorological range of 4 km using equation (1). These theoretical values agreed with Elterman's values where the range of wavelengths involved overlapped. There is no limitation in the theory used to derive equation (1) which would preclude its use at 10.2μ .

The definition and choice of the equation for the signal-to-noise ratio is discussed in detail in section 4 of the basic report. As used in the computer programs, the signal-to-noise ratio (S/N) is given by

$$S/N = S_d^2 P_c^2 / \left\{ 2qB[S_d(P_b + P_c) + I_d] \right\} \quad (2)$$

S_d is the detector responsivity, given by

$$S_d = \eta q / h\nu, \quad (3)$$

where

- η is the detector quantum efficiency,
- q is the electronic charge (coulombs),
- h is Planck's constant (joule-sec),
- ν is the carrier frequency (Hz),
- P_c is the received carrier power (watts),
- B is the electrical bandwidth of the system (Hz),
- P_b is the background power incident on the detector (watts), and
- I_d is the detector dark current (amperes).

The model for the background noise power is discussed in section 5 of the basic report. As implemented in the computer programs,

$$\tilde{P}_b = P_o + 4.75 \times 10^{-3} / \left\{ \lambda^{13/2} [\exp(2.44/\lambda) - 1] \right\}, \text{ daytime,} \quad (4)$$

$$= P_o + 8.3 \times 10^{-3} / \left\{ \lambda^{13/2} [\exp(2.44/\lambda) - 1] \right\}, \text{ nighttime,} \quad (5)$$

$$P_o \equiv 0, \lambda < 1.8\mu$$

$$\equiv 1.2 \times 10^8 / \left\{ \lambda^5 [\exp(50/\lambda) - 1] \right\}, \lambda \geq 1.8\mu.$$

The neglect of the P_o term avoids a numerical problem in the computations without altering the results. In these equations, λ is in micrometres, and \tilde{P}_b is in $W m^{-2} Sr^{-1} \mu^{-1}$. In other words, \tilde{P}_b is the background spectral radiance. It thus is necessary to multiply \tilde{P}_b by the receiver aperture area, the receiver optical bandwidth, and the receiver solid angle FOV in order to obtain P_b . Although the aperture area and optical bandwidth are specified, care must be exercised in the value used for the solid angle intercepted by the receiver field of view. It can be shown that for a circularly symmetric FOV of full angle θ , the solid angle intercepted is

$$2\pi [1 - \cos(\theta/2)]. \quad (7)$$

For small θ this reduces to $\pi\theta^2/4$. In the OTH case, it is reasonable to expect that the receiver FOV may be broader vertically (full angle θ_1) than horizontally (full angle θ_2) (see appendix E). This permits accommodating the vertical fan beam, while minimizing the background power received horizontally. As an approximation, the solid angle intercepted by the receiver field of view for computing the background power is calculated as $\pi\theta_1\theta_2/4$ for the OTH case. A circularly symmetric FOV is assumed for the line-of-sight (LOS) case.

For the OTH case, it is necessary to know $f(\theta)$ for $\theta = 0^\circ$, where $f(\theta)$ is the gain over isotropic for aerosol scattering at the scattering angle θ (ie, the ratio of the actual scattering cross section at angle θ to that of an isotropic scatterer of identical total scattering cross section). This is available in Deirmendjian's book³⁵ as a function of wavelength and aerosol size distribution. Values for two distributions, a continental haze "L" and a marine haze "M", are stored as a function of wavelength by the computer programs, and "log-log" interpolation is used to generate $f(0^\circ)$ for a particular wavelength.

³⁵ Deirmendjian, D., *Electromagnetic Scattering on Spherical Polydispersions*, American Elsevier Publishing Company, Inc, 1969

APPENDIX B: OTH PROGRAM DESCRIPTION

The OTH propagation model, as described in appendix E, is incorporated into an interactive program. This program is designed to permit the user to choose the range and step size of the independent variable, to easily vary parameter values, and to print out the path loss and signal-to-noise ratio as a function of the independent variable in tabular form.

The program will be described by referring to the line numbers of the various program modules and their subsets. A sample console listing and output precede the program listing. The program is written in BASIC, and has been run on a Data General NOVA 800 computer. It should execute without modification on any other manufacturer's computer under a BASIC interpreter which accepts standard Dartmouth BASIC. The only exception to this statement is the use of a form of the INPUT statement which includes a string of text to be printed prior to the question mark which requests a user response. These statements can be replaced by a PRINT statement and the standard INPUT statement if required.

The computation portion of this program is marginally compute bound for the pencil beam case and strongly compute bound for the fan beam case (using a teletype as the output device). For comparison, compute bound FORTRAN programs tend to execute on the NOVA 800 at from 1 to 3 times the speed of execution for the same program (level G compiler) on an IBM 360/67 running under OS. Of course, a compute bound BASIC program will execute on the order of a factor of ten times slower on the NOVA 800 than a FORTRAN program doing the same computations. The response time of the interactive program is quite adequate.

10-450: Set up parameter and variable values.

This section of the program initializes the variable and parameter values. The arrays dimensioned in statements 30 and 35 are used as follows:

- W, B Wavelength and associated value (respectively) of the extinction coefficient at $\lambda = 0.55\mu$, $V = 4\text{km}$. This forms the table used by the interpolation routine to compute $\beta(V, \lambda)$ using Elterman's model (see appendix A).
- X, Y Temporary arrays used as the working storage of the interpolation routine.
- P Stores the parameter values.
- N, M Wavelength and associated value (respectively) of the forward scattering coefficient, $f(0)$, for a marine haze aerosol distribution.
- O, L The same as N, M, but for a continental haze aerosol distribution.
- V Stores the three possible independent variable values.

The subroutine at 4130 is called to fill the tables used for interpolation and to put the default parameter values into P. The aerosol distribution to be assumed is chosen, and the fan or pencil (0° divergence) beam case is specified. For the fan beam case, the default beam angle is printed as a reminder; this is the angle over which the received power is averaged. For the pencil beam case the default receiver vertical field of view value is printed. For both cases, the program integrates the received power over this field of view. If the user decides to change any of the default parameter values, the subroutine at statement 4570 is called.

There are three possible independent variables: wavelength, path length, and meteorological range. The user enters the starting value for the desired independent variable, values for the other two, specifies which of the three is the independent variable and then enters the increment and number of independent variable values to be looped over. Finally, the choice is made between day or night background power values to be used in computing the signal-to-noise ratio.

460-630: Begin the loop over the independent variable, and compute path loss

This series of statements controls calls to the various subroutines necessary to compute the path loss. At statement 630, P5 is the path loss, defined as follows:

$$P5 = \frac{P_{rec}}{P_{trans} A_{rec} f(0^\circ)} \quad (B1)$$

where P_{rec} is the received power, P_{trans} is the transmitted power, A_{rec} is the area of the receiver aperture in m^2 , and $f(0^\circ)$ is the forward scattering coefficient (see appendix A).

635-971: Computation of signal-to-noise ratio

Depending on the aerosol distribution chosen, the scattering coefficient is calculated in lines 650-830. The background power is computed in lines 850-950. The test on the value of λ at line 872 and its subsequent results avoid an underflow problem at line 875. This does not affect the accuracy of the result. At line 971, S1 is the signal-to-noise ratio, defined as given in equation 2) of appendix A.

1000-1050: Output

As currently written, line 1000 prints the value of the independent variable, the path loss, the path loss in dB, the signal-to-noise ratio, and the signal-to-noise ratio in dB. The program then gives the user the option of terminating execution or initiating another run.

2500-2590: Integration over field of view

This subroutine integrates the path loss over the receiver field of view; the result is Z3. The variables are as follows:

- H1, H2 Height of transmitter, receiver in km
- R1 4/3 earth radius, in km
- D1 propagation range, in km
- F2 vertical field of view of the receiver, rads.

The integration loop is from 2550 to 2580. The choice of 0.003 radian as the integration step size is arbitrary, a choice that provides adequate accuracy for most practical fields of view while maintaining reasonable response time for the program. For a much longer run in which execution time can become quite significant, the step size can be chosen as F2/5. This provides accuracy consistent with the accuracy of the model. The

number of iterations through this loop, and the number of iterations through the loop which starts at line 2620, control the primary execution speed versus accuracy tradeoff possible for the programs in this and the following appendix.

2600-3230: Average over fan beam and compute path loss

This routine, and the short auxiliary routine in lines 3500-3520, compute the path loss, Z5, as given in equation B1). The additional variables not already defined are as follows:

- P1, P2 Azimuthal pointing angles (transmitter, receiver) in radians, measured relative to the great circle path.
- B \emptyset the extinction coefficient in km^{-1}
- H \emptyset the aerosol lapse rate, in km^{-1} (the aerosol density as a function of height, h, is proportional to $\exp(-h/H\emptyset)$)
- A1, A2 elevation angles (transmitter, receiver) of the beam in radians, relative to the local horizontal, measured positive downwards.
- F1 vertical fan angle of the transmitter, in radians

The details of the computations of this routine can be deduced by comparison with the equations in appendix E. See also the comments under "Caution."

4000-4450: Default model parameters

The parameters (stored in array P) their default values, units, and the names of the variables to which they are equated (if other than the P array) are listed in lines 4030-4170. The units used for these parameters were chosen to facilitate interactive input.

4460-4550: Equate Variables and Convert Units

This routine equates the P array values to the variables used in the other routines, converting units as required. Note that some parameters are used directly from the P array. Unit conversion for these values is carried out where they are used.

4560-4710: Changes parameter values interactively

6000-6170: Interpolation

This routine performs "log-log" interpolation on tabular data. Arrays Y and X store the dependent and independent tabular values. The values must be monotonically increasing, but need not be equally spaced. There are M1 table entries, and Y1 = Y(X9) is the value returned. The dimension statement (line 30) assumes $M1 \leq 50$. Extrapolation is performed if required.

7000-7170: Evaluates $\beta(V, \lambda)$

This routine evaluates the extinction coefficient, B \emptyset (in km^{-1}) for a given value of wavelength in microns, L5, and a given value of meteorological range in km, V5. The method used is described in appendix A.

Caution

There is a potential numerical difficulty with this program as it appears in the listing. Care should be taken when running this program in single precision arithmetic. Care was taken to assure that this numerical problem would not and did not affect any of the numerical values presented in this report.

Program Listing:
OTH Modeling Program

```

RUN
AEROSOL DISTRIBUTION: MARINE(1) OR CONTINENTAL(2):1

FAN(1) OR PENCIL(2) BEAM:2
DEFAULT VERTICAL FIELD OF VIEW= 1 DEGREES.
PARAMETER CHANGES (1=YES, 0=NO):1

ENTER SUBSCRIPT OF PARAMETER TO BE CHANGED (FOR A LIST
OF SUBSCRIPTS AND CURRENT VALUES, LIST LINES 4010
TO 4170): ? 5

NEW VALUE: ? 1.2987

NEXT SUBSCRIPT (0 IF DONE): ? 0

INPUT VARIABLES. ENTER START VALUE FOR INDEPENDENT VAR
1. WAVELENGTH: ? 1.06
2. PATH LENGTH: ? 20
3. METEOROLOGICAL RANGE: ? 10

INPUT SUBSCRIPT OF INDEPENDENT VARIABLE: ? 2

INCREMENT, NUMBER OF VALUES: ? 10,15

DAY(1) OR NIGHT(2):1

```

20	1.42987E-10	-98.4471	8932.73	30.5009
30	8.75197E-12	-110.579	160.329	22.0502
40	6.74769E-13	-121.709	1.23466	.915507
50	5.5935E-14	-132.523	8.68066E-03	-20.6145
60	5.27055E-15	-142.782	7.72184E-05	-41.1223
70	5.65393E-16	-152.477	8.88765E-07	-60.5122
80	6.29178E-17	-162.012	1.10063E-08	-79.5836
90	7.9084E-18	-171.019	1.73889E-10	-97.5974
100	1.06892E-18	-179.711	3.17675E-12	-114.98
110	1.57904E-19	-188.016	6.93233E-14	-131.591
120	2.50858E-20	-196.006	1.74965E-15	-147.571
130	4.37443E-21	-203.591	5.32032E-17	-162.741
140	8.19636E-22	-210.864	1.86783E-18	-177.287
150	1.71979E-22	-217.645	8.22333E-20	-190.85
160	3.78912E-23	-224.216	3.98972E-21	-203.991

```

END OF RUN. ANOTHER (1=Y, 0=NO): ? 0

END AT 9999
*

```

```

0010 REM OTH PROPAGATION MODELING PROGRAM.
0020 REM MEGATEK CORPORATION, DECEMBER, 1975
0030 DIM W(21),B(21),X(50),Y(50),P(14),M(13),L(10),N(13)
0035 DIM O(10),V(3)
0037 DEF FNA(X)=10*.434295*LOG(X)
0040 LET R1=4*6370/3
0060 REM FILL PARAMETER ARRAY.
0070 GOSUB 4130
0080 INPUT "AEROSOL DISTRIBUTION: MARINE(1) OR CONTINENTAL(2):",Q1
0090 PRINT " "
0092 INPUT "FAN(1) OR PENCIL(2) BEAM:",Q4
0094 IF Q4=2 GOTO 0097
0095 PRINT "DEFAULT FAN ANGLE=";P(6);" DEGREES."
0096 GOTO 0110
0097 PRINT "DEFAULT VERTICAL FIELD OF VIEW=";P(7);" DEGREES."
0100 REM CHECK TO SEE IF ANY PARAMETER CHANGES
0110 INPUT "PARAMETER CHANGES (1=YES, 0=NO):",Q2
0120 PRINT " "
0130 IF Q2=0 GOTO 0210
0140 GOSUB 4570
0150 REM DETERMINE INDEPENDENT VARIABLE. VARIABLES ARE:
0160 REM 1 WAVELENGTH (MICRONS) L5
0170 REM 2 PATH LENGTH (KM) D1
0180 REM 3 METEROLOGICAL RANGE (KM) V5
0210 PRINT "INPUT VARIABLES. ENTER START VALUE FOR INDEPENDENT VAR"
0220 PRINT "1. WAVELENGTH:";
0230 INPUT V(1)
0240 PRINT " "
0250 PRINT "2. PATH LENGTH:";
0260 INPUT V(2)
0270 PRINT " "
0280 PRINT "3. METEROLOGICAL RANGE:";
0290 INPUT V(3)
0300 PRINT " "
0370 PRINT "INPUT SUBSCRIPT OF INDEPENDENT VARIABLE:";
0380 INPUT Q6
0390 PRINT " "
0400 LET V1=V(Q6)
0410 PRINT "INCREMENT, NUMBER OF VALUES:";
0420 INPUT V2,V3
0430 PRINT " "
0440 REM DAY OR NIGHT AFFECTS BACKGROUND POWER VALUE.
0450 INPUT "DAY(1) OR NIGHT(2):",Q3
0460 REM*****LOOP OVER INDEPENDENT VARIABLE STARTS HERE*****
0470 FOR Q5=1 TO V3
0480 REM CALCULATE P5=PR/(PT*A*F), WHERE PR=POWER RECEIVED, PT=
0490 REM POWER TRANSMITTED, A=RECVR AREA, F=SCATTERING F'N.
0495 LET V(Q6)=(Q5-1)*V2+V1
0500 REM CALCULATE EXTINCTION COEFFICIENT, IF V(1) OR V(2) HAS CHANGED.
0510 IF Q5=1 GOTO 0540
0520 IF Q6<>3 GOTO 0540

```

```

0530 GOTO 0570
0540 LET V5=V(3)
0550 LET L5=V(1)
0560 GOSUB 7050
0570 LET D1=V(2)
0580 IF Q4=1 GOTO 0620
0590 REM PENCIL BEAM
0600 GOSUB 2510
0605 LET P5=23
0610 GOTO 0650
0615 REM FAN BEAM
0620 GOSUB 2600
0630 LET P5=24
0635 REM*****AT THIS POINT P5="FATH LOSS" AS DEFINED ABOVE*****
0640 REM COMPUTE SCATTERING FUNCTION, F5
0650 IF Q1=2 GOTO 0750
0655 REM MARINE HAZE
0660 FOR I1=1 TO 13
0670 LET X(I1)=NL(I1)
0680 LET Y(I1)=M(I1)
0690 NEXT I1
0700 LET M1=13
0710 LET X9=V(1)
0720 GOSUB 6030
0740 GOTO 0830
0750 REM CONTINENTAL HAZE.
0760 FOR I1=1 TO 10
0770 LET Y(I1)=L(I1)
0780 LET X(I1)=OL(I1)
0790 NEXT I1
0800 LET M1=10
0810 LET X9=V(1)
0820 GOSUB 6030
0830 LET F5=Y1
0840 REM P6=RECEIVED POWER
0850 LET P6=P5*P(13)*3.14159*P(12)*P(12)*F5
0860 REM COMPUTE S/N RATIO.
0870 REM COMPUTE P7=BACKGROUND.
0871 LET P8=0
0872 IF V(1)<1.8 GOTO 0880
0875 LET P8=1.2E+08/(V(1)+5*(EXP(50/V(1))-1))
0880 IF Q3=2 GOTO 0950
0890 REM DAYTIME BACKGROUND
0900 LET P7=4750/(V(1)+6.5*(EXP(2.44/V(1))-1))+P8
0930 GOTO 0960
0940 REM NIGHTTIME BACKGROUND
0950 LET P7=.0083/(V(1)+6.5*(EXP(2.44/V(1))-1))+P8
0960 LET P7=P7+6.28318*(1-COS(F2/2))*3.14159*P(12)*P(12)*P(14)
0970 LET S1=2*1.60219E-19*P(10)*(P(9)*(P7+P6)+P(11))
0971 LET S1=P(9)+P(9)*P6+P6/S1
0980 REM*****AT THIS POINT S1=SNR*****

```

```

0990 REM*****OUTPUT ROUTINE SHOULD BE INSERTED HERE*****
1000 PRINT V(Q6),P5,FNA(P5),S1,FNA(S1)
1010 NEXT Q5
1020 PRINT "END OF RUN. ANOTHER (1=Y, 0=NO):"
1030 INPUT Q8
1040 IF Q8=0 GOTO 9999
1050 GOTO 0080
2500 REM FOV INTEG
2510 LET A3=ATN(SQR(2*H2/R1))
2520 LET A4=COS(A3)*COS(P2)+SIN(A3)*(D1/(2*R1)+(H2-H1)/D1)
2530 LET A4=A4/SQR(1+(D1/(2*R1)+(H2-H1)/D1)*(D1/(2*R1)+(H2-H1)/D1))
2540 LET A4=ATN(SQR(1-A4*A4)/A4)
2545 LET Z3=0
2550 FOR B2=A4 TO A4+F2 STEP .003
2560 GOSUB 3000
2570 LET Z3=Z3+Z5*.003
2580 NEXT B2
2590 RETURN
2600 REM FAN AVG
2610 LET A5=ATN(SQR(2*H1/R1))
2615 LET Z4=0
2620 FOR A6=-A5 TO -A5+F1 STEP F1/5
2630 LET A1=-A6
2640 GOSUB 2510
2650 LET Z4=Z4+Z3*.2
2655 NEXT A6
2660 RETURN
3000 REM Z5=PR/(PT+A(SQM)*F(Q))
3010 LET R1=COS(A1)*COS(P1)+SIN(A1)*(D1/(2*R1)+(H1-H2)/D1)
3020 LET R1=R1/SQR(1+((H2-H1)/D1-D1/(2*R1))*(H2-H1)/D1-D1/(2*R1)))
3030 LET R1=ATN(SQR(1-R1*R1)/R1)
3040 LET Z1=D1*SIN(R2)/SIN(R1+R2)
3050 LET Z2=D1*SIN(R1)/SIN(R1+R2)
3060 LET A2=SIN(A1)*COS(D1/R1)-COS(P1)*COS(A1)*SIN(D1/R1)
3070 LET A2=(A2+Z1+H2-H1+D1*D1/(2*R1))/Z2
3080 LET A2=ATN(A2/SQR(1-A2*A2))
3090 LET Y9=SQR(R1/(2*H0))*TAN(A1)
3095 LET YR=Z1*COS(A1)/SQR(2*R1*H0)
3096 LET X1=-Y9
3097 GOSUB 3510
3098 LET G2=G1*SGN(-Y9)
3099 LET Y1=YR-Y9
3100 GOSUB 3510
3110 LET G2=G2-G1*EXP(2*YR*Y9-YR*YR)*SGN(YR-Y9)
3120 LET G2=G2+EXP(Y9*Y9)*(SGN(YR-Y9)-SGN(-Y9))
3130 LET L1=-B0*SQR(2*R1*H0)*G2+.886227*EXP(-H1/H0)/COS(A1)
3145 LET L1=EXP(L1)
3150 LET Y9=SQR(R1/(2*H0))*TAN(A2)
3160 LET YR=Z2*COS(A2)/SQR(2*R1*H0)
3170 LET X1=-Y9
3180 GOSUB 3510
3185 LET G2=G1*SGN(-Y9)
3190 LET X1=YR-Y9
3195 GOSUB 3510
3200 LET G2=G2-G1*EXP(2*YR*Y9-YR*YR)*SGN(YR-Y9)

```

```

3205 LET G2=G2+EXP(Y9*Y9)*(SGN(Y8-Y9)-SGN(-Y9))
3206 LET L2=-R0+SOR(2*R1+H0)+G2*.886227*EXP(-H1/H0)/COS(A2)
3207 LET L2=EXP(L2)
3210 LET Z5=H1+Z1+Z1*COS(A1)+COS(A1)/(2*R1)-Z1*SIN(A1)
3220 LET F5=.000001*L1+L2+R0*EXP(-Z5/H0)/(4*3.14159*D1*SIN(B1))
3230 RETURN
3500 REM G1(X1)
3510 LET T1=1/(1+.47047*ABS(X1))
3520 LET G1=(((.747856*T1)-9.5879RE-02)*T1+.348024)*T1
3530 RETURN
4000 REM SUBROUTINE TO SET MODEL PARAMETERS.
4010 REM SUB QUANTITY                                DEFAULT NAME
4020 REM                                             VALE
4030 REM 1 TRANSMITTER HEIGHT (M)                    25      H1 (KM)
4040 REM 2 RECEIVER HEIGHT (M)                       25      H2 (KM)
4050 REM 3 AZ. POINTING ANGLE (DEG) REL. TO          0       P1 (RAD)
4060 REM 4 GREAT CIRCLE PATH (1=TRANS, 2=RECVR)      0       P2 (RAD)
4070 REM 5 AEROSOL LAPSE RATE (KM)                   100     H0 (KM)
4080 REM 6 VERTICAL FAN ANGLE(DEG)-FAN CASE ONLY     4       F1 (RAD)
4090 REM 7 VERTICAL FIELD OF VIEW (DEG)              1       F2 (RAD)
4100 REM 8 ELEVATION ANGLE (DEG) REL. TO LOCAL      0       A1 (RAD)
4110 REM      HORIZ. OF TRANS. (POS. DOWNWARDS)
4120 REM 9 DETECTOR RESPONSIVITY                     .065    P(9)
4130 REM 10 SYSTEM ELECTRICAL BANDWIDTH (HZ)        7E7     P(10)
4140 REM 11 DETECTOR DARK CURRENT (AMPS)            1E-14   P(11)
4150 REM 12 RECEIVER APERTURE RADIUS (M)            .05     P(12)
4160 REM 13 TRANSMITTER POWER (W)                   1E6     P(13)
4170 REM 14 RECEIVER OPTICAL BANDWIDTH (MICRONS)  1E-3    P(14)
4180 RESTORE
4190 FOR I9=1 TO 14
4200   READ P(I9)
4210 NEXT I9
4220 DATA 25,25,0,0,100,4,1,0,.065,7E+07,1E-14,.05,1E+06,.001
4230 REM STUFF W AND B ARRAYS FOR EXTINCTION COEFFICIENT.
4240 FOR I9=1 TO 21
4250   READ W(I9),B(I9)
4260 NEXT I9
4270 DATA .27,2,.28,1.89,.3,1.78,.32,1.67,.34,1.56
4280 DATA .36,1.45,.38,1.4,.4,1.3,.45,1.15,.5,1.05,.55,.966
4290 DATA .6,.86,.65,.78,.7,.73,.8,.64,.9,.58,1.06,.52
4300 DATA 1.26,.47,1.67,.4,2.17,.36,10,.312
4310 REM STUFF SCATTERING COEFFICIENTS - M, N=
4320 REM VALUE, WAVELENGTH FOR MARINE HAZE; L, O=VALUE, WAVELENGTH
4330 REM CONTINENTAL HAZE.
4340 FOR I9=1 TO 13
4350   READ N(I9),M(I9)
4360 NEXT I9
4370 DATA .45,10.31,.7,5.176,1.19,2.862,1.45,2.423,1.61,2.224
4380 DATA 1.94,1.939,2.25,1.776,3,1.103,3.9,.9216,5.3,.6851
4390 DATA 6.05,.5279,8.15,.4154,10,.3256
4400 FOR I9=1 TO 10
4410   READ O(I9),L(I9)
4420 NEXT I9

```

```

4430 DATA .45,3.725,.7,2.415,1.19,1.52,1.94,.9252,3,.4411
4440 DATA 3.9,.3458,5.3,.2891,6.05,.243,8.15,.1971,16.6,.1393
4445 GOSUB 4470
4450 RETURN
4460 REM EQUATE VARIABLES TO P ARRAY AND CONVERT UNITS.
4470 LET H1=P[1]*.001
4480 LET H2=P[2]*.001
4490 LET P1=P[3]*1.74533E-02
4500 LET P2=P[4]*1.74533E-02
4510 LET H0=P[5]
4520 LET F1=P[6]*1.74533E-02
4530 LET F2=P[7]*1.74533E-02
4540 LET A1=P[8]*1.74533E-02
4550 RETURN
4560 REM SUBROUTINE TO CHANGE PARAMETER VALUES.
4570 PRINT "ENTER SUBSCRIPT OF PARAMETER TO BE CHANGED (FOR A LIST"
4580 PRINT "OF SUBSCRIPTS AND CURRENT VALUES, LIST LINES 4010 "
4590 PRINT "TO 4170):";
4600 INPUT I9
4610 PRINT " "
4620 IF I9=0 GOTO 4700
4630 PRINT "NEW VALUE:";
4640 INPUT P[I9]
4650 PRINT " "
4660 PRINT "NEXT SUBSCRIPT (0 IF DONE):";
4670 INPUT I9
4680 PRINT " "
4690 GOTO 4620
4700 GOSUB 4470
4710 RETURN
6000 REM LINEAR INTERPOLATION ON A LOG-LOG SCALE. M1=NUMBER OF
6010 REM POINTS IN X AND Y, WHICH STORE TABULAR VALUES. Y1=
6020 REM Y(X9) IS VALUE RETURNED. X IS MONOTONICALLY INCREASING.
6030 LET I7=M1-1
6032 IF X9>X[I7] GOTO 6120
6035 FOR I7=M1 TO 1 STEP -1
6040 IF X9>=X[I7] GOTO 6090
6050 NEXT I7
6060 LET I5=1
6070 LET I6=2
6080 GOTO 6140
6090 IF X9>X[I7] GOTO 6120
6100 LET Y1=Y[I7]
6110 RETURN
6120 LET I5=17
6130 LET I6=17+1
6140 LET M9=(LOG(Y[I6])-LOG(Y[I5]))/(LOG(X[I6])-LOG(X[I5]))
6150 LET B9=-M9*LOG(X[I5])+LOG(Y[I5])
6160 LET Y1=EXP(M9*LOG(X9)+B9)
6170 RETURN

```

```

7000 REM EVALUATES BETA = B0 (IN KM^-1) BY INTERPOLATION USING
7010 REM ELTERMAN'S MODEL (APPLIED OPTICS, 9, 1804-10, 1970).
7020 REM INPUTS ARE V5, THE METEOROLOGICAL RANGE IN KM, AND
7030 REM L5, THE WAVELENGTH IN MICRONS. B IS ASSUMED FILLED
7040 REM WITH THE 21 VALUES OF BETA FOR V5=4 KM. L STORES
7045 REM THE WAVELENGTHS.
7050 IF L5>=.2 GOTO 7090
7070 PRINT "WAVELENGTH OUT OF RANGE FOR BETA. L5=",L5
7080 STOP
7090 IF L5>11 GOTO 7070
7100 FOR I7=1 TO 21
7110 LET X(I7)=W(I7)
7120 LET Y(I7)=B(I7)
7130 NEXT I7
7140 LET X9=L5
7145 LET M1=21
7150 GOSUB 6030
7160 LET B0=Y1*((3.91/V5)-.0116)/((3.91/4)-.0116)+.0116
7170 RETURN
9999 END

```

APPENDIX C: LOS PROGRAM DESCRIPTION

The line of sight (LOS) propagation model is inherent in the OTH model described in appendix E. The basic quantity calculated is the fraction of power remaining in the beam after propagating a distance z measured along the beam. In the notation of appendix E, this is $\ell(z, \alpha)$, given in equation 7) of that appendix (where α is the angle with respect to the local horizontal). The LOS program was derived from the OTH interactive program described in appendix C. As a result, the program comments given in appendix B for all lines numbered 4230 and higher apply to the LOS program.

The subroutine from line 3000 to line 3158 computes $\ell(z, \alpha)$. Appendix E, (in equation 7 and the accompanying footnote) gives the expression for $\ell(z, \alpha)$ and a numerical approximation for the error function required to compute it. However, certain values of the parameters cause overflow to occur in evaluating the exponentials if this expression is used directly. The code given in the listing takes advantage of the fact that the $\exp(-x^2)$ term in $\text{erf}(x)$, for the values of x involved, partially cancels the exponential term multiplying the G function which causes the problem. This eliminates the overflow. Lines 3500-3530 evaluate $G_1(x)$, where

$$G(x) = (\sqrt{\pi}/2)[1+(1-G_1(x)\exp(-x^2)\text{sgn}(x))]$$

and the G function is as defined in appendix E.

The rest of the statements in the LOS program carry out three loops over the parameters of interest, and print a table of results. The columns contain the path loss, and the signal-to-noise ratio for the four combinations of powers of 1 MW and 1 kW, and receiver fields of view of 1° and 60° . Each row is a different wavelength. Lines 225-351 assign values to the other system and geometric parameters. Their meaning is documented in the program remarks, and the variables used (primarily the P array) are consistent with the description of appendix B. The three loops are, from outer to inner, over the values of meteorological range, propagation distance, and wavelength. A separate table, giving the columnar values as a function of wavelength, is produced for each value of meteorological range. The values of meteorological range (in km) used are inserted via the data statement at line 110. The values of distance (in km) are inserted at statement 160, and the wavelength values (in microns) are inserted at statements 210-221.

The only real difference, other than looping and parameter value initialization, between the computations in the LOS program and the analogous ones in the OTH program is found in lines 435-480. Two LOS cases were considered. In the first, which substitutes the lines of code given below for those in the listing, it was assumed that operational advantages (primarily covertness) might cause the RPV to be flown at the minimum altitude necessary to propagate over the desired range. The lines given below compute this minimum height and the associated elevation angle of the transmitted beam. The geometry is as shown in figure C1. The parameters shown are as follows:

- h_t = altitude of transmitter
- h_r = altitude of receiver (RPV)
- α = elevation angle with respect to horizontal (+ downwards)
- a = radius of earth ($k=4/3$ is refraction correction)
- z = propagation distance along path
- D = propagation distance over earth

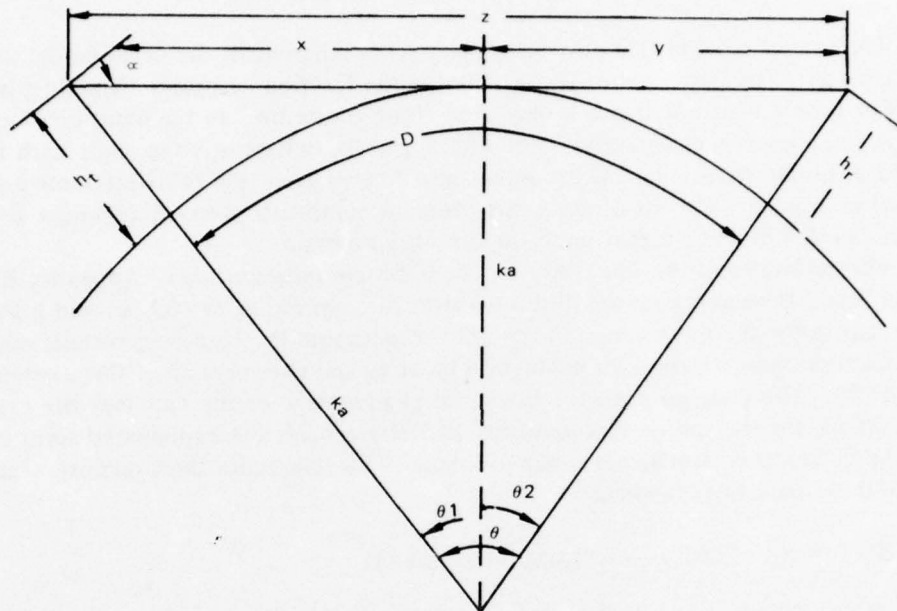


Figure C1. Geometry used to compute minimum RPV altitude.

The following geometrical relationships hold:

$$\begin{aligned}
 x &= [(ka + h_t)^2 - (ka)^2]^{1/2} \\
 y &= [(ka + h_r)^2 - (ka)^2]^{1/2} \\
 z &= x+y = (2ka h_t)^{1/2} + (2kah_r)^{1/2}
 \end{aligned}
 \tag{C1}$$

The minimum value of h_r for a given z and h_t is thus

$$h_r = \left[z - (2kah_t)^{1/2} \right]^2 / 2ka
 \tag{C2}$$

The approximation that $z \cong D$ is made. This can be seen to be good for practical values of D by noting that, using the angles defined in the Figure,

$$D = \theta ka = ka\theta + ka\theta_2
 \tag{C3}$$

$$\theta_1 = \arctan \left[(2kah_t)^{1/2} / ka \right]
 \tag{C4}$$

$$\theta_2 = \arctan \left[(2kah_r)^{1/2} / ka \right]
 \tag{C5}$$

If θ_1 and θ_2 are small, the small angle approximations for expressions (C4) and (C5) may be substituted into expression (C3) to yield expression (C1), ie, $D \cong z$. As an example: $h_r = 3\text{km}$, $\theta_2 \cong 0.035$ rad, for which the approximation is excellent. From geometry, it also follows that $\alpha = \theta_1$. The lines which should replace lines 435-480 in the listing are given in figure C2.

The code in the listing, lines 435-480, treats the second LOS case. Given an over-the-ground communication range, D , and values for the transmitter and receiver heights, the slant range, z , and elevation angle with respect to the horizontal at the transmitter, α , are computed. The geometry is shown in figure C3. From the law of cosines, with $R \equiv ka$,

$$z^2 = (R + h_t)^2 + (R + h_r)^2 - 2(R + h_t)(R + h_r)\cos\theta \quad (C6)$$

Noting that $\theta = D/R$, expanding $\sin\theta$, and keeping only the most significant terms in the result yields

$$\alpha = \cos^{-1} \left\{ (D/z) \left[1 - D^2/(6R^2) + h_r/R \right] \right\} \quad (C7)$$

Note that in the LOS program listing, the arctangent (ATN) function must be used because BASIC has no arccosine. This requires some method of determining the sign of α (which is positive if the LOS is below the horizontal and negative if above). To do this the length of the horizontal path ($\alpha = 0$) between the transmitter and a point above the receiver is computed (Z6, lines 473-475) and compared with z . If z is larger than this value, $\alpha < 0$; if z is shorter, $\alpha > 0$. For very small values of α , or for $h_t \sim h_r$, cancellation errors can cause problems in this comparison. If this is a problem for a case of interest, it is suggested that $\text{SQR}(Z6)$ be expanded as a power series in $1/R$.

The user is urged to heed the "Caution" in appendix B. It applies to the LOS program as well.

```

0435 REM H2=RECEIVER HEIGHT
0436 REM CALCULATE MIN H2 (KM) FOR GIVEN D1, H1.
0440 REM APPROXIMATION: D1 (OVER GROUND)=Z5 (SLANT RANGE).
0450 LET Z5=H1/C2]
0460 LET D1=Z5
0470 LET H2=Z5-SQR(2*R1*H1)
0472 LET H2=H2*H2/(2*R1)
0473 REM A1=ELEVATION ANGLE, POSITIVE DOWNWARDS, RAD.
0475 LET A1=ATN(SQR(2*R1*H1)/R1)
0476 LET Z1=Z5
0480 REM LOOP OVER WAVELENGTH

```

Figure C2. Code to calculate minimum receiver height necessary to maintain line of sight.

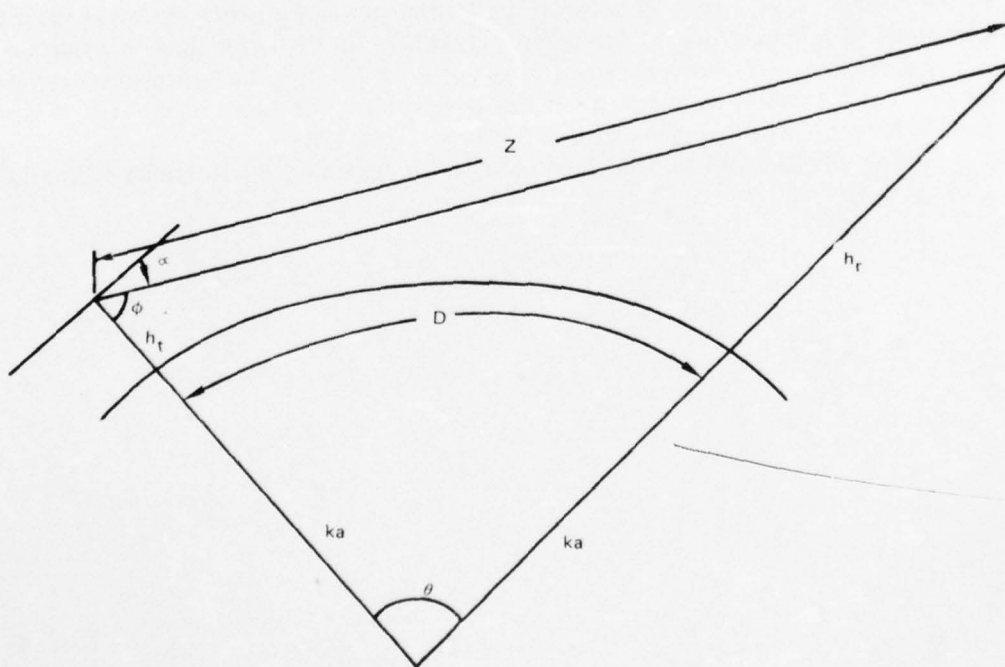


Figure C3. Geometry used to compute elevation angle and slant range from transmitter to RPV.

Program Listing:
LOS Modeling Program

```
10 REM LINE OF SIGHT PROPAGATION MODELING PROGRAM.
20 REM MEGATEK CORPORATION, DECEMBER 1975
30 DIM W(21),B(21),X(50),Y(50),G(9),H(13),I(21),P(15)
40 DEF FNA(X)=10*.434295* LOG (X)
50 RESTOR
55 REM R1=4/3 EARTH RADIUS (KM)
60 LET R1=4*6370/3
70 REM G=MET. RANGE LOOP VALUES (KM)
80 FOR I1=1 TO 9
90 READ G(I1)
100 NEXT I1
110 DATA 4, 8, 10, 15, 20, 30, 50, 70, 90
120 REM H=DISTANCE LOOP VALUES (KM)
130 FOR I1=1 TO 13
140 READ H(I1)
150 NEXT I1
160 DATA 20, 40, 60, 80, 100, 125, 150, 175, 200, 225, 250, 275, 300

170 REM I=WAVELENGTH LOOP VALUES (MICRONS)
180 FOR I1=1 TO 21
190 READ I(I1)
200 NEXT I1
210 DATA .4,.5,.6,.7,.8,.9,1,1.1,1.2,1.3
220 DATA 1.6,2.1,2.3,3.5,3.8,4.1,4.6,4.9
221 DATA 8,9,10.2
225 REM P1=AZ. POINTING ANGLE (RAD)
230 LET P1= 0
240 REM H1=TRANS. HEIGHT (KM)
245 LET P(1)=7
250 LET H1=.001*P(1)
260 REM H0=LAPSE RATE (KM)
270 LET H0=1/.77
272 REM P9=RECEIVER FIELD OF VIEW (RAD)
273 LET P(15)=1
274 LET P9=P(15)*1.74533E-2
275 REM D3=TRANSMITTER DIVERGENCE (RADS)
276 LET D3=.001
280 REM P(9)=DETECTOR RESPONSIVITY, P(10)=SYSTEM ELECTRICAL
```

```

285 REM BANDWIDTH (HZ), P(11)=DETECTOR DARK CURRENT (AMPS),
287 REM P(12)=RECEIVER APERTURE RADIUS (M),P(13)=TRANSMITTER POWER

300 REM (W), P(14)=RECEIVER OPTICAL BANDWIDTH (MICRONS)
310 LET P[9]=.065
320 LET P[10]=7E+7
330 LET P[11]=1E-14
340 LET P[12]=.05642
350 LET P[13]=1E+6
351 LET P[14]=.0001
352 REM STUFF B & W ARRAYS.
353 GOSUB 4230
370 REM LOOP OVER MET. RANGE
380 LET C1= 0
390 LET C1=C1+1
400 LET V5=G(C1)
401 PRINT
403 PRINT
405 PRINT "V=";V5;"KM, HT=";P[1];"KM."
406 PRINT TAB(25);"FOV=1"; TAB(35);"FOV=1";
407 PRINT TAB(45);"FOV=60"; TAB(55);"FOV=60"
408 PRINT TAB(25);"P=1 MW"; TAB(35);"P=1 KW";
409 PRINT TAB(45);"P=1 MW"; TAB(55);"P=1 KW"
410 PRINT "RANGE"; TAB(7);"LAMBDA"; TAB(15);"PATH LOSS";
411 PRINT TAB(25);"S/N"; TAB(35);"S/N"; TAB(45);"S/N";
412 PRINT TAB(55);"S/N"; TAB(65);"HR"
420 LET C2=0
430 LET C2=C2+1
435 REM H2=RECEIVER HEIGHT
440 LET H2=2.5
445 LET D1=H[C2]
450 LET Q9=D1*D1
455 REM
460 LET Q8=H1+H2
463 LET Q7=(H1-H2)*(H1-H2)
465 LET Z5= SQR (Q9+Q8*Q9/R1+Q7-Q9*Q9/(12*R1*R1))
470 LET A1=(D1/Z5)*(1-Q9/(6*R1*R1)+H2/R1)
471 LET A1= ATN ( SQR (1-A1*A1)/A1)
472 LET A1=-A1
473 LET Z6=(H2*H2-H1*H1+2*R1*(H2-H1))
474 IF Z6< 0 GOTO 477
475 IF Z5< SQR (Z6) GOTO 477
476 LET A1=-A1
477 LET Z1=Z5

```

```
480 REM LOOP OVER WAVELENGTH
490 LET C3=0
500 LET C3=C3+1
505 LET C6=15
510 LET L5=I(C3)
520 REM COMPUTE B0
530 GOSUB 7050
540 GOSUB 3010
541 IF L1>=1E-30 GOTO 0549
542 IF C3<>1 GOTO 0546
543 PRINT H(C2); TAB(7);L5; TAB(15);"←-300";
544 PRINT TAB(64);INT(H2*1000+.5)
545 GOTO 0784
546 PRINT TAB(7);L5; TAB(15);"←-300"
547 GOTO 0784
548 REM P9=RECEIVER FIELD OF VIEW (RADS)
549 FOR C4=1 TO 2
```

```

550 LET P(15)=1
551 IF C4=1 GOTO 0553
552 LET P(15)=60
553 LET P9=P(15)*1.74533E-02
554 REM LOOP OVER POWER
555 FOR C5=1 TO 2
556 LET P(13)=1E+06
557 IF C5=1 GOTO 0565
558 LET P(13)=1000
559 REM P6=RECEIVED POWER=L1*PT*A/(PI*(25*D3/2)^2)
560 REM *****AT THIS POINT L1 IS PATH LOSS. COMPUTE SNR=S1*****
561 REM P6=RECEIVED POWER=L1*PT*A/(PI*(25*D3/2)^2)
562 LET P6=25*D3*1000/?
563 LET P6=L1*P(13)*3.14159*P(12)*P(12)/(3.14159*P6*P6)
564 LET C6=C6+10
565 REM P6=BACKGROUND.
566 REM FORCE PROGRAM TO DAYTIME BACKGROUND.
567 LET Q3=1
568 LET P8=0
569 IF L5<1.8 GOTO 0650
570 LET P8=1.2E+08/(L5+5*(EXP(50/L5)-1))
571 IF Q3=2 GOTO 0680
572 REM DAYTIME BACKGROUND
573 LET P7=4750/(L5+6.5*(EXP(2.44/L5)-1))+P8
574 GOTO 0690
575 REM NIGHTTIME BACKGROUND.
576 LET P7=.0083/(L5+6.5*(EXP(2.44/L5)-1))+P8
577 LET P7=P7*(3.14159/4)*P9*P9*3.14159*P(12)*P(12)*P(14)
578 LET S1=2+1.60219E-19*P(10)*(P(9)*(P7+P6)+P(11))
579 LET S1=P(9)*P(9)*P6*P6/S1
580 REM *****AT THIS POINT S1=SNR*****
581 REM *****OUTPUT ROUTINE SHOULD BE INSERTED HERE*****
582 IF S1<1E-30 GOTO 0753
583 IF C6=55 GOTO 0749
584 IF C6<>25 GOTO 0746
585 IF C3<>1 GOTO 0751
586 PRINT H(C2); TAB(7);L5; TAB(15);FNA(L1);
587 PRINT TAB(C6);FNA(S1);
588 GOTO 0780
589 GOTO 0791
590 PRINT TAB(7);L5; TAB(15);FNA(L1);
591 GOTO 0746
592 IF C6=55 GOTO 0811
593 IF C6<>25 GOTO 0757
594 IF C3<>1 GOTO 0761
595 PRINT H(C2); TAB(7);L5; TAB(15);FNA(L1);
596 PRINT TAB(C6);"←-300";
597 GOTO 0780
598 GOTO 0811
599 PRINT TAB(7);L5; TAB(15);FNA(L1);
600 GOTO 0757

```

```

760 NEXT C5
782 NEXT C4
784 IF C3=21 GOTO 8800
790 GOTO 8500
791 IF C3<>1 GOTO 8794
792 PRINT TAB(C6);FNA(S1); TAB(64);INT(H2*1000+.5)
793 GOTO 8780
794 PRINT TAB(C6);FNA(S1)
795 GOTO 8780
800 IF C2=13 GOTO 8820
810 GOTO 8430
811 IF C3<>1 GOTO 8814
812 PRINT TAB(C6);"←-300"; TAB(64);INT(H2*1000+.5)
813 GOTO 8780
814 PRINT TAB(C6);"←-300"
815 GOTO 8780
820 IF C1=9 GOTO 8840
830 GOTO 8390
840 PRINT
850 PRINT
860 PRINT
870 GOTO 9999
880 PRINT H(C2); TAB (7); FNA(L1)
890 GOTO 784
3000 REM COMPUTE L1=PATH LOSS FOR LINE OF SIGHT.
3010 REM
3090 LET Y9= SQRT (R1/(2*H0))* TAN (A1)
3100 LET Y8=Z1* COS (A1)/ SQRT (2*R1*H0)
3110 LET X1=-Y9
3120 GOSUB 3510
3130 LET G2=G1* SGN (-Y9)
3140 LET X1=Y8-Y9
3150 GOSUB 3510
3160 LET G2=G2-G1* EXP (2*Y8*Y9-Y8*Y8)* SGN (Y8-Y9)
3165 LET G2=G2+ EXP (Y9*Y9)*( SGN (Y8-Y9)- SGN (-Y9))
3170 LET L1=-B0* SQRT (2*R1*H0)*G2*.886227* EXP (-H1/H0)/ COS (A1)
3175 LET L1= EXP (L1)
3180 RETURN
3500 REM G1(X1)
3510 LET T1=1/(1+.47047* ABS (X1))
3520 LET G1=(((.747856*T1)-9.58798E-2)*T1+.348024)*T1
3530 RETURN
4230 REM STUFF W AND B ARRAYS FOR EXTINCTION COEFFICIENT.
4240 FOR I9=1 TO 21
4250 READ W(I9),B(I9)
4260 NEXT I9

```

```

4270 DATA .27, 2, .28, 1.89, .3, 1.78, .32, 1.67, .34, 1.56
4280 DATA .36, 1.45, .38, 1.4, .4, 1.3, .45, 1.15, .5, 1.05, .55
4285 DATA .966
4290 DATA .6, .86, .65, .78, .7, .73, .8, .64, .9, .58, 1.06, .52
4300 DATA 1.26, .47, 1.67, .4, 2.17, .36, 10, .312
4310 RETURN
6000 REM      LINEAR INTERPOLATION ON A LOG-LOG SCALE.  M1=NUMBER OF
6010 REM      POINTS IN X AND Y, WHICH STORE TABULAR VALUES. Y1=
6020 REM      Y(X9) IS VALUE RETURNED.  X IS MONOTONICALLY INCREASING
.
6030 LET I7=M1-1
6032 IF X9>X[I7] GOTO 6120
6035 FOR I7=M1 TO 1 STEP -1
6040   IF X9>=X[I7] GOTO 6090
6050 NEXT I7
6060 LET I5=1
6070 LET I6=2
6080 GOTO 6140
6090 IF X9>X[I7] GOTO 6120
6100 LET Y1=Y[I7]
6110 RETURN
6120 LET I5=I7
6130 LET I6=I7+1
6140 LET M9=( LOG (Y[I6]) - LOG (Y[I5])) / ( LOG (X[I6]) - LOG (X[I5]))
6150 LET B9=-M9* LOG (X[I5]) + LOG (Y[I5])
6160 LET Y1= EXP (M9* LOG (X9) + B9)
6170 RETURN
7000 REM      EVALUATES BETA = B0 (IN KM^-1) BY INTERPOLATION USING
7010 REM      ELTERMAN'S MODEL (APPLIED OPTICS, 9, 1804-10, 1970).
7020 REM      INPUTS ARE V5, THE METEOROLOGICAL RANGE IN KM, AND
7030 REM      L5, THE WAVELENGTH IN MICRONS.  B IS ASSUMEE FILLED
7040 REM      WITH THE 21 VALUES OF BETA FOR V5=4 KM.  L STORES
7045 REM      THE WAVELENGTHS.
7050 IF L5>=.2 GOTO 7090
7070 PRINT "WAVELENGTH OUT OF RANGE FOR BETA.  L5=",L5
7080 STOP
7090 IF L5>11 GOTO 7070
7100 FOR I7=1 TO 21
7110   LET X[I7]=W[I7]
7120   LET Y[I7]=B[I7]
7130 NEXT I7
7140 LET X9=L5
7145 LET M1=21
7150 GOSUB 6030
7160 LET B0=Y1*((3.91/V5)-.0116)/((3.91/4)-.0116)+.0116
7170 RETURN
9999 END

```

APPENDIX D: REFERENCES

1. Naval Research Laboratory Report 6152, Experimental Observations of Forward Scattering of Light in the Lower Atmosphere, by JA Curcio and LF Drummeter, Jr, 30 September 1964
2. Megatek Report R2005-039-IF-1, Propagation Model for a Laser-Type Beyond-the-Horizon Communications Link, by PH Levine, 15 December 1975
3. Siegman, AE, "The Antenna Properties of Optical Heterodyne Receivers, Proceedings of the IEEE, v 54, p 1350-1356, 1966
4. Pratt, WK, Laser Communication Systems, John Wiley & Sons, 1969
5. Gagliardi, RM, "The Effect of Timing Errors in Optical Digital Systems," IEEE Transactions on Communication Technology, COM-20, p 87-93, 1972
6. Gagliardi, RM and S Karp, "M-ary Poisson Detection and Optical Communication," IEEE Transactions on Communication Technology, COM-17, p 208-216, April 1969
7. Naval Electronics Laboratory Center Technical Document 447, Periscope Aircraft-Submarine Optical Communications System (PERASOCS): Preliminary Definition and Analysis, by R Anderson, D Adrian and WR Stone, 1 September 1974
8. RCA, Electro-Optics Handbook, 1974
9. Karp, S and RM Gagliardi, "The Design of a Pulse-Position Modulated Optical Communication System," IEEE Transactions on Communication Technology, COM-17, p 670-676, 1969
10. Karp, S, EL O'Neill and RM Gagliardi, "Communication Theory for the Free-Space Optical Channel," Proceedings of the IEEE, v 58, p 1611-1625, 1970
11. Naval Electronics Laboratory Center Technical Note 2672, * Voice Communication with a Flashlamp-Excited Blue-Green Dye Laser, by JE Celro, EJ Schimitschek, and JA Trias, 23 April 1974
12. LaRocca, AJ, "Methods of Calculating Atmospheric Transmittance and Radiance in the Infrared," Proceedings of the IEEE, v63, p 75-94, 1975
13. United States Air Force, Handbook of Geophysics and Space Environment, SL Valley, Editor, 1965
14. Naval Electronics Laboratory Center Technical Note 2714, * Radiated Background Noise in the 10 - 45 GHz Band, by DB Sailors, DJ Adrian and PH Levine, 24 June 1974
15. Kopeika, NS, and J Boldogna, "Background Noise in Optical Communication Systems," Proceedings of the IEEE, v 58, p 1571-1577, 1970
16. McDonnell Douglas Report F-063, Marine Weather of the World, June 1968
17. Naval Weapons Center, China Lake, Technical Note 4056-16, Weather Effects on Infra-red Systems for Point Defense, by FE Nicodemus, May 1972

18. Electro-Optical Systems Report 4440, Final III, Laser Systems Study, Part III, Effects of Clouds, by GA Cato, LW Carrus and KJ von Essen, 14 December 1975
19. Naval Electronics Laboratory Center Technical Note 2923,* Optical SATCOM: Effects of Clouds on Global Availability of Optical Satellite Communications Links, by SW Green and RA Greenwell, 1 May 1975
20. Geusic, JE, WB Bridges and JI Panklove, "Coherent Optical Sources for Communications," Proceedings of the IEEE, v58, p 1419-1439, June 1970
21. 1975 Laser Focus Buyers' Guide, Advanced Technology Publications, Inc, 1975
22. McIntyre, C, et al, "Optical Components and Technology in Laser Space Communications Systems," Proceedings of the IEEE, v 58, p 1491-1503, 1970
23. Roche, AI, and AM Title, "Tilt Tunable Ultra Narrow Band Filters for High Resolution Infrared Photometry," Applied Optics, v 14, p 765-769, 1975
24. Harris, SE, STK Nieh and DK Winslow, "Electronically Tunable Acousto-Optic Filter," Applied Physics Letter 15, p 325, 1969
25. Kusters, JA, DA Wilson and DL Hammond, "Optimum Crystal Orientation for Acoustically Tuned Optical Filters," Journal of the Optical Society of America, v 64, p 434-440, 1974
26. Naval Electronics Laboratory Center Technical Report 1990, Possible Use of Organic Dyes and Inorganic Compounds in Liquid as Wide-Aperture, Narrowband, Optical Filters, by JA Trias (in preparation)
27. Senitzky, B, "Narrowband Ultraviolet Vapor Filter," Applied Optics, v 14, p 238-244, 1975
28. Melchior, H, MB Fisher and FR Arams, "Photodetectors for Optical Communication Systems," Proceedings of the IEEE, v 58, p 1466-1486, 1970
29. Leverenz, DJ, and OL Gaddy, "Subnanosecond Gating Properties of the Dynamic Cross-Field Photomultiplier," Proceedings of the IEEE, v 58, p 1487-1490, 1970
30. Medved, D, "Photodiodes for Fast Receivers," Laser Focus, v 10, p 45-47, 1974
31. Aviation Week and Space Technology, March 17, 1975
32. Pratt, WK, LS Stokes and R Hinckley, "Optimization of Optical Communication Systems," Proceedings of the IEEE, v 58, p 1737-1740, 1970
33. Woodman, Douglas P, "Limitations in Using Atmospheric Models for Laser Transmission Estimates," Applied Optics, v 13, p 2193-2195, 1974
34. Elterman, L, "Relationships Between Vertical Attenuation and Surface Meteorological Range," Applied Optics, v 9, p 1804-1810, 1970
35. Deirmendjian, D, Electromagnetic Scattering on Spherical Polydispersions, Elsevier Publishing Company, Inc, 1969

*NELC technical notes are informal documents intended primarily for use within the Center.

**Appendix E: Propagation Model for a Laser-Type
Beyond-the-Horizon Communication Link**

(This appendix was issued as a Megatek Corporation
Informal Report. It is included here for
completeness and ease of reference in the same
form as originally published)

MEGATEK CORPORATION

INFORMAL REPORT

Title : Propagation Model for a Laser-Type Beyond-the-Horizon Communication Link
Number : R2005-039-IF-1
Contract No. : N00123-75-C-0328
NELC Task : MEG-TA-039
Date : 15 December 1975

Submitted to:

**Naval Electronics Laboratory Center
Code 2500
San Diego, California 92152**

PROPAGATION MODEL FOR A LASER-TYPE BEYOND-THE-HORIZON COMMUNICATION LINK

GENERAL

King and Kainer¹ have discussed beyond-the-horizon propagation of laser beams by means of scattering from clouds and hazes and have specifically considered the use of this propagation mode for communications. In the present study a more detailed model is given for this forward scatter optical communications channel in the cloud-free case, ie where scattering arises solely from atmospheric "haze" aerosols. The model takes explicit account of: a) the vertical falloff in aerosol concentration; b) refraction and c) Earth's curvature, neglect of which can lead to severe errors in path loss estimates at ranges of interest in beyond-the-horizon communications. Indeed, it is found that proper exploitation of the a) above can lead to novel strategies for reducing path loss, eg optimally elevated beams or vertical fans.

DETAILED MODEL

VERTICALLY INHOMOGENEOUS ATMOSPHERE

The atmosphere is taken to be horizontally homogeneous but both the local refractivity N , and extinction coefficient β are assumed to decrease exponentially with height h :

$$1) \quad N = N_0 \exp \left[-h/H_N \right]$$

$$2) \quad \beta = \beta_0 \exp \left[-h/H_e \right]$$

where the zero subscript refers to the conditions at the Earth's surface. In the CCIR standard atmosphere $N_0 = 289$ and $H_N = 7.34$ km. We make the simplifying though reasonable assumption that extinction arises solely from aerosol scattering with unity albedo, thus ignoring both molecular Rayleigh scattering and any absorption in the aerosol Mie scattering. Then for the wavelength range of .5 to 10 microns, β_0 will lie typically in the range.

$$3) \quad 10^{-2} \text{ km}^{-1} < \beta_0 < 2 \times 10^{-1} \text{ km}^{-1}$$

depending on visibility, although still higher values of β_0 are obviously possible in the case of ground fog. H_e in equation 2) is identified with the lapse rate in aerosol concentration - a quantity which is not well characterized statistically and whose magnitude is typically of the order of 1 km.

REFRACTION

As a result of the vertical decrease in refractivity, light rays in the atmosphere are curved (concave downwards) rather than straight. Thus a laser beam will gain in altitude less rapidly with increasing range than would be the case in vacuum, and this effect may be accommodated to an acceptable degree of accuracy by introducing the concept of a fictitious Earth radius R' related to the true radius R by:

$$4) \quad R' = kR$$

where the factor k is determined by the surface refractivity, N_0 , as shown in Table 1.

TABLE 1. EARTH'S RADIUS CORRECTION COEFFICIENT (k)
FOR VARIOUS SURFACE REFRACTIVITIES (N_0)

N_0	k
250	1.232
289	1.305
301	1.333
350	1.489
400	1.767

Following standard practice, the value $k = 4/3$ will be adopted in the present study. In this so-called "4/3 Earth" approximation, it suffices to ignore refraction throughout the model calculations (ie assume straight line light paths) and then to remedy this neglect by the simple expedient of using an Earth radius = 8393 km in any numerical evaluations.

EARTH'S CURVATURE EFFECTS

Due to the curvature of the Earth the altitude of a laser beam will not vary linearly with range. Specifically, if a laser beam is projected from a height H in a direction making an angle α below the local horizontal as shown in figure 1, then a simple geometrical construction yields the relationship

$$5) \quad (R + h)^2 = (R + H - Z \sin \alpha)^2 + Z^2 \cos^2 \alpha$$

where h is the altitude corresponding to a distance Z along the beam. Solving for h , one finds

$$6) \quad h(Z, \alpha) = H - Z \sin \alpha + Z^2 \cos^2 \alpha / 2R + 0(1/R^2)$$

BEAM ATTENUATION

Consider a laser beam (non-divergent) projected is shown in figure 1, and let $\varrho(z, \alpha)$ denote the fraction of power remaining in the beam after propagating a distance z measured along the beam. Then from 2), there follows

$$7) \quad \varrho(z, \alpha) = \exp \left\{ - \int_0^z \beta_0 \exp \left[-h(z, \alpha)/H_e \right] dz \right\}$$

which after some algebra, may be written

$$\begin{aligned} \varrho(z, \alpha) = \exp & \left\{ -\beta_0 \sec \alpha \sqrt{2RH_e} \exp\left(-H - \frac{R}{2} \tan^2 \alpha\right)/H_e \right. \\ & \left. \times \left[G\left(\frac{z \cos \alpha}{\sqrt{2RH_e}} - \sqrt{\frac{R}{2H_e}} \tan \alpha\right) - G\left(-\sqrt{\frac{R}{2H_e}} \tan \alpha\right) \right] \right\} \end{aligned}$$

where*

$$G(x) = \sqrt{\frac{\pi}{2}} \int_0^x e^{-u^2} du \equiv \sqrt{\frac{\pi}{2}} \operatorname{erf}(x)$$

BEYOND-THE-HORIZON PROPAGATION MODEL

As shown in figure 2, in the absence of clouds we may distinguish two primary mechanisms for beyond-the-horizon propagation: viz. single and multiple scattering from atmospheric aerosols. Since aerosol scattering tends to be peaked in the forward direction and to be virtually free of absorption at the optical and infrared wavelengths of interest, it is meaningful to think in terms of an "aura" of multiply (forward) scattered photons surrounding the laser beam. As discussed in the Appendix, this aura will in general attenuate less rapidly with distance than the direct beam and, were it not for the effect of the nearby Earth's surface, would be the dominant source of radiance at long ranges. However, the effect of the Earth's surface is to remove energy from the aura by a combination of absorption and diffuse scattering so that, as shown in the Appendix, for near-surface transmitter/receiver links the aura will attenuate with range (D) approximately as $e^{-\beta_0 D/D}$, a rate of attenuation more rapid (as will be seen) than that of the singly scattered component. For this reason, the beyond-the-horizon propagation model is limited to the singly scattered component. It should be borne in mind, however, that at ranges less than about 100 km, the aura can – under favorable conditions (see Appendix) – be the dominant component.

*A useful numerical approximation for the error function is

$$\operatorname{erf}(x) = 1 - (a_1 t + a_2 t^2 + a_3 t^3) e^{-x^2} + E(x) \quad x \geq 0$$

where

$$t = \frac{1}{1 + Px} \quad P = .47047 \quad a_1 = .3480242$$

$$a_2 = -.0958798 \quad a_3 = .7478556$$

and

$$|E(x)| \leq 2.5 \times 10^{-5}$$

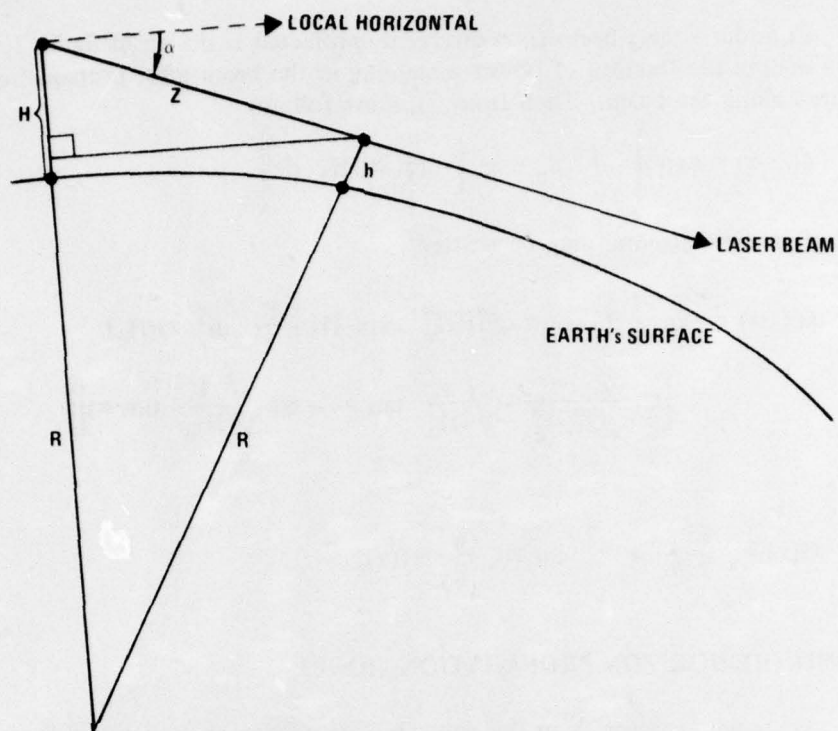


Figure 1. Geometry for Evaluating Earth's Curvature Effects.

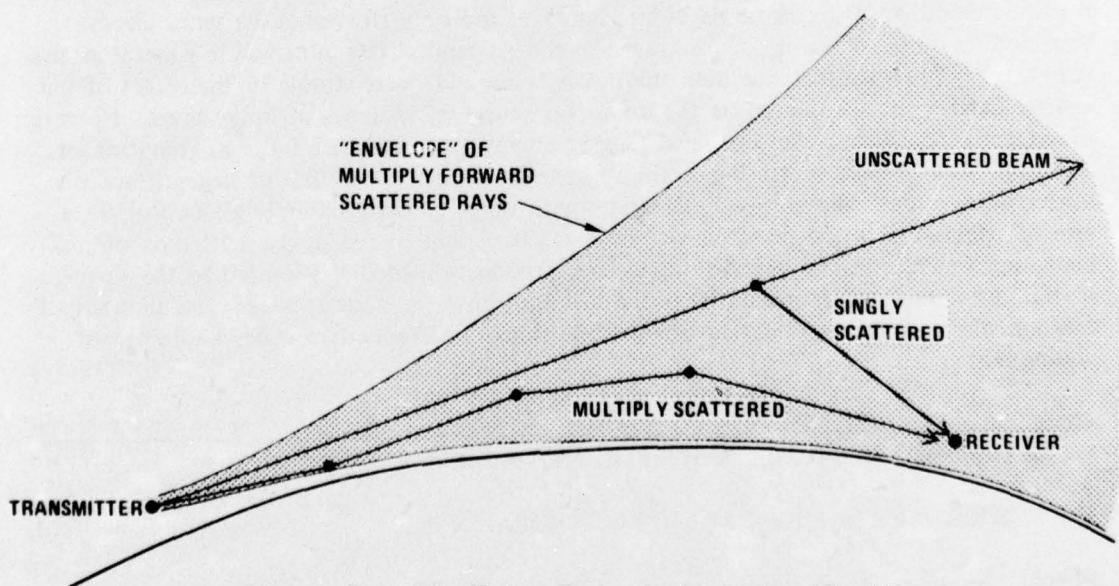


Figure 2. Beyond the Horizon Propagation Mechanisms (Cloud Free Case).

Consider the geometry shown in Figure 3 and let the receiver aperture (area = A) be oriented normal to the line of sight to the scattering element. Then if P_T is the transmitted power and dP_R the power received which enters the receiver optics at elevation angles between β_2 and $\beta_2 + d\beta_2$, there follows

$$10) \quad \frac{dP_R}{P_T \cdot A} = \frac{f(\beta_1 + \beta_2)}{4\pi z_2^2} \ell(z_2, \alpha_2) \left[\frac{-\partial}{\partial z_1} \ell(z_1, \alpha_1) \right] dz_1$$

where $(-)\alpha_1$ is the elevation angle of \vec{z}_1 , ℓ is defined in equation 8), and $f(\theta)$ is the gain over isotropic for aerosol scattering at the scattering angle θ , ie the ratio of the actual scattering cross section at angle θ to that of an isotropic scatterer of identical total scattering cross section.

From the geometrical relations

$$11) \quad z_1 = D' \sin \beta_2 / \sin(\beta_1 + \beta_2) \quad z_2 = D' \sin \beta_1 / \sin(\beta_1 + \beta_2)$$

$$d\beta_2 = \frac{dz_1}{z_2} \sin(\beta_1 + \beta_2)$$

and the result obtainable from 8)

$$12) \quad \frac{-\partial \ell}{\partial z} = \ell \beta_0 \exp \left\{ - \left[\frac{H}{H_e} + \frac{z^2 \cos^2 \alpha}{2H_e R} - \frac{z \sin \alpha}{H_e} \right] \right\}$$

there follows from 10)

$$13) \quad \frac{dP_R}{P_T \cdot A} = \frac{\beta_0 d\beta_2 f(\beta_1 + \beta_2)}{4\pi D' \sin \beta_1} \ell(z_1, \alpha_1) \ell(z_2, \alpha_2) \exp \left\{ - \left[\frac{H_1}{H_e} + \frac{z_1^2 \cos^2 \alpha_1}{2H_e R} - \frac{z_1 \sin \alpha_1}{H_e} \right] \right\}$$

where z_1 and z_2 are to be evaluated from 11).

It now only remains to relate the angles β_1 and β_2 to the elevation and azimuth angles at the transmitter and receiver respectively. To do this, we set up the geometry shown in figure 4. The transmitter and receiver are taken to lie in the y-z plane and the laser beam direction is specified by the angles α_1 (measuring the negative elevation angle) and ϕ_1 measuring the azimuth relative to the great circle path between transmitter and receiver. α_2 and ϕ_2 are analogously defined for the line of sight between the receiver and the scattering element. We find for β_1 the relation:

$$14) \quad \cos \beta_1 = \frac{\cos \alpha_1 \cos \phi_1 \sin \Omega (R+H_2) - \sin \alpha_1 [(R+H_2) \cos \Omega - R-H_1]}{\sqrt{(R+H_2)^2 \sin^2 \Omega + ((R+H_2) \cos \Omega - R-H_1)^2}}$$

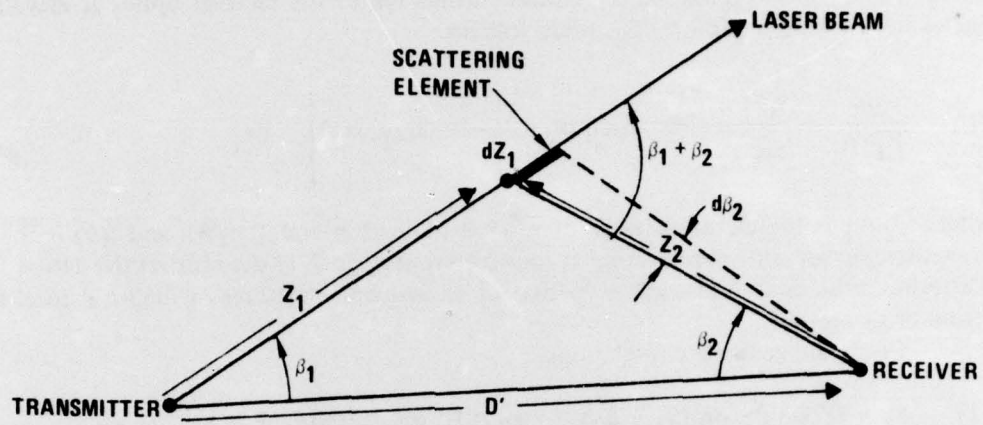


Figure 3. Geometry for Single Scattering Model

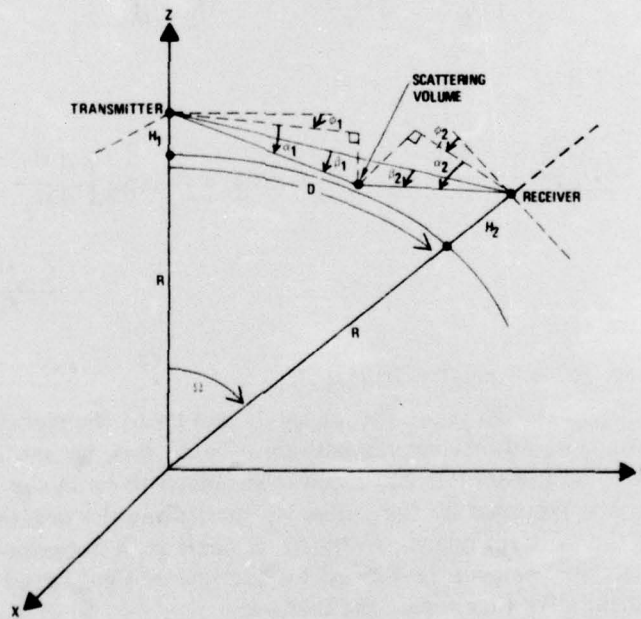


Figure 4. Scattering Geometry.

which can be approximated by

$$15) \quad \cos \beta_1 \approx \frac{\cos \alpha_1 \cos \phi_1 + \sin \alpha_1 \left(\frac{D}{2R} + (H_1 - H_2)/D \right)}{\sqrt{1 + \left(\frac{H_2 - H_1}{D} - \frac{D}{2R} \right)^2}}$$

For α_2 , we find

$$16) \quad -\sin \alpha_2 = \left[z_1 \cos \alpha_1 \cos \phi_1 \sin \Omega - (R + H_2) + (R + H_1) \cos \Omega - z_1 \sin \alpha_1 \cos \Omega \right] / z_2$$

which can be approximated by

$$17) \quad -\sin \alpha_2 \approx \frac{z_1}{z_2} \left[\cos \phi_1 \cos \alpha_1 \frac{D}{R} - \sin \alpha_1 \right] + \frac{H_1 - H_2 - D^2/2R}{z_2}$$

In 14-17), D is the ground range from transmitter to receiver and

$$18) \quad \Omega = D/R$$

Thus the basic propagation model is defined by equations 13), 11), 14) and 16), where $f(\beta_1 + \beta_2)$ is to be determined from a given aerosol size distribution model. Since 13) is in differential form, it must be integrated over the field of view of the receiver optics. To do this, we assume the field of view is positioned as shown in figure 5.* Then, if the field of view is F_2 radians, we must integrate 13) over the range

$$19) \quad \beta_{\min} \leq \beta_2 \leq \beta_{\min} + F_2$$

where (cf. 15)):

$$20) \quad \cos \beta_{\min} = \frac{\cos \alpha_2 \cos \phi_2 + \sin \alpha_2 \left(\frac{D}{2R} + (H_2 - H_1)/D \right)}{\sqrt{1 + \left(\frac{H_1 - H_2}{D} - D/2R \right)^2}}$$

*Note that the laser beam in the present model appears to the receiver as a line source. In practical cases, the received power will increase linearly with field of view for fields of view out to about 5 degrees.

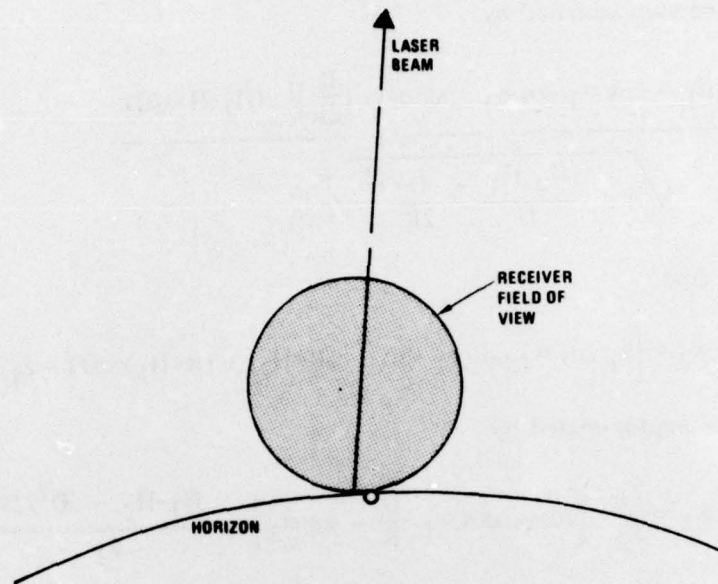


Figure 5. Field of View Placement.

A generalization is now added to the model: thus far we have considered the laser beam to be non-divergent; we now allow the beam to be spread in the vertical plane by F_1 radians, ie we consider the beam to be a vertical fan rather than a line. The reason for this generalization is that it turns out from 13) that the received power will be a maximum if the laser beam direction is elevated above the horizon by an angle which depends on the range D and the vertical lapse rate in aerosol concentration, H_e . There may thus be a practical advantage in spreading the beam in elevation and to accommodate this possibility we introduce the vertical fan angle F_1 and average 13) over the range of beam elevation angles:

$$21) \quad \alpha_{\min} \leq -\alpha_1 \leq \alpha_{\min} + F_1$$

where

$$22) \quad \tan \alpha_{\min} \approx \sqrt{\frac{2H_1}{R}}$$

Finally, with the understanding that both the field of view (F_2) and fan angle (F_1) are less than about five degrees, we can approximate the scattering function $f(\beta_1 + \beta_2)$ in 13) by its value in the forward direction, $f(0)$, thereby removing it from the field of view and fan integrations. Then, we may define an overall transmission T for the beyond-the-horizon link as:

$$23) \quad P_R = P_T \cdot T$$

where from 13)

$$24) \quad T = \frac{\beta_0 \cdot A \cdot f(0)}{4\pi D} \frac{1}{F_1} \int_{\alpha_{\min}}^{\alpha_{\min}+F_1} d\alpha_1 \int_{\beta_{\min}}^{\beta_{\min}+F_2} d\beta_2 \frac{\rho(z_1, \alpha_1) \rho(z_2, \alpha_2)}{\sin\beta_1}$$

$$\times \exp \left\{ - \left[\frac{H_1}{H_e} + \frac{Z_1^2 \cos^2 \alpha_1}{2H_e R} - \frac{Z_1 \sin \alpha_1}{H_e} \right] \right\}$$

NUMERICAL RESULTS

EFFECT OF VERTICAL BEAM WIDTH

As a first application of the model, we examine the dependence of the transmission function on the vertical beam width, i.e. the fan angle F_1 . To this end we assume the following typical parameter values:

Receiver and Transmitter height (H_1, H_2) = 25 meters

Azimuth angles (ϕ_1, ϕ_2) = 0 (ie no offset from great circle)

Sea level extinction coefficient (β_0) = 0.1 km^{-1}

Receiver field of view (F_2) = 1°

Vertical lapse rate in aerosol concentration (H_e) = 1.3 km

Effective Earth's radius (R) = 8393 km (i.e. "4/3 Earth" model)

and compute the quantity $T/(A \cdot f(0))$, where A is the receiver aperture in square meters and $f(0)$ is the forward direction "gain over isotropic" for the aerosol Mie scattering,* as a function of ground range D and fan angle F_1 . The results are shown in figure 6.

It is seen that for ranges below 100 km the transmission is highest for a non-divergent beam, whereas at greater ranges transmission improves with increasing fan angle. (The effect saturates near 4° ; calculations for 8° fan angles are very close to those for 4°). Since from a practical standpoint tracking and pointing requirements in the elevation plane are far less severe for a vertical fan than for a non-divergent beam pointed at the horizon it is clear that a (nominally 4°) vertical fan would be the preferred mode in a communication system - particularly since figure 6 indicates that the penalty paid at short ranges (ie $<100 \text{ km}$) is less than about 3 dB.

DEPENDENCE ON EXTINCTION COEFFICIENT

In figures 7 and 8, the quantity $T/A \cdot f(0)$ is plotted as a function of range and sea level extinction coefficient for both a non-divergent beam and a 4° vertical fan. Parameter values used are identical to those listed above. Comparing the two figures it is seen that the vertical fan is particularly advantageous at low visibilities (high β_0). For example, at 130 km range and $\beta_0 = .2$ the gain is about 26 dB.

*Typically $f(0)$ can be as large as 10 while A will be of the order of .1 meters² so that $f(0) \cdot A$ is of order unity.

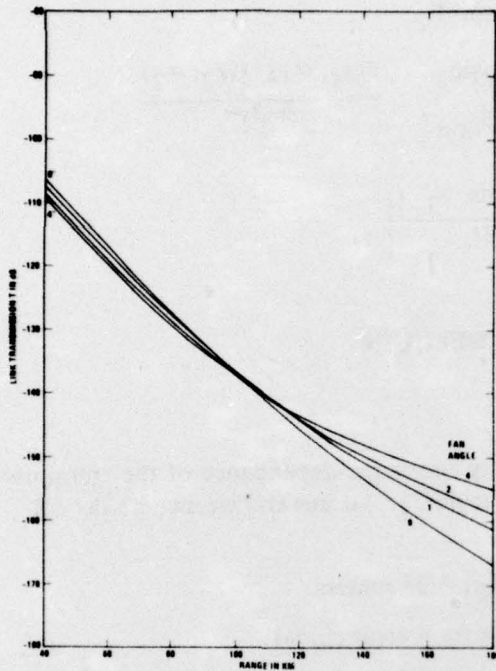


Figure 6. Effect of vertical beam width on Path Loss Extinction Coefficient = 0.1 KM^{-1}

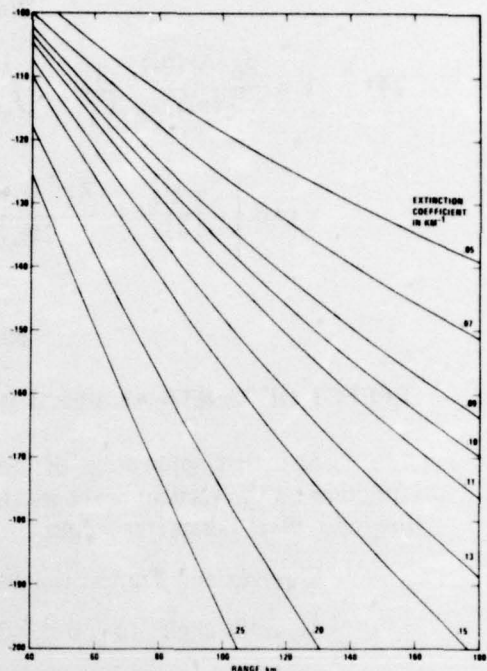


Figure 7. Laser Beam Path Loss in Beyond-the-Horizon Propagation: Single Scattering Model (0 Vertical Beam Width)

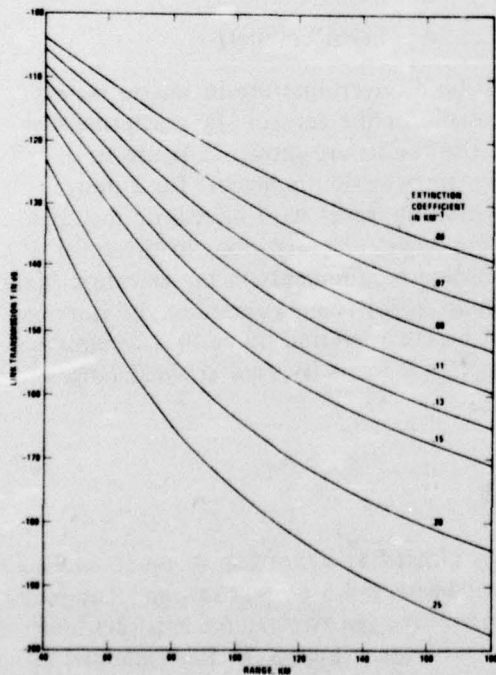


Figure 8. Laser Beam Path Loss in Beyond-the-Horizon Propagation: Single Scattering Model (4 Vertical Beam Width)

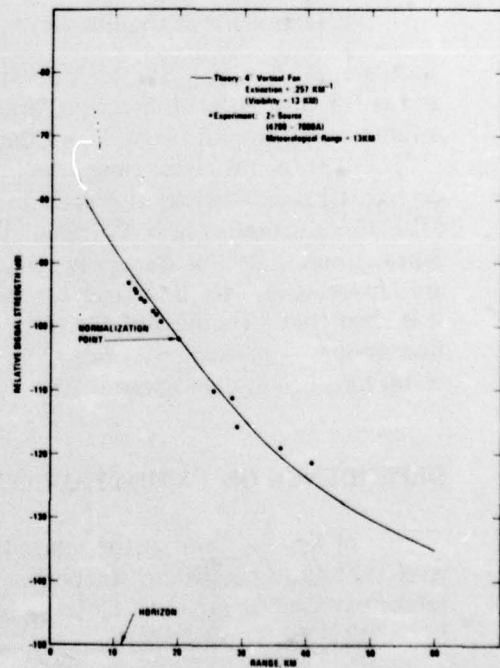


Figure 9. Comparison of Path Loss Predictions with NRL Observation.

The monotonic increase of transmission with decreasing extinction coefficient (ie increasing visibility) is noteworthy since at some point this trend must reverse ($T \rightarrow 0$ as $\beta_0 \rightarrow 0$). If -130 dB is taken as a typical system threshold, then it is seen that for the range of extinction coefficients considered (.05 to .25 km^{-1}), the maximum range for communication varies from about 140 to 40 km respectively.

COMPARISON WITH FIELD OBSERVATIONS

Transmission data for beyond-the-horizon laser propagation is not apparently available. A limited test of the model for the 4° vertical fan was possible once it was realized that an isotropic (ie 2π) source should behave (in the elevation plane) approximately as a small angle vertical fan since aerosol scattering is primarily in the near forward direction and consequently photons emitted appreciably away from the horizontal will not be scattered to beyond the horizon ranges.

In 1964, Curcio and Drummer² at the Naval Research Laboratory reported the results of an experiment in which an uncollimated 6000 joule xenon flash lamp was mounted about 3 meters above water level on the cabin of a small boat. During night time measurements, the boat traveled a course on Chesapeake Bay up to a maximum range to the receiver of 41 km. The receiving system had a 3° field of view and was similarly located at 3 meters height. The meteorological range, monitored by a transmissometer, was 13 km.

In figure 9, the Naval Research Laboratory data of visible light intensity (in the 4700-7000 A band) vs. range is compared with the predictions of the 4° fan model for $H_1 = H_2 = 3$ meters. The extinction coefficient was chosen to be $\beta_0 = .2575$ which is what one estimates at 6000 A for a 13 km visibility using scaling laws discussed elsewhere³. Since only relative transmission data were given in the Naval Research Laboratory report, a comparison of transmission vs. range was possible by adjusting the theoretical curve to the experimental data at one range chosen arbitrarily at 20 km - and observing the fit at other ranges. As seen in figure 9, the agreement is reasonably good. Clearly, however, this limited data cannot be construed as a test of the model at the ranges of practical interest, ie of the order of 100 km, and further experiments would be needed for this purpose.

DISCUSSION

An analytical model for beyond-the-horizon laser propagation has been developed based upon the single scattering approximation. Numerical results suitable for estimation of received power levels in specific systems have been given. The model appears to be in reasonable agreement with limited field data on beyond-the-horizon optical propagation at (relatively close) ranges up to 40 km. A more conclusive field test of the model, particularly at longer ranges, would be necessary to assess its utility for beyond-the-horizon optical communications system design.

A clear conclusion of the study is the desirability of providing a vertical beam divergence of the order of 4° as a means of increasing the received signal at distances greater than 100 km and to relax beam pointing and tracking requirements in the elevation

plane. This is a particular consequence of the decrease of aerosol concentration with height. It is recognized, however, that a vertical fan will reduce the bandwidth of the link due to the increased multipath delay.

Implicit in the model is the neglect of multiple scattering, a semi-quantitative justification for which is given in the Appendix for the limit of long ranges. The transmission estimates of the present model should therefore be viewed as conservative, perhaps by as much as 10 dB at ranges below 100 km where the aura can under favorable conditions be dominant.

APPENDIX: MULTIPLE SCATTERING

Consider a perfectly collimated beam propagating in a homogeneous medium far from any boundaries. Then from multiple scattering theory⁴ it is known that if the scattering law emphasizes forward scattering so that the r.m.s. scattering angle $\bar{\theta} \ll 1$, then an "aura" of multiply scattered photons will develop (similar to that shown in figure 2) whose radial extent, r , increases as the $3/2$ power of the distance z along the beam. More specifically, if the mean free path for scattering is ϱ , then

$$A-1) \quad r = C z^{3/2} \bar{\theta} / \varrho^{1/2}$$

where C is a constant of order unity.

Unfortunately, this result cannot be directly applied to the problem at hand because of the proximity of the Earth's surface to the beam. A downward scattering, even at an angle small compared to $\bar{\theta}$, will result in the photon striking the surface at which point it is either diffusely reflected into non-forward directions or absorbed but in any event lost to the aura. Only those forward scatterings at sufficiently small angles to avoid hitting the surface will contribute to the aura.

We can accommodate this situation by the following approximate device. Let us assume the aura to be built up from multiple scattering events for which the individual scattering angles are all less than or equal to some critical angle θ_c . That is, if the actual differential scattering cross section is $\sigma_a(\theta)$, then the effective cross section $\sigma_e(\theta)$ is

$$A-2) \quad \sigma_e(\theta) = \begin{cases} \sigma_a(\theta) & \theta \leq \theta_c \\ 0 & \theta > \theta_c \end{cases}$$

Assuming for simplicity a homogeneous medium of aerosol density N , then the extinction coefficient, β , for the laser beam is given by

$$A-3) \quad \beta_{\text{direct}} = N \int_0^\pi 2\pi \sin\theta \sigma_a(\theta) d\theta$$

The effective extinction coefficient for the aura, β_{aura} , is

$$A-4) \quad \beta_{\text{aura}} = N \int_{\theta_c}^\pi 2\pi \sin\theta \sigma_a(\theta) d\theta = \beta \{1 - \phi(\theta_c)\}$$

where

$$A-5) \quad \phi(\theta_c) \equiv \frac{\int_0^{\theta_c} \sin\theta \sigma_a(\theta) d\theta}{\int_0^\pi \sin\theta \sigma_a(\theta) d\theta}$$

If $F_0(z)$ is the total radiant flux in the direct (ie unscattered) beam at a distance z along the beam, and $F_1(z)$ is that in the aura (where these fluxes have been integrated over the beam and aura cross sections) then the equations of transfer are

$$\text{A-6) } \frac{dF_0}{dz} = \beta F_0$$

$$\frac{dF_1}{dz} = \beta \phi^{1/4} F_0 - \beta(1 - \phi^{1/4}) F_1$$

from which we obtain for the aura flux

$$\text{A-7) } F_1 = P_T e^{-\beta(1 - \phi^{1/4})z} [1 - e^{-\beta \phi^{1/4} z}]$$

where P_T is the initial flux in the direct beam.

Now since the scattering coefficient for the aura (ie those scatterings which do not deplete the aura) is given by

$$\text{A-8) } N \int_0^{\theta_c} 2\pi \sin \theta \sigma_a(\theta) d\theta = \beta \phi^{1/4}(\theta_c)$$

we may rewrite A-1) in the form

$$\text{A-9) } r = \phi z^{3/2} \Theta_c \beta^{1/2} \phi^{1/2}(\theta_c)$$

where ϕ' is of order unity. Then, the power P_R received by a detector of area A located within the aura at a distance z along the beam is

$$\text{A-10) } P_R = \frac{F_1 \cdot A}{\pi r^2} = \frac{P_T A \phi' e^{-\beta(1-\phi)z} [1 - e^{-\beta \phi z}]}{\pi z^3 \beta \theta_c^2 \phi(\theta_c) \phi^2}$$

where ϕ' is of order unity and depends on the position of the detector within the aura, the field of view, detector orientation, etc.

It remains to estimate ϕ_c and, from the scattering law, $\phi(\theta_c)$. To do this we consider a beam launched from the Earth's surface with elevation angle θ_e , and we neglect the Earth's curvature. Clearly $\theta_c \approx \theta_e$ since a downward scattering at an angle $> \theta_e$ will intersect the surface. Since, from A-9), the aura radius at a given range increases as θ_c increases, if the aura is to intersect the Earth's surface at a given range D , then the beam must have an elevation angle $\theta_e = \theta_c$ satisfying the relationship $D\theta_c = r$ or:

$$\text{A-11) } \phi D^{3/2} \theta_c \beta^{1/2} \phi^{1/2}(\theta_c) = D \theta_c$$

that is

$$\text{A-12) } \phi(\theta_c) = \frac{1}{\phi^2 D \beta}$$

Equation A-12) determines θ_c once the functional form of $\phi(\theta)$ has been determined from the scattering law. To proceed further, we idealize the aerosol Mie scattering cross section as

$$A-13) \sigma(\theta) \approx \begin{cases} \text{constant} \times \left(1 - \left(\frac{\theta}{\theta_0}\right)^n\right) & 0 \leq \theta \leq \theta_0 \\ 0 & \theta > \theta_0 \end{cases}$$

Then from A-5)

$$A-14) \phi(\theta) \approx \left(\frac{n+2}{n}\right) \left(\frac{\theta_c}{\theta_0}\right)^2 \left[1 - \frac{2}{n+2} \left(\frac{\theta_c}{\theta_0}\right)^n\right]$$

If the range D is large, ie $D\beta \gg 1$ than from A-12) and A-14) we find

$$A-15) \left(\frac{\theta_c}{\theta_0}\right)^2 \approx \frac{n}{n+2} \frac{1}{\phi^2 D \beta} \frac{1}{\left[1 - \frac{2}{n+2} \left(\frac{n}{n+2} \frac{1}{\phi^2 D \beta}\right)^{n/2}\right]}$$

Finally, introducing A-15) and A-12) into A-10) we obtain the result

$$A-16) \frac{P_R}{P_{TA}} = \frac{e^{-\beta D \beta}}{\pi D} \frac{1}{\theta_0^2} \left[\frac{\phi' \phi^2 [e^{1/\phi^2} - 1]}{\left(\frac{n}{n+2}\right)} \right] \left[1 - \frac{2}{n+2} \left(\frac{n}{n+2} \frac{1}{2 D \beta}\right)^{n/2} \right]$$

To estimate ϕ , we note that in the Arnush⁴ calculation

$$A-17) \langle r^2 \rangle = \frac{2}{3} \beta z^3 \langle \theta \rangle$$

In the model A-13), $\langle \theta \rangle \approx 2/3 \theta_c$ from which we estimate $\phi \approx 2/3$.

From Deirmendjian's⁵ Mie scattering calculations for marine haze models, we deduce $n \approx 1$ and θ_0 ranging from about 9° in the visible (4500A) to about 30° at 1.19 microns.

In order to compare A-18) with the single scattering results from the text, we must relate θ_0 to the quantity $f(o)$ - the gain over isotropic in the forward direction. Since

$$A-18) f(o) = \frac{\sigma(o)}{4\pi}$$

and

$$A-19) \int_0^\pi 2\pi \sin \theta \frac{\sigma(\theta)}{4\pi} d\theta = 1$$

then from A-13) for $n = 1$ and small θ

$$A-20) \quad 2\pi f(\theta) \int_0^{\theta_0} \theta \left(1 - \frac{\theta}{\theta_0}\right) d\theta = 1$$

or

$$A-21) \quad \frac{\pi f(\theta) \theta_0^2}{3} = 1$$

Then since the first bracketed term on the right hand side of A-16) is about 10 (for $\phi' = 1, \phi = 2/3, n = 1$) we arrive finally at the following estimate for large D

$$A-22) \quad \frac{P_R}{P_T A f(\theta)} = \frac{10 \beta e^{-\beta D}}{3D} = T$$

which can now be compared to the results for T shown in the text. This is carried out in figure A-1 where we compare A-22) with $\beta = .1$ to the results from figure 6 in the text.

Two features of this comparison are noteworthy. First it is seen that at large distances the single scattering model will dominate by virtue of its more gradual fall-off with range. When the extinction coefficient is $.1 \text{ km}^{-1}$, the cross over point is between 130 and 150 km depending on wavelength. Under poor visibility conditions, this cross over point will shift to shorter ranges. At $\beta = .257 \text{ km}^{-1}$ (visibility = 13 km at 6000 Å), for example, the single scattering will dominate at ranges greater than about 75 km.

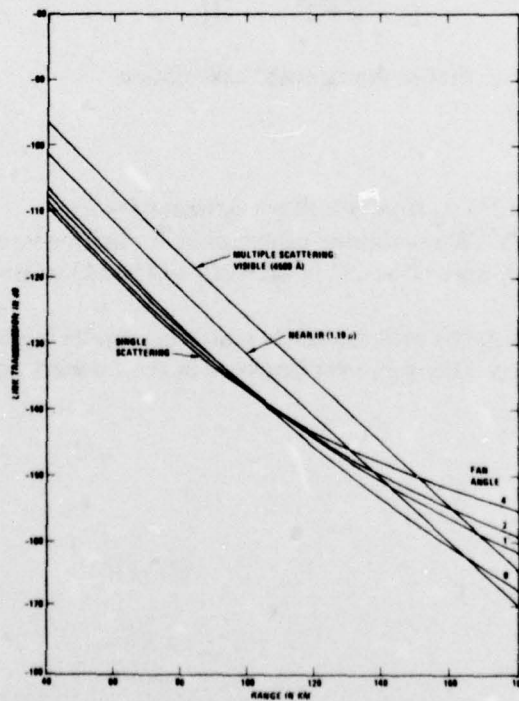


Figure A-1. Comparison of Single and Multiple Scattering.
Extinction Coefficient = 0.1 KM^{-1}

On the other hand, however, it is significant that at shorter ranges, the aura can exceed the single scattered component by about 10 dB. Thus if conditions are right (specifically that the vertical beam divergence be such that energy is radiated at the critical elevation angle, θ_c , determined by A-12) then it is expected that at the shorter ranges (nominally: under 100 km), a bright point-like source due to the aura should be superimposed on the line source due to single scattering.*

Clearly, if communications system design is to be based upon detection of the aura, a more detailed and rigorous treatment of the multiple scattering problem – perhaps via Monte Carlo simulation – would be required. The approach adopted in the present study is the more conservative one of basing detection on the single scattered component whose transmission properties can be modeled in a relatively straightforward manner.

*Indeed, this is precisely what Curcio and Drummer³ observed at a 45 km range when the meteorological range was 20-25 km.

REFERENCES

1. King, M and S Kainer, Some Parameters of a Laser-Type Beyond-The-Horizon Communication Link, Proc IEEE, vol 53, pp 137-141, February 1965
2. Curcio, JA and LF Drummeter, Jr, "Experimental Observations of Forward Scattering of Light in the Lower Atmosphere," NRL Report 6152, US Naval Research Laboratory, September 30, 1964.
3. Adrian, DJ, PH Levine, WR Stone, "Extended Line-of-Sight Electro-Optical Communications Study," Megatek Report Number R2005-039-F-1.
4. Arnush, D, Underwater Light-Beam Propagation in the Small-Angle-Scattering Approximation, Jour Opt Soc Amer, vol 62, pp 1109-1111, September 1972.
5. Deirmendjian, D, Scattering and Polarization Properties of Water Clouds and Hazes in the Visible and Infrared, Appl Optics, vol 3, pp 187-196, February 1964.